DISCLAIMER

This report was prepared as an account of work sponsored by an agency of the United States Government. Neither the United States Government nor any agency thereof, nor any of their employees, makes any warranty, express or implied, or assumes any legal liability or responsibility for the accuracy, completeness, or usefulness of any information, apparatus, product, or process disclosed, or represents that its use would not infringe privately owned rights. Reference herein to any specific commercial product, process, or service by trade name, trademark, manufacturer, or otherwise does not necessarily constitute or imply its endorsement, recommendation, or favoring by the United States Government or any agency thereof. The views and opinions of authors expressed herein do not necessarily state or reflect those of the United States Government or any agency thereof. Reference herein to any social initiative (including but not limited to Diversity, Equity, and Inclusion (DEI); Community Benefits Plans (CBP); Justice 40; etc.) is made by the Author independent of any current requirement by the United States Government and does not constitute or imply endorsement, recommendation, or support by the United States Government or any agency thereof.

Final Technical Report (RD&D Projects)

Project Title:
Developing an Energy-Conscious Traffic Signal Control System for Optimized Fuel Consumption in Connected Vehicle Environments

FOA No.: DE-FOA-0002197

Award No.: DE-EE0009208

Lead Institution: University of Tennessee at Chattanooga

Project Team Members:
University of Tennessee at Chattanooga (UTC), Georgia Institute of Technology, University of Pittsburgh, Oak Ridge National Laboratory (ORNL), and City of Chattanooga

Technical Point of Contact:
Mina Sartipi
Guerry Professor, Department of Computer Science and Engineering, UTC
Email: mina-sartipi@utc.edu, Phone: 423-425-5336

Business Point of Contact:
Meredith Perry
Assistant Vice Chancellor of Research, UTC
Email: meredith-perry@utc.edu, Phone: 423-425-2232

Principal Investigator: Mina Sartipi, UTC

Other Key Personnel (Co-PIs):
UTC: Osama A. Osman, Yu Liang, Dalei Wu
Georgia Institute of Technology: Michael Hunter and Angshuman Guin
University of Pittsburgh: Aleksandar Stevanovic
ORNL: Abhilasha Saroj and Adian Cook

Table of Contents

Section 1: Executive Summary

The project titled “Developing an Energy-Conscious Traffic Signal Control System for Optimized Fuel Consumption in Connected Vehicle Environments” addresses energy-related challenges associated with adaptive traffic control systems by integrating connected vehicles (CV) and connected infrastructure (CI). The system developed in this project, a CV-based adaptive traffic control system, aims to improve fuel consumption in mixed traffic environments by capitalizing on emerging CV and CI communication technologies, as well as leveraging recent advances in Artificial Intelligence (AI), optimization, and edge computing.

The system was tested at the MLK Smart Corridor, an urban testbed managed by the University of Tennessee at Chattanooga (UTC) and the City of Chattanooga. The system was validated through extensive simulations, both Software-in-the-Loop (SILS) and Hardware-in-the-Loop (HILS), and was further implemented and tested in real-world conditions at several intersections along the corridor.

The Fuel Consumption Performance Index (FC-PI) and the Ecological Performance Index (Eco-PI) were developed as the key components for evaluating the system’s impact on fuel consumption and emissions. These metrics provided a comprehensive means of understanding the impact of traffic signal control optimization in mixed traffic environments.

The report presents an in-depth analysis of the Eco-PI, FC-PI, adaptive traffic control system integration, and the testing and field implementation of the system. The results demonstrate significant reductions in fuel consumption and emissions, showcasing the system’s capability to contribute to more sustainable urban traffic management. The report also documents the challenges encountered and recommendations for scaling and further improving the system.

Section 2: Introduction

The growing complexity of urban traffic systems and the increasing need for efficient transportation management have driven the development of advanced traffic control systems. This project aimed to address the challenge of optimizing fuel consumption in connected vehicle (CV) environments through the development of an energy-conscious traffic signal control system. This research leverages deep-learning techniques for real-world vehicle counting and integrates these observations into an adaptive traffic control system, specifically tailored for connected and intelligent transportation infrastructure.

Motivation

The primary motivation behind this work was to enhance traffic management efficiency and minimize emissions from vehicles. Traditional traffic signal control systems often fall short in achieving optimal performance due to their reliance on outdated technologies and lack of real-time data integration. By incorporating deep learning-based vehicle detection and advanced adaptive control algorithms, this research sought to improve fuel efficiency and reduce the environmental impact of traffic.

Objectives

This report details the comprehensive research and development undertaken to achieve these goals. This project was executed in several stages, including the development of a deep learning-based framework for vehicle detection, the integration of hardware-in-the-loop (HIL) simulation for testing adaptive control strategies, and the implementation of field tests to evaluate system performance in real-world scenarios. The culmination of this work is an innovative traffic signal control system designed to meet the demands of a modernizing traffic environment

Section 3: Methodology

3.1 Deep Learning Framework

The primary objective of this part of the research is centered around accurately counting the number of vehicles present in each lane at various intersections. To accomplish this task, we have developed a sophisticated framework based on YOLOv7. This framework has been carefully designed and implemented to efficiently process and analyze traffic data obtained from GRIDSMART systems. By leveraging the capabilities of YOLOv7, we aim to provide a robust and effective solution for automating vehicle counting tasks, thereby contributing to improved traffic management and enhanced transportation planning.

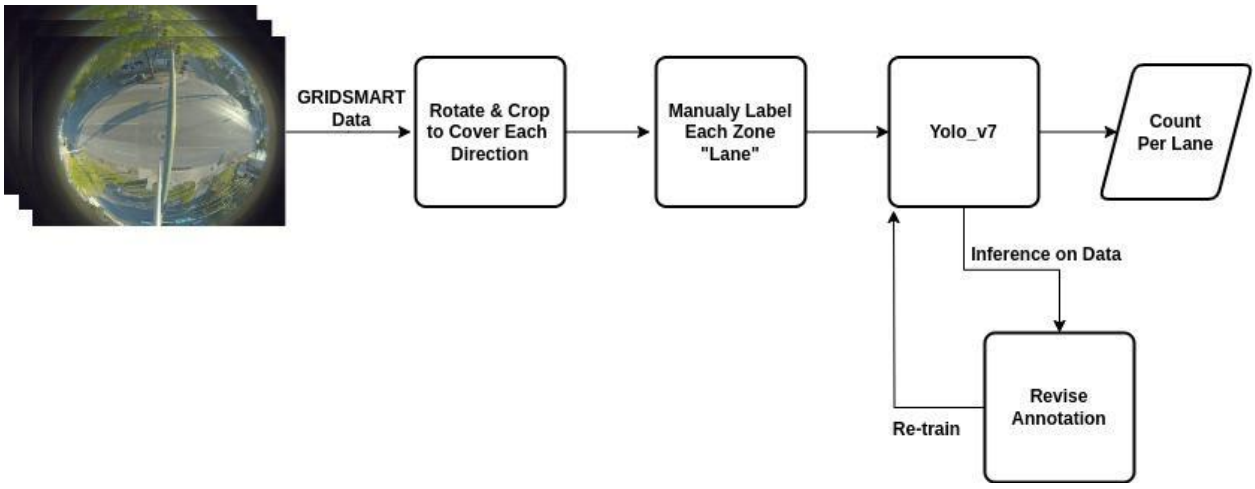

Fig. 1: System Pipeline

Initially, as a proof of concept, we picked one intersection, Central, and subsequently, four distinct approaches were formulated, each corresponding to a specific geographic direction of a lane (East, West, North, and South).

To validate the feasibility and effectiveness of these approaches, comprehensive data was collected, capturing the necessary “proof of concept” for all four directions. The acquired data was then meticulously annotated using the CVAT annotation tool, where a total of 2000 images were manually labeled to facilitate the training process. YOLOv7 was used as our object detectors due to its accurate results compared to its predecessors.

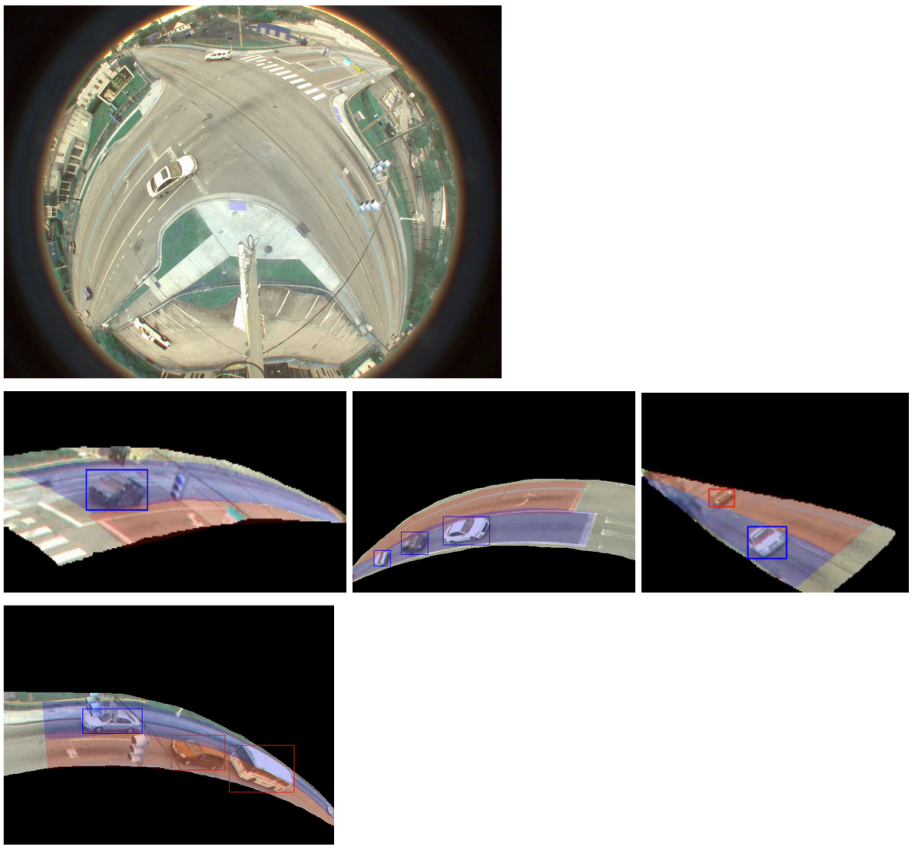

Fig. 2: Intersection at MLK Blvd and Central Ave.

After testing on the Central intersection, using the initially annotated 2000 images, we determined that additional data was needed for other approaches because of variation in camera locations. To address this, we annotated an additional 1200 images, specifically targeting the unseen approaches to expand the dataset. Using the trained YOLOv7 model in inference mode, we obtained preliminary annotation data from various times of day, including night, early morning, and morning periods. This dataset, consisting of 5100 images, was reformatted and uploaded to CVAT for revision and accuracy checks. In total, 8310 images (2000+1200+5110) were accurately annotated and used for retraining the model, ensuring robustness and adaptability to different traffic scenarios.

To ensure the system operates fast enough, maintaining a maximum delay of 1 second (a crucial requirement for controlling traffic lights based on real-time occupancy data), we deployed the framework across two virtual instances. The first instance, equipped with a Tesla V100 GPU (32GB), handles five intersections each with four approaches. The second instance, running on a P100 GPU (12GB), manages three intersections. Through extensive testing, we verified that the

system processes at least 3 frames per second per intersection per approach, effectively ensuring a real-time environment.

The vehicle counts for each intersection and approach are stored in files and made available via a RESTful API. This API, built using Flask, was chosen for its simplicity and ability to handle high throughput with minimal overhead. Flask's lightweight architecture makes it ideal for real-time applications, as it allows fast, asynchronous requests and responses, significantly reducing latency. By employing Flask's threaded mode, we ensure that the API can handle multiple requests simultaneously without blocking, making it capable of delivering real-time traffic data quickly enough to meet the system's 1-second maximum delay requirement.

3.2 DGMARL System Development

3.2.1 Model Overview

The DGMARL framework formulates the traffic signal control problem as a Multi-Agent Markov Decision Process (MDP). Each intersection is represented as a node in a spatial-temporal graph, and the roads between intersections are modeled as edges. The reinforcement learning agents control the signal phases at each intersection, to maximize a cumulative reward defined by the reduction in vehicle delays, stops, and environmental impacts (measured by Eco-PI).

Figure 3 shows the architecture of DGMARL. The architecture has the following features:

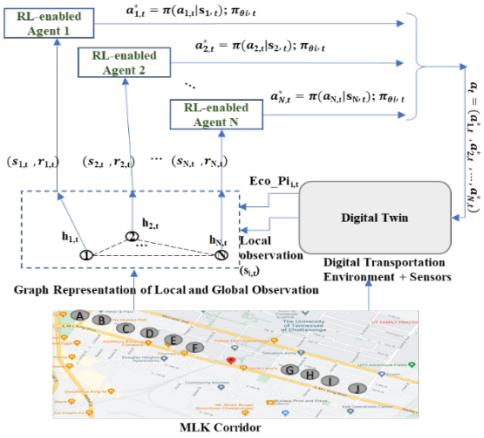

Fig. 3: DGMARL

- A spatial-temporal graph neural network is used to formulate the temporal and spatial features of the whole transportation network. Each intersection is modeled as a node of the graph and the roads connecting the two interactions are modeled as edges of the graph.
- As a decentralized scheme, on each node, an Advantage Actor Critic (A2C) reinforcement learning agent generates actions to control the traffic lights at the corresponding intersection.
- The DGMARL integrates the black-box reinforcement learning framework and traffic dynamics derived from the temporal and spatial correlation between intersections.

3.2.2 Simulation Environment

The VISSIM micro-simulator was used to test and evaluate the DGMARL model. The network was configured with real-world traffic data from MLK Blvd during peak hours observed on Dec.

15th, 2022. The state and reward functions were derived from VISSIM, with simulations conducted for durations ranging from 1 to 24 hours to evaluate performance under varying traffic conditions.

3.2.3 Mathematical Model

Initially, a mathematical model was developed to optimize traffic signal timing based on observed demand at intersections along MLK Blvd, using the VISSIM micro-simulation platform for evaluation. The model tracked traffic data such as vehicle occupancy, signal start times, and cycle duration, and then identified optimal phase durations while considering constraints like maximum cycle length. Initial tests showed a 12.32% improvement in Eco-PI, but further adjustments, such as modifying green light durations, increased performance to 40.12%. Integrating a dynamic stop penalty further enhanced overall performance by 45.63% though some intersections, like Magnolia, showed mixed results. However, this method was preliminary and did not include constraints like red clearance, but it provided valuable insights into traffic flow, helping to identify key elements for developing a machine learning model to optimize traffic signal timing.

3.2.4 Integrating Math Model with DGMARL

We developed a multi-agent learning model using the Advantage Actor Critic (A2C) policy and integrated it with the VISSIM network for MLK Blvd through a DGMARL-compatible Python script and COM interface. The DGMARL algorithm employs a neural network-based “critic” to estimate the state-value function and an “actor” to update policy distribution based on the critic’s recommendations. The model was trained and validated across multiple scenarios, incorporating constraints like minimum phase duration and maximum cycle lengths. We have analyzed the model’s performance under various conditions, adjusting parameters such as the number of episodes, learning rate, simulation duration, batch size, and learning frequency.

Input and output of the DGMGRL model is shown in Table 1.

Table 1: Input and Output of DGMARL

DGMARL Input		
Runtime Properties Needed from Field	**Sub algorithm – Eco_PI Calculation**	**Static Properties or Configurations available from the field**
1. Detector's value - Traffic Occupancy 2. Each signal's current status 3. Number of vehicles in each lane - every second	Vehicle_ID, LaneID, Vehicle_speed	Intersection Id, Associated Signal Controller Id, Signal Group ids and Associated Phases, Left turn phases, Link Ids and Lanes - associated to phases, Detectors Ids associated to phases, MinGreen, RedClearanceTime, YellowTime, Ped Recall, Walk time, Flashing Don't Walk time
DGMARL Output		
Action: 0 : Stay in current phase 1 & Phase_id: Switch to the Phase_id which has highest traffic demand		

3.2.5 Integration Pedestrian Recall and Physical Constraints to DGMARL

To adhere to existing field constraints and provide a safe environment for users, we have included safety measures such as pedestrian recall, minimum green duration, and maximum cycle length as constraints in DGMARL.

In the initial effort, since pedestrian input was not yet configured in VISSIM, we treated pedestrian requests as recalls, using default timings for “pedestrian walk” and “flashing don’t walk” whenever the phase was green. The minimum phase duration was set to the higher value between the configured minimum green duration and pedestrian recall timing. However, the maximum cycle length constraint caused delays, as the DGMARL agent had to serve fixed phase sequences even when there was no traffic demand. To resolve this, we removed the maximum cycle constraint and introduced a phase sequence-free model in the next effort. This improvement allowed DGMARL to switch to the phase with the highest traffic occupancy. We also included right-turn movements in the Eco-PI calculation to account for stops and delays caused by yielding to oncoming traffic. Also, we integrated an optimization frequency parameter (Δt) to account for data communication latency between the field and VISSIM, trained and tested the model with a 5-second optimization frequency.

3.3 Digital Twin System Design

The design philosophy of the digital twins is driven by the need to address a few key challenges. Traditional traffic management systems often rely on static timing for traffic signals and are slow to respond to real-time changes in traffic flow. This results in congestion, delays, and inefficiency. A system that can utilize real-time data from sensors and GPS-enabled vehicles to dynamically adjust traffic control systems would be a much-improved alternative. This helps improve traffic flow, reduce congestion, and optimize road usage by reacting instantly to changing conditions. A sign of robustness in a system is the ability to use current and historical information to gain foresight into how a system may change over time. The availability of real-

time data offers the opportunity to employ deep analytics in the form of machine learning models to predict incidents ahead of time. Prior explorations of digital twins and the incorporation of streaming field data have shown the necessity to accommodate data flaws. These come in many forms and varying degrees, from data being riddled with gaps or entirely missing.

To handle the scaling of such a deeply integrated system, a three-tier approach was adopted for this study. Each tier is incrementally more complex than the previous. The primary differences are in the method of the simulation itself and the data sources. The simpler models allowed for more efficient testing of changes in the development of algorithms with faster than real-time trial runs. A breakdown of the Tiers is as follows:

- Tier 1 involved a VISSIM model that was prepopulated with archived data. The data is manually incorporated into the model through the VISSIM interface itself.
- Tier 2 was developed to test the ingestion of data in a pseudo real-time environment. The archived data was periodically streamed to the VISSIM model which dynamically adapted to the changes.
- Tier 3 is the real-time digital twin which uses data streamed directly from the field devices. This data is then ingested by VISSIM, and the model is updated accordingly.

Tier 1

The incorporation of archived data into the VISSIM model directly results in the simplest version of the digital twin. This model serves as a foundation for subsequent development stages. Data, such as traffic volumes, signal timings and turn movements, are incorporated into the simulation in advance, enabling the testing of optimization algorithms in a controlled environment. By using archived data, scenario testing can be done efficiently without the added complexities of real-time data.

The MLK corridor Tier 1 model is prepopulated with one minute aggregate traffic volume data and ten-minute turn movement data provided by the City of Chattanooga. Two versions were created for the same tier, for both the PM peak and 24-hour traffic scenarios.

Tier 2

With the successful creation of a Tier 1 model, a few key modifications were made to bring it closer to real world elements. The method of incorporating archived data was changed to that of a streaming model. The SPaT, traffic volumes, and turn count data were communicated to the

model during its runtime unlike the Tier 1 method of loading it prior to a simulation run. This incremental advancement in the model helped lay the groundwork for the Tier 3 system.

Tier 3

The final tier integrates real-time data streams into the simulation model. By utilizing actual field data, the model becomes a real-time representation of the smart corridor, capable of reflecting live traffic conditions. Modifications in this tier include the ingestion of real-time volume, turn count, and SPaT data, enabling the model to continuously adjust based on live data inputs. The consistent data streams from the MLK corridor allowed for real-time performance monitoring and optimization of traffic signal timings for fuel efficiency.

3.4 Digital Twin Model Development

3.4.1 Digital Twin Modules

In this study, the Digital Twin is developed using vehicle real-time and historic volume count, turn count, and Signal Phasing and Timing (SPaT) data available from approximately 2.1 miles of Martin Luther King Smart Corridor, Chattanooga, Tennessee, consisting of 11 signalized intersections. A smart corridor Digital Twin model architecture typically includes four key components as shown in Figure 4.

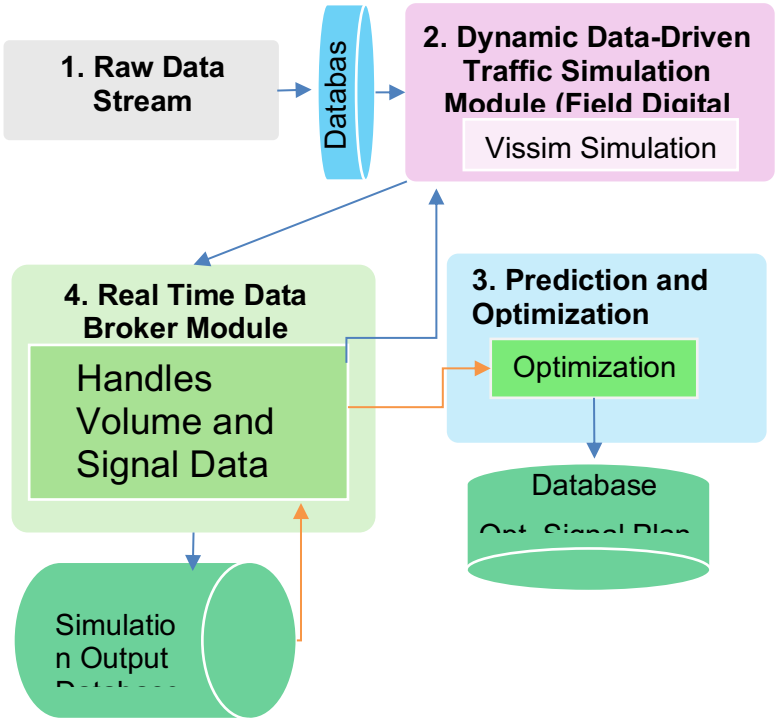

Fig. 4: Digital Twin Architecture

Module 1: Raw Data Stream Processing Module - includes processing of raw data to parse, format, and store the data in a database. From the physical MLK Smart Corridor, the left,

through, and right turn vehicle counts per lane at the 11 intersections are obtained. This data is processed to obtain approach level (Eastbound, Westbound, Northbound, and Southbound) volume and turn counts. Further, 10 Hz Signal Phase and Timing (SPaT) data is obtained from the signal controllers in the corridor.

Module 2: Dynamic Data-Driven Traffic Simulation Module - includes PTV-Vissim microscopic traffic simulation model of the Smart Corridor, dynamically driven using volume, turn movement ratios, and signal indications data (from Module 1). In this implementation, intersection approach level 1-minute aggregate volume counts, 10-minute aggregate turn counts data, and signal timing are dynamically driven using PTV-Vissim's COM module. Using COM the signal indications can be driven using external SPaT (Signal Phasing and Timing) data or PTV-Vissim's internal Ring Barrier Controller (RBC) module.

Module 3: Prediction and Optimization Module or Simulation Testbed Application Module - consists of tools and algorithms to process simulation outputs based on the requirements of the application. This module contains processes or algorithms that are driven using outputs from the Digital Twin simulation. In this study, the outputs such as detector occupancy, each direction approach level vehicle count aggregates, vehicle velocity, and current signal state, etc are generated from the PTV-Vissim simulation model in the Dynamic Data Driven Traffic Simulation Module are used as inputs for prediction and optimization for the signal timing plan.

Module 4: Real Time Data Broker Module - handles real time dynamic data transactions between modules. This module consists of a Flask based web service to handle data transactions/communication between other three modules.

3.4.2 Three-Tier Incremental Framework for Digital Twin Development

The three-tier incremental framework used for the MLK Smart Corridor study is described in this section. The framework includes the development of structures for execution of replicate trials faster than real time, enabling efficient testing and development of algorithms and applications in the first two tiers, leading to the development of the final digital twin in the last tier.

Tier 1 - Development of Prepopulated Offline Simulation

The developed Vissim model provides the base simulation construction (Vissim link and connector layout, signal placement, etc.) that is harnessed in all three Tiers. While basic Vissim model development is often a partially manual process, the authors advise the development of scripts for converting archived data into the input file formats utilized by the underlying

simulation, enabling the ability to efficiently test developed algorithms under different conditions (e.g., weekday vs weekend, growth scenarios, etc.). Minimization of the manual effort required to test differing scenarios is critical to the overall usability and effectiveness of such a platform. Scripts used for data preparation and prepopulating Vissim model may be found at https://github.com/hunter- guin-gatech/MLK_Digital_Twin. Detailed guidance for developing the underlying Vissim model may be found in Hunter, 2021 (1).

In this tier, for the MLK corridor, the Vissim simulation model of the corridor is populated with one-minute volume and ten-minute aggregate turn movement ratio data for a representative time period. In Tier 1, traffic signals are controlled using Vissim's Ring Barrier Controller (RBC) feature which emulates typical signal control features found in most traffic signal controllers deployed in the field. For example, the MLK corridor signal timing plans and phase diagrams provided by the City of Chattanooga were used to configure the RBCs. For the MLK case study two versions of the prepopulated Vissim model were created: 1) a PM peak model that simulates the 3 PM to 6 PM period, and 2) a 24- hour version that simulates an entire day. These models provide an efficient means for developing and testing optimization algorithms on a simulation testbed much faster than real time. These models are used to conduct initial studies for development of local and global signal timing optimization algorithms.

Tier 2 - Development of Pseudo Digital Twin (Driven with Archived Data)

The goal of Tier 2 is the development of a dynamically driven simulation model, i.e., data is streamed to the model during runtime rather than pre-populated prior to model execution as in Tier 1. Dynamic streaming data includes volumes (demand), intersection turn ratios, and SPaT data. The model differs from the model in Tier 1 in its ability to drive the simulation during runtime using archived field data streams in their original formats. Further, it is highlighted that in this model the signal indications are controlled using field received SPaT messages, not the internal Vissim RBC. Thus, the implemented signal phase times will match the field directly, rather than relying on the accuracy of the simulation signal control emulator (i.e., Vissim's RBC feature).

This effort includes development of the digital twin architecture modules (Figure 4). It differs from the real time data-driven digital twin (Tier 3) as it simulates data from an archival data stream rather than a real time stream. The key developments found in Tier 2 related to the digital twin architecture (Figure 4) include:

- Module 1: Development and integration of hardware and software for receiving and processing of data streams in sync with wall clock time.
- Module 2: Integration of the Tier 1 simulation model into the system, enabling volume and signal control to be driven by external data streams.
- Modules 3 and 5: Development of the application specific functions. In this case study this involved the development of the traffic signal optimization algorithms for module 3 and the second simulation instance for module 5, which ingests SPaT data from module 3 instead of field SPaT data.
- Module 4: Development of a Flask [28] based web service to handle data transactions/communication between modules, and fetching of archival volume, turn counts, and SPaT data from the database.

Tier 2 introduces two significant benefits in the three-tier approach to the digital twin platform. Firstly, it contains the development of the digital twin architecture necessary to utilize real time (or wall clock time) data streams. Importantly, the ability to utilize archived data streams to simulate real time streams allows for simplified error checking in dynamic execution of system components. Secondly, Tier 2 allows for replicability under identical streamed field conditions when testing developed optimization algorithms or other smart corridor applications.

The Tier 2 platform can be used to simulate any day as long as the archived data is available for that day. This allows for testing and refinement of different strategies implemented in Module 3, capturing the variations across days of the week, holidays, and special events. Vissim's inbuilt evaluation measures such as route travel time and delay, approach queue length, etc., are used by Module 3 for evaluation and optimization.

Tier 3 - Development of Real Time Data Driven Digital Twin

Tier 3 contains the development of the digital twin driven using real time streaming volume, turn count, and SPaT data. Module developments from Tier 2 are utilized with minor modifications. The key modifications made in Tier 3 are:

- Module 1: Data ingestion programs are created to receive and process real time data from field devices and inject the processed data into relational MySQL database tables. The system input configuration is modified to point to the database tables for real time data streams instead of streams generated from archived data.

- Module 2: Model verification, validation, and calibration may be extended to validate real time simulation performance.
- Module 4: Service configuration modified to point to real time database tables instead of archived data tables.

3.5 Fuel Consumption Performance Index (Eco FC-PI)

The goal of this task is to develop an environmental-based objective function for control optimization. To achieve this goal, we developed a novel performance measure referred to as Ecological Performance Index (Eco-PI). The Eco-PI is a performance measure that characterizes impact of signal timings on excessive FC and vehicular emissions at signalized intersections by looking at how various operational and traffic conditions impact unnecessary vehicular stops at controlled intersections. Eco-PI is a scalable performance measure that can be estimated on various spatial levels–from an Eco-PI for a specific traffic movement (related to a signal phase) through an Eco-PI for a whole intersection (in order to be able to find the right balance for various traffic movements) to an Eco-PI for the entire road network.

The development of the Eco-PI is based on the well-known concept of Performance Index, a performance measure which has been used for decades in traffic signal optimization processes to derive a right balance of delays versus stops when optimizing traffic signals (*2-9)*. The PI achieves balance through a linear combination of delays and stops (mainly for major through movements), where the key factor is the stop penalty "K", which represents a weighting factor, or a stop equivalency measured in seconds of delay. However, the PI is neither properly defined (especially from the point of its technical derivation), nor is it comprehensively evaluated for several impacting factors. A more technical outcome of these omissions is the fact that the PI is used as a single deterministic formula *(6-8),* as opposed to being a family of relationships that depend on several operational factors. Specifically, the contemporary signal optimization practice assigns a constant value (e.g., 10 seconds) to the K and it does not recognize it as a parameter that is dependent on various operational conditions.

The goal of using the Eco-PI is to reduce fuel consumption and various pollutant emissions caused by traffic signals. However, previous studies *(9-10)* have shown that one or more pollutant criteria do not linearly correlate with FC. That suggests that most likely an Eco-PI that minimizes other emissions/pollutant criteria. Therefore, we defined the Eco-PI as a generic performance measure that can be derived to reduce FC and any other pollutants (e.g., HC, CO,

NOx, CO_2, and PMs). As a consequence, a specific intersection or a network Eco-PI could be defined as one from a family of similar PIs, all based on different environmental factors. For example, FC-PI, HC-PI, CO-PI, NOx-PI, CO_2-PI, and PMs-PI are all members of the Eco-PI family that are derived specifically to reduce FC, HC, CO, NOx, CO_2, and PMs, respectively. Our research, however, focused on a methodology to derive an FC-PI considering impacts of various operation conditions (e.g., cruising speed) on the K value.

3.4.1 Major Factors Impacting Stop-Related Fuel Consumption

When developing an FC-PI, the K factor becomes the number of seconds of delay that consume the same amount of fuel equivalent to the action of stopping (deceleration and acceleration). Thus, the value of K is significantly impacted by the FC experienced during a stopping maneuver, which eventually impacts the total value of FC-PI. The major factors (driving conditions) that impact FC during a stop at a signalized intersection are those that impact the acceleration phase of the entire stop-and-go maneuver. While the same, or other, factors may significantly impact the deceleration phase too, such impacts are usually of much lower significance as much less fuel is always consumed during the deceleration phase. Thus, it is logical to pay more attention to what happens on the acceleration side of the maneuver, which is the major driving phase for increased FC. For this reason, we mainly focused on those factors that impact FC mainly during the acceleration phase, which are: 1. Distribution of vehicular types and engines; 2. Proportion of heavy vehicles in fleet distribution; 3. Driver's behavior; 4. Road gradient; 5. Cruising speed; and 6. Wind effect.

3.4.2 Development of the FC-PI

Observing the kinematics and dynamics of a vehicle stopping at an intersection microscopically, shown in fig. 5, was the essence of deriving the FC-PI. When a vehicle stops at a signalized intersection, it must go through three driving phases, as shown in fig. 5a. Firstly, the vehicle decelerates from its original cruising speed to zero (deceleration phase)> secondly, the vehicle waits for the signal to turn green, during which time the vehicle's engine idles (idling phase). Thirdly, once the signal turns green, the vehicle accelerates from zero to its cruising speed (acceleration phase). Those three phases form the concept of the "Cruising Speed Stop Profile" (CSSP), where cruising speed after acceleration is assumed to be the same as before the deceleration phase.

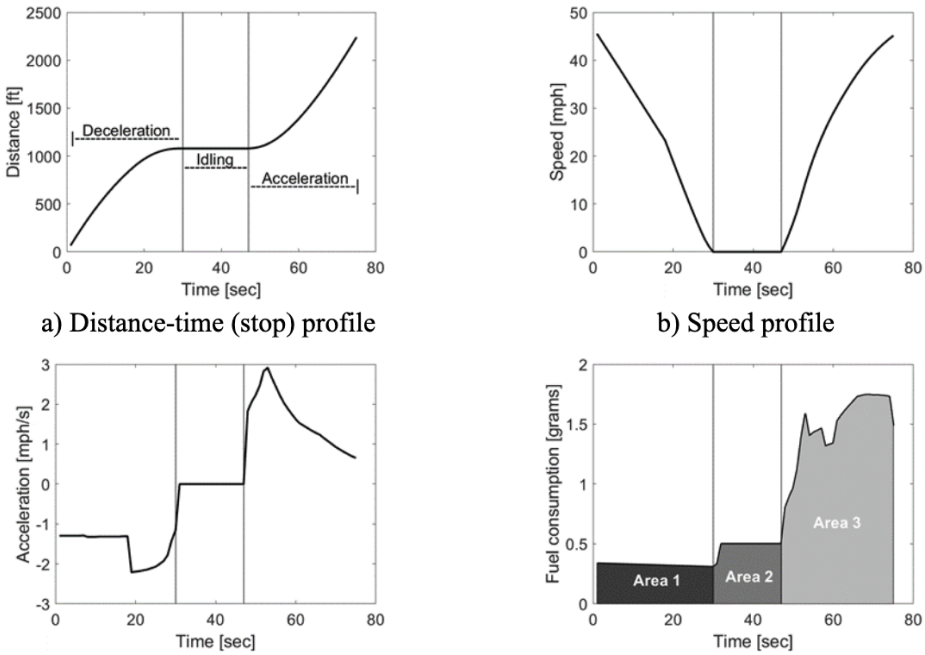

Fig. 5: Dynamics and Kinematics of a Stopped Vehicle

Part b of Fig. 5 shows the CSSP of the same vehicle, where the speed foes from its cruising value to zero, and then back to the cruising value. Part c shows how acceleration changes during the process, which directly impacts FC, shown in part d. It can be stated that for CSSP, the total amount of fuel consumed is:

$$FC_{CSSP} = FC_D + FC_I + FC_A$$

Where: FC_{CSSP} – total fuel consumed during a CSSP [gallons, liters, or grams], FC_D – fuel consumed during the deceleration phase; [same unit as FC_{CSSP}], FC_I – fuel consumed during the idling phase; [same unit as FC_{CSSP}], FC_A - fuel consumed during the acceleration phase; [same unit as FC_{CSSP}].

While the FC curves shown in Figure 1d are hypothetical, it is obvious that fuel consumed during the acceleration mode is by far greater than fuels consumed either during braking or idling at the intersection. While this simple concept (including FC) has not been shown in relation to the PI concept before, it has been clear since late '60s (*10)* that idling mode can be associated with 'pure' delay (stopped delay, to be more precise) while braking and acceleration are associated with a full stop, or a car's maneuver to decelerate from its cruising speed to zero and then accelerate back to the cruising speed. That suggests that it is crucial to separate 'delays' from 'stops', the two commonly used traffic performance measures for signalized intersections. Such separation is achieved only by separately identify extra FC attributed to a stopping event FC_{DA} ($FC_D + FC_A$) from that attributed to the stopped delay (FC_I) (or waiting time in the queue at traffic signals).

Now, following that the K factor is the number of seconds of delay that consume the same amount of fuel consumed by a stopping event, we can say that FC_{DA} is equal to an equivalency factor 'constant' (K_e) multiplied by the FC_I, as expressed in Equation 2.

$$FC_{DA} = K_e \cdot FC_I \quad (2)$$

By rearranging Equation 2, the unitless constant (K_e) can be expressed as shown in Equation 3.

$$K_e = \frac{FC_D + FC_A}{FC_I} \quad (3)$$

The idling phase duration varies based on the red interval's length. Therefore, the next step is to divide FC_I by the total idling time (T_I) in seconds, as shown in Equation 4. That is important to assign the number of seconds of stopped delay that is equivalent to a stopping event, which is the stop penalty (K).

$$K = \frac{(FC_D + FC_A) \cdot T_I}{FC_I} \quad (4)$$

Naturally, K values will be different for various movements based on several factors. For example, it is obvious that total fuel consumed on a movement with a high truck percentage in the fleet will be larger than total fuel consumed on a movement with light-duty vehicles only. Thus, we define a movement-specific K_i for each movement *i*:

$$K_i = \frac{(FC_D + FC_A)_i \cdot T_{I_i}}{FC_{I_i}} \quad (5)$$

Next, one can define an FC-Performance Index (FC-PI) for a network of traffic signals with *i* movement, and a given analysis period (e.g., an hour), as:

$$FC - PI = \sum_{i=1}^{n} D_i + \frac{(FC_D + FC_A)_i \cdot T_{I_i}}{FC_{I_i}} \cdot S_i \quad (6)$$

While all of the variables have been introduced above, the index *i* applies to each eligible movement in the network and the *n* is the total number of eligible movements.

3.4.3 Investigating Impact of Operating Factors Contributing to Eco-PI

When investigating the individual impact of a particular factor (e.g., vehicle type) on FC, all other factors (e.g., cruising speed, road gradient, fleet distribution, driver behavior, and wind speed) were kept constant, at their default values (discussed next). A total of 74 experiments were designed to cover a wide range of variables for each of the investigated operational condition factors. Table 2 shows a summary of the variables that were tested individually for each investigated factor. It should be noted that we adopted various vehicle types from CMEM.

Table 2 Variables for various operational conditions impacting FC

Vehicle type		Fleet distribution		Driver behavior		Road gradient		Cruising speed		Wind effect	
Variable	FC (g)	Variable	FC (g)	Variable	FC (g)	Variable	FC (g)	Variable	FC (g)	Variable	FC (g)
LDV1	56.6	100:0	56.6	Func1	45.7	-7	34.8	20	16.1	50 tailwinds	473.8*
LDV2	57.2	99:1	62.5	Func2	47.2	-6	37.6	25	21.8	40 tailwinds	505.6
LDV3	55.5	98:2	68.7	Func3	49.5	-5	40.8	30	27.2	30 tailwinds	510.8
LDV4	52.5	97:3	74.4	Func4	51.9	-4	43.5	35	36.7	20 tailwinds	513.3
LDV5	57.8	96:4	80.1	Func5	53.2	-3	46.3	40	46.4	10 tailwinds	525.6
LDV6	54.6	95:5	86.5	Func6	55.4	-2	49.6	45	56.6	No wind	549.0
LDV7	55.5	94:6	92.3	Func7	56.3	-1	52.7	50	70.3	10 headwinds	587.2
LDV8	59	93:7	98.4	Func8	58.4	0	56.6	55	85.5	20 headwinds	628.5
LDV9	58.7	92:8	104.1	Func9	60.5	1	59.2	60	106.6	30 headwinds	690.8
LDV10	111.2	91:9	110.9	Func10	62.2	2	63.7	65	135.3	40 headwinds	835.4
LDV11	56.8	90:10	117.6	Func11	63.7	3	67.1			50 headwinds	979.5

LDV12	55.9		Func12	65.4	4	71.1	Not applicable	
HDDV1	816.5				5	75.0		*Values are for
HDDV2	894.4	Not applicable	Not applicable		6	80.2		HDDVs
HDDV3	549.0				7	85.6		

Fig. 6 shows the process of modeling traffic at the testbed intersection, performing various experiments, post-processing data trajectories from VISSIM, estimating FC (based on trajectories) in the CMEM, and post-processing FC estimates in Matlab to compute the value of K. A default value for each of the evaluated factors was identified, as a reference value used when comparing FC results, to ensure consistent comparisons. Light-duty vehicle 1 (LDV1), Heavy-duty vehicle Diesel vehicle 3 (HDDV3), no heavy vehicles, 12 deterministic acceleration-deceleration functions, level terrain, 45 MPH, and no wind were selected as default values for LD vehicle type, HDD vehicle type, driving behavior, road gradient, cruising speed, and wind speed, respectively.

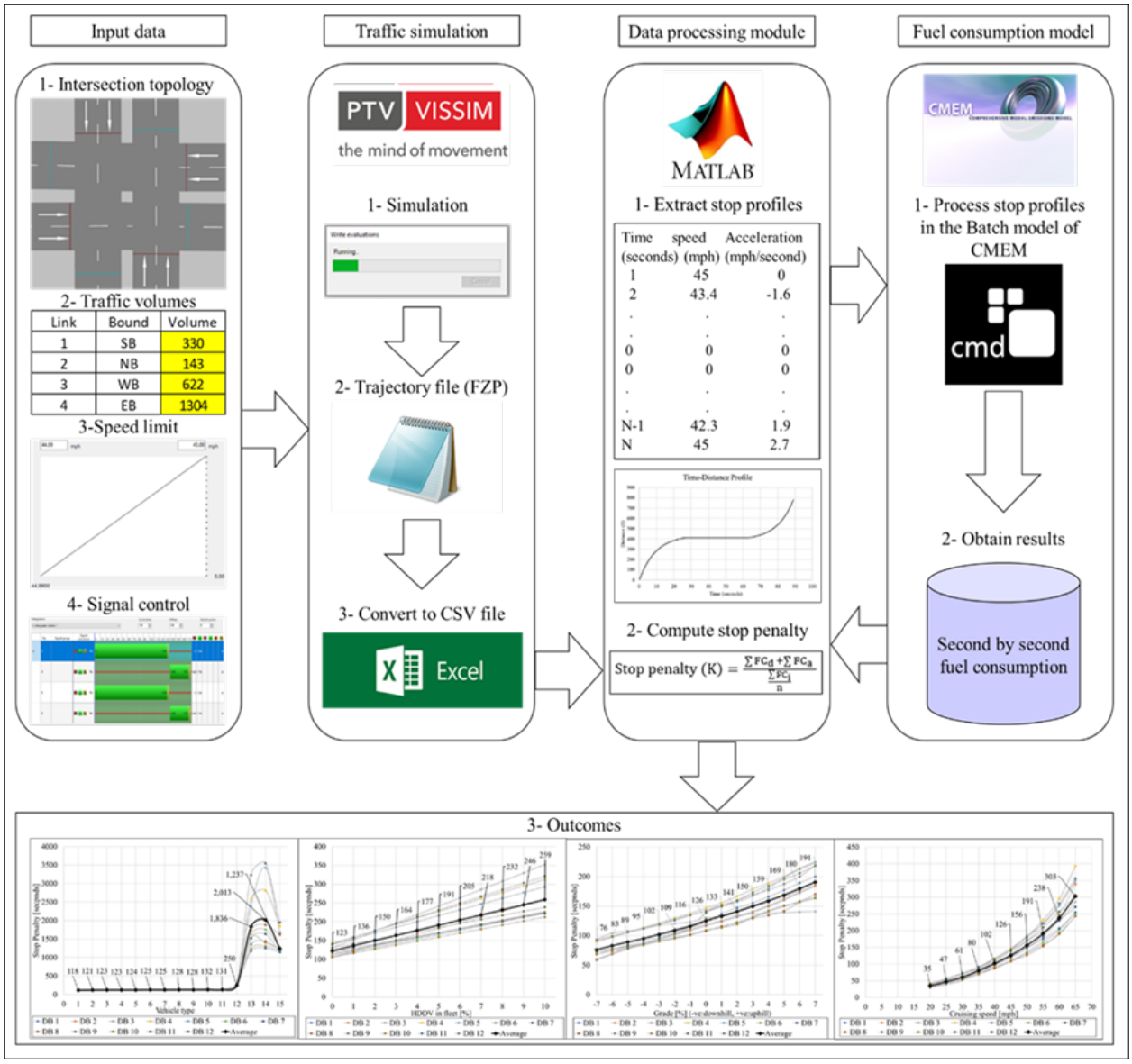

Fig. 6: VISSIM-Matlab-CMEM connection

3.4.4 Developing Regression Equations Based on Simulation

The amount of consumed fuel (in grams), for a CSSP representing each of the various experiments, are presented in Table 2. For each of the results from Table 2, the values of K are illustrated (for each variable individually) as a function of a specific FC factor in Fig. 7.

Each of the charts in Fig. 7 (except 7c) includes 13 data series out of which 12 represent deterministic deceleration-acceleration functions investigated in the study, and the bold line represents an average of those 12 data series. Fig. 7c is an exception because it already shows the impact of various driving behaviors on K value. Results of the experiments with various vehicle types (columns 1 and 2 in Table 2) show that each vehicle type consumes a different amount of fuel. Such difference in FC is mainly apparent when comparing LDVs and HDDVs between various vehicle types as visualized in Fig. 7, which illustrates the FC results during the same CSSP regime for three vehicle types: LDV10, LDV11, and HDDV3. The variations in FC between different vehicle types will result in various K values as shown in fig. 7a, which depict that stop penalty ranges between 118-second to 250-second for various LDVs

Such a conclusion can also be reached by observing the stop penalties of HDDVs, which resulted in ~9-15 times higher values than the stop penalty from the LDVs. These facts are expected to result in a significant impact on the K value, when calculated for a fleet of vehicles with a high HDDV percentage.

Fig. 7b shows that the K factor follows an approximately linear relationship with an increase in the percentage of HDDVs. Based on fig. 7b, we can conclude that every increase of 1% of HDDVs in the fleet costs around 11 seconds of extra waiting-idling time (based on the equivalent FC) for every additional stop at a traffic signal. Similarly, every increase of 1% of the road gradient costs 6 to 11 seconds of extra waiting-idling time, as shown in fig. 7c.

As seen from fig. 7d, there is no clearly recognizable pattern to correlate variations of the K factor with some intuitive expectations related to different driving behaviors, because such behaviors are usually based on unique mental and physical characteristics of the drivers. Nevertheless, the impact of those differences is significant on the K value (ranging from 105 to 147 seconds for various deceleration-acceleration functions).

In relation to the cruising speed, the K factor growth seems to follow an exponential equation, as shown in fig.7e. This is especially observable for cruising speeds higher than 45 MPH. This

finding can be interpreted as if stopping a vehicle at a higher cruising speed introduces a much more significant interruption than stopping a vehicle traveling at a slower speed.

Results of the wind speed and direction have shown, as expected, that headwinds cause the HDDV to generate more energy (which requires more fuel) to overcome the energy of the wind blowing in the opposite direction. Those results are reflected on the K value as depicted in fig. 7f; thus, they confirm the importance of including wind effect in K calculations, especially for fleets with a high percentage of HDDVs. To summarize, the results indicate that the K factor should be much larger than used by current signal timing practices and that it should be defined differently for various traffic movements and intersections, depending on their operating and traffic conditions.

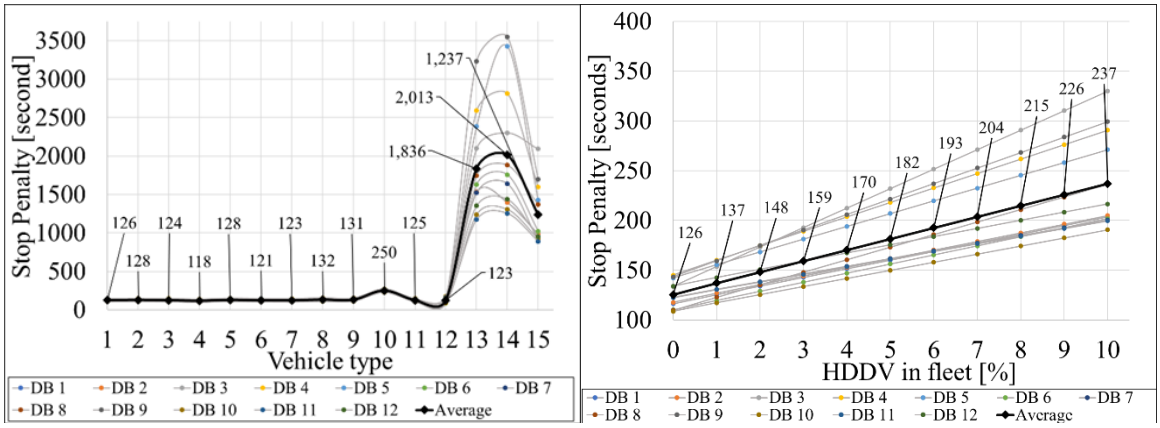

a)vehicle type b) fleet distribution

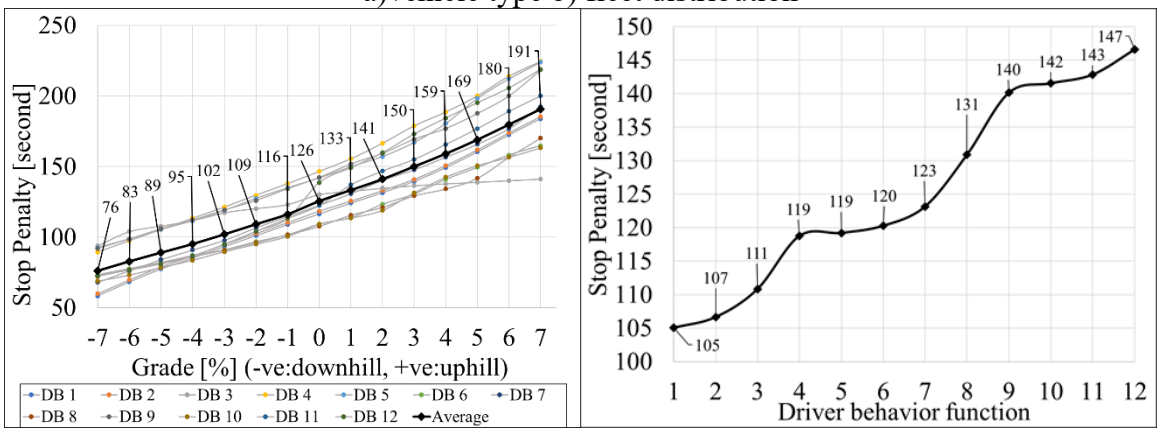

c) road gradient d) driving behavior

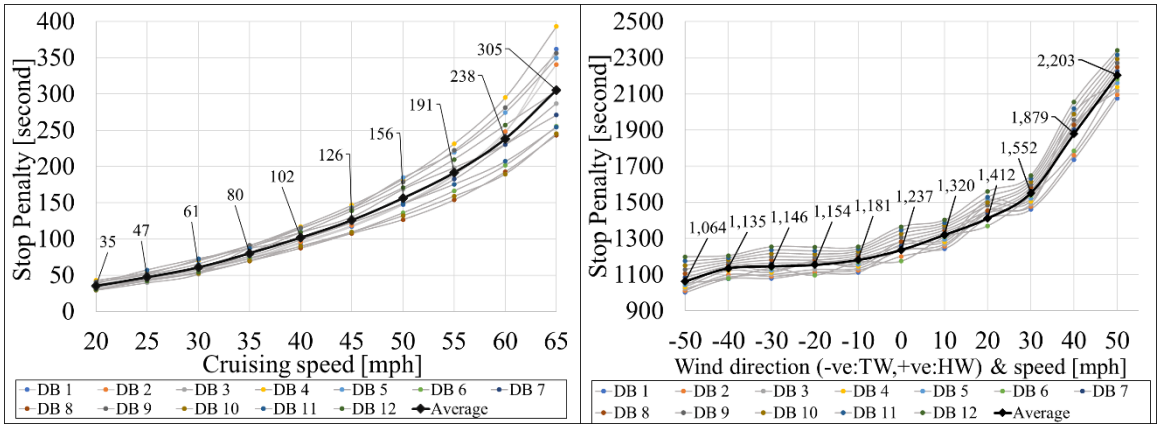

e) cruising speed f) wind effect

Fig.7: Impact of various operational condition on stop penalty (K); DB: driver behavior

Finally, fig. 8 presents regression equations to compute the K factor considering the individual impacts of percentage of heavy vehicles in fleet, road gradients, cruising speeds, and wind effects. It should be noted that when developing a regression equation for one of the four above-mentioned factors, the default values of all of the other factors (and the 12 deterministics driving behavior functions (shown in fig. 7d) were used. Also, those equations were developed with the assumption that the final cruising speed is the same as the initial cruising speed.

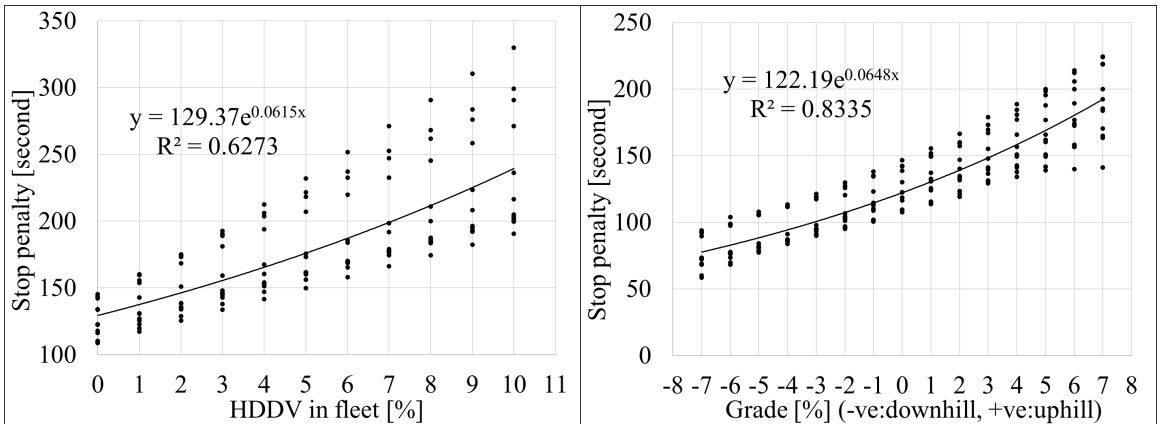

a)percentage of HDDVs in fleet b) slope during acceleration phase

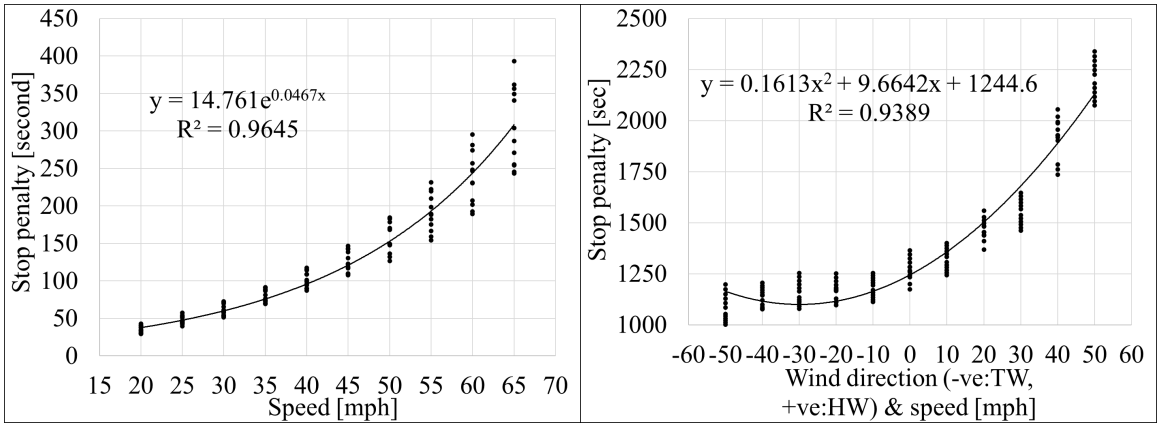

c) cruising speed d) aerodynamic effect of wind speed and direction

Fig. 8: Regression models to computer stop penalty

Table 3 presents the coefficient of determination and the range of each of the developed regression equations, based on existing simulation results.

Table 3 Regression equations to compute the stop penalty

Factor	Equation	Range	R^2
x_{pHV}: % of HDV	$K = 129.37 \cdot e^{0.0615 \cdot x_{pHV}}$	$x_{pHV} = [0, 10]$	0.6273
x_{RG}: Road gradient (%)	$K = 122.19 \cdot e^{0.0648 \cdot x_{RG}}$	$x_{RG} = [-7, 7]$	0.8335
x_{cs}: Cruising speed (mph)	$K = 14.761 \cdot e^{0.0467 \cdot x_{cs}}$	$x_{cs} = [20, 65]$	0.9645
x_{WE}: Wind effect (mph)	$K = 0.1613 \cdot {x_{WE}}^2 + 9.6642 \cdot x_{WE} + 1244.6$	$x_{WE} = [-50, 50]$	0.9389

It should be noted that the equations in Table 3 can be used to compute the K factor required to minimize FC, but not necessarily any of the pollutant emissions. Fig. 9 shows the difference in the K values required to minimize various pollutant emissions and FC under various cruising speeds with all other operation conditions are identical. One can conclude, from fig. 9, that the stop penalty has a different value for each pollutant criteria at each speed. For example, a K value of 70 seconds will minimize HC at a speed of 45-mph, whereas a much larger K of 225 seconds is needed to minimize NOx at the same speed. While some of the criteria yield to very similar Ks (for like cruising speeds), e.g., FC and CO2, the others are quite different (e.g., HC and NOx). A careful analysis of these values could help us define signal optimization strategies for various areas in the cities based on their sensitivity to particular emission and pollution criteria.

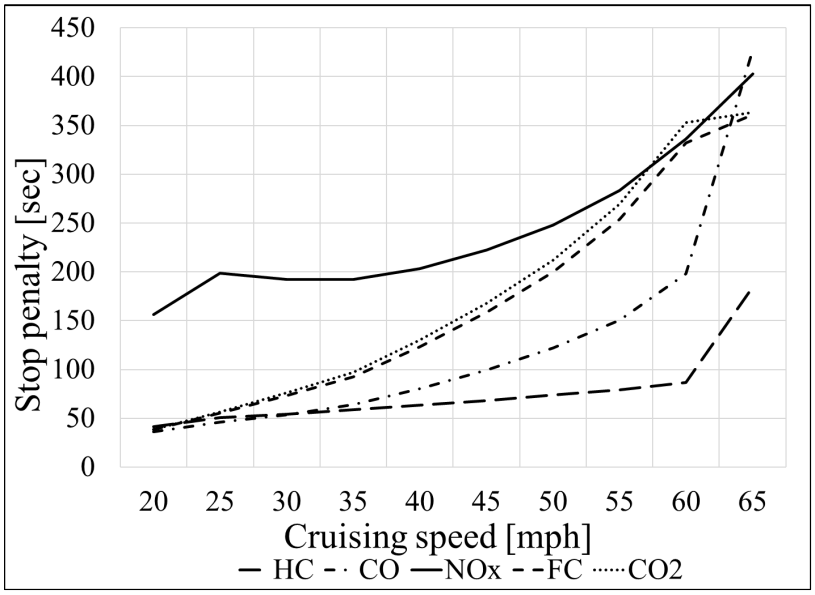

Fig. 9: Impact of a single stop-and-go event of excess emissions

3.4.5 Data Required for Eco-PI Computation

Each of the delays, number of stops, and the stop penalty must be determined in order to compute the Eco-PI. Considering that two most important data types needed for delay and number of stops estimations are volumes (vehicular arrivals) and signals phasing and timing data, they are examined in Table 4. Data are organized per attribute (e.g., type, source, etc.) and their utilization in optimization procedures, offline (pretimed), online (adaptive), and online CV

(adaptive CV). Please note that several data sources might be considered to collect the necessary data in some instances (see Vehicle arrivals downstream in Table 4).
As concluded before, all of the tested operating factors have significant impact on the stop penalty. For that reason, it is crucial to include the impact of all of those operating factors on the stop penalty when computing the Eco-PI. Table 5 presents the data required to include each of the factors with a major impact on the stop penalty. Finally, Table 6 summarizes the cruising speeds and road gradients for individual signalized intersections at M.L. King Blvd. Initial speed and final speed in Table 6 represents the cruising speeds at the start of the deceleration phase and after the end of the acceleration phase, respectively. Also, EB, WB, NB, SB, RT, TH, and LT stand for Eastbound, Westbound, Northbound, Southbound, Right-turn, Through, and Left-turn, respectively.

Table 4 Required data for estimating delay and number of stops

Optimization type \ Data attribute	Type	Source	Spatial coverage	Temporal coverage	Importance
Vehicle arrivals downstream					
Offline - Pretimed	Traffic counts	GridSmart TMCs / Counts	Intersection movement	15-minutes bins / Second-by-second	High
Online - Adaptive	Traffic counts	GridSmart Counts	Intersection movement	Second-by-second	High
Online CV – Adaptive CV	Traffic counts	CV data (BSM)	Exact location of vehicle	Same as Online	Medium
Vehicle arrivals upstream					
Offline - Pretimed	Traffic counts	GridSmart Counts	After upstream intersection	Aggregated based on second-by-second data	Low
Online - Adaptive	Traffic flow rate	GridSmart Counts / Video data	After upstream intersection	Second-by-second / TBD (resolution of video analytics)	High
Online CV – Adaptive CV	Traffic flow rate	CV data (BSM)	Exact location of vehicle	Second-by-second	Medium
Signal phasing and timing data					
Offline - Pretimed	Signal timing elements	Signal timing sheets	Intersection movement	Peak period or hour	High
Online - Adaptive	Signal timing elements	GridSmart Events	Intersection movement	Second-by-second	High
Online CV – Adaptive CV	Signal timing elements	Same as Online	Same as Online	Same as Online	Medium

Table 5 Required data for each of the factors impacting the stop penalty

Optimization type \ Data attribute	Type	Source	Spatial coverage	Temporal coverage	Importance
Fleet composition and Vehicle type					
Offline - Pretimed	Vehicle shape	GridSmart Counts	Intersection movement	Second-by-second	Medium
Online - Adaptive	Vehicle shape	Video data / GridSmart Counts	Intersection movement	TBD (resolution of video analytics) / Second-by-second	High
Online CV – Adaptive CV	Exact vehicle model	CV data (Embed in BSM)	Exact location of vehicle	Second-by-second	High
Driving behavior					
Offline - Pretimed	Trajectory data	Probe GPS / Video data	Before & After StopLine/ TBD (camera view)	Second-by-second / TBD (resolution of video analytics)	High
Online - Adaptive	Trajectory data	Video data	TBD (camera view)	TBD (resolution of video analytics)	Medium
Online CV – Adaptive CV	Trajectory data	CV data (BSM), individual CV	Same as Online and for multiple intersections	Second-by-second	High
Road gradient					
Offline - Pretimed	Grade of the terrain	Maps with altitude	Intersection approach	NA	High
Online - Adaptive	Grade of the terrain	Same as Offline	Same as Offline	Same as Offline	Low
Online CV – Adaptive CV	Grade of the terrain	Same as Offline + BSM	Exact location of vehicle	Second-by-second	Medium
Cruising speed					
Offline - Pretimed	Speed limit	Google maps	Intersection approach	NA	High
Online - Adaptive	Speed distribution	Video data /GridSmart Realtime	TBD (camera view) / Intersection movement	TBD (temporal resolution of video analytics) / Second-by-second	Medium
Online CV – Adaptive CV	Speed distribution	CV data (BSM)	Exact location of vehicle	Second-by-second	Medium
Wind effect					
Offline - Pretimed	Wind speed & direction	Dark Sky	TBD	TBD	Low
Online - Adaptive	Wind speed & direction	Dark Sky (API)	TBD	TBD	Medium
Online CV – Adaptive CV	Wind speed & direction	Dark Sky (API)	Same as Online	Same as Online	Medium

Table 6 Cruising speeds and road gradients on intersections of the area of study

Intersection	Parameter/movement	EB RT	EB TH	EB LT	WB RT	WB TH	WB LT	NB RT	NB TH	NB LT	SB RT	SB TH	SB LT
Carter St	Initial speed (mph)	30	30	30	25	25	25	30	30	30	30	30	30
	Final speed(mph)	30	30	30	25	25	25	30	30	25	25	30	30
	Deceleration slope (%)	-0.8	-0.8	-0.8	-0.1	-0.1	-0.1	0.1	0.1	0.1	-0.4	-0.4	-0.4
	Acceleration slope (%)	0.2	-0.2	0.4	0.3	0.3	0.1	0.4	0.2	0.1	0.3	-0.1	0.0
Broad St	Initial speed (mph)	30	30	30	25	25	25	30	30	30	20	20	20
	Final speed(mph)	20	25	30	30	30	25	30	20	25	25	30	30
	Deceleration slope (%)	0.2	0.2	0.2	-1.6	-1.6	-1.6	-0.2	-0.2	-0.2	0.0	0.0	0.0
	Acceleration slope (%)	0.5	1.1	0.8	0.3	-0.1	0.0	0.9	0.3	0.0	-0.3	0.0	1.1
Market St	Initial speed (mph)	25	25	25	25	25	25	30	30	30	30	30	30
	Final speed(mph)	30	25	30	30	25	30	25	30	25	25	30	25
	Deceleration slope (%)	1.5	1.5	1.5	-1.9	-1.9	-1.9	-0.5	-0.5	-0.5	1.5	1.5	1.5
	Acceleration slope (%)	1.0	2.0	-1.1	-1.9	-1.7	0.3	1.9	-1.7	-1.3	-0.9	1.1	2.2
Georgia St	Initial speed (mph)	25	25	25	25	25	25	30	30	30	30	30	30
	Final speed(mph)	30	25	30	30	25	30	25	30	25	30	25	30
	Deceleration slope (%)	1.9	1.9	1.9	-1.0	-1.0	-1.0	-0.9	-0.9	-0.9	-1.1	-1.1	-1.1
	Acceleration slope (%)	0.7	1.4	1.3	0.3	-1.9	-0.1	1.3	0.6	-1.7	-2.3	0.0	0.8
Lindsay St	Initial speed (mph)	25	25	25	25	25	25	30	30	30	30	30	30
	Final speed(mph)	30	25	30	30	25	30	25	30	25	30	25	30
	Deceleration slope (%)	1.3	1.3	1.3	1.7	1.7	1.7	-1.7	-1.7	-1.7	-3.7	-3.7	-3.7
	Acceleration slope (%)	1.3	-1.1	1.9	2.2	-1.0	1.1	-1.2	1.8	-0.8	-1.3	0.7	-1.5
Houston St	Initial speed (mph)	25	25	25	25	25	25	30	30	30	30	30	30
	Final speed(mph)	30	25	30	30	25	30	25	30	25	30	25	30
	Deceleration slope (%)	-1.6	-1.6	-1.6	2.3	2.3	2.3	-1.1	-1.1	-1.1	-4.3	-4.3	-4.3
	Acceleration slope (%)	0.8	-1.5	1.7	4.4	0.9	0.3	-1.4	5.0	1.2	0.8	-0.4	-1.8
Douglas St	Initial speed (mph)	25	25	25	25	25	25	30	30	30	30	30	30
	Final speed(mph)	30	25	30	30	25	30	25	30	25	30	25	30
	Deceleration slope (%)	-0.5	-0.5	-0.5	-1.0	-1.0	-1.0	0.4	0.4	0.4	-2.3	-2.3	-2.3
	Acceleration slope (%)	-0.3	1.1	1.9	2.2	0.3	-0.5	1.1	1.8	0.7	-0.2	-0.9	0.2
Peeples St	Initial speed (mph)	25	25	-	-	25	25	30	-	30	-	-	-
	Final speed(mph)	30	25	-	-	25	30	25	-	25	-	-	-
	Deceleration slope (%)	0.3	0.3	-	-	-1.5	-1.5	3.3	-	3.3	-	-	-
	Acceleration slope (%)	-2.3	1.4	-	-	0.5	-1.9	1.3	-	0.9	-	-	-
Magnolia St	Initial speed (mph)	25	25	25	25	25	25	30	30	30	30	30	30
	Final speed(mph)	30	25	30	30	25	30	25	30	25	30	25	30
	Deceleration slope (%)	3.3	3.3	3.3	-4.3	-4.3	-4.3	3.2	3.2	3.2	-1.8	-1.8	-1.8
	Acceleration slope (%)	-1.8	3.7	2.2	1.1	-3.2	-2.6	3.6	1.4	-2.0	-3.1	-1.6	2.4
Central St	Initial speed (mph)	35	35	35	35	35	35	30	30	30	30	30	30
	Final speed(mph)	30	35	30	30	35	30	35	30	35	30	35	30
	Deceleration slope (%)	-5.4	-5.4	-5.4	5.8	5.8	5.8	-1.7	-1.7	-1.7	-0.4	-0.4	-0.4
	Acceleration slope (%)	1.2	-5.5	-1.5	1.5	5.1	5.1	-5.7	-1.4	2.6	4.4	1.1	-3.3

3.6 Evaluation of Analytical Models for Eco-PI estimation

Analytical models for *EcoPI* estimation were introduced in the proposed framework for the development of constraints for local optimization mainly to relate available traffic data (e.g., volumes, arrivals on green) and signal timing parameters (e.g., green times, cycle length) with *EcoPI* value. As defined earlier, the main performance measures for *EcoPI* estimation are delay (d_{m_i}), number of stops (N_{m_i}), and stop penalty (K_{m_i}), which need to be estimated per movement (m) of each intersection (i). Thus, we define the *EcoPI* as:

$$EcoPI_{total}^{i} = \sum_{m=1}^{8} d_{m_i} + K_{m_i} * N_{m_i} \qquad (7)$$

$$d_{m_i} = \frac{0.38 * CL^i\left(1 - g_{m_i}/CL^i\right)^2}{1 - y_{m_i}} * PF_{m_i} \qquad (8)$$

$$PF_{m_i} = \frac{1 - POG_{m_i}}{1 - g_{m_i}/CL^i} * \frac{1 - y_{m_i}}{1 - y_{m_i} * \left(\frac{CL^i}{g_{m_i}}\right) * POG_{m_i}} * \left[1 + y_{m_i} * \frac{1 - POG_{m_i} * CL^i/g_{m_i}}{1 - g_{m_i}/CL^i}\right] \qquad (9)$$

$$N_{m_i} = 0.9 \times \frac{1 - g_{m_i}/CL^i}{1 - y_{m_i}} \qquad (10)$$

where:

$EcoPI_{total}^{i}$= Eco performance index of intersection i,

m= movement number of the intersection (for standard four-legged intersection m_{max} = 8),

i= intersection number,

d_{m_i}= stopped delay at movement m of intersection i (*sec/veh*),

PF_{m_i}= progression adjustment factor at movement m of intersection i,

K_{m_i}= stop penalty of movement m of intersection i,

N_{m_i}= number of stops at movement m of intersection i,

CL^i = cycle length at intersection i (*sec*),

g_{m_i}= green time for movement m of intersection i (*sec*),

y_{m_i}= ratio of volume and saturation flow rate at movement m of intersection i,

POG_{m_i}= percentage of arrivals on green at movement m of intersection i.

An important traffic characteristic that needs to be included in the analytical models for *EcoPI* is the percentage of vehicles arriving on green *POG*. The *POG* accounts for vehicular arrival patterns, which is a traffic flow characteristic that (in addition to traffic volume) impacts the *EcoPI*. Thus, if analytical models do not account for *POG* appropriately, such *EcoPI* estimates may be inaccurate and unreliable. We recently noticed that the previously proposed analytical model for estimating number of stops (eq. 7) is not very accurate when estimating performance of coordinated movements. We reviewed several other models from the literature and decided to update the analytical formulation of *EcoPI*, to improve estimation of the number of stops. We decided to use the model proposed by Bonneson (2008) because it is capable of accounting for arrival patterns while estimating the number of stops (*14*). The formulation of the subject model is as follows:

$$IF\ d_{a_{m_i}} \leq \left(1 - POG_{m_i}\right) g_{m_i} X_{m_i} \rightarrow\ N_{m_i} = \frac{1 - POG_{m_i}\left(1 + \frac{d_{a_{m_i}}}{g_{m_i}}\right)}{1 - POG_{m_i} X_{m_i}} \qquad (23)$$

$$IF\ d_{a_{m_i}} > \left(1 - POG_{m_i}\right) g_{m_i} X_{m_i} \rightarrow\ N_{m_i} = \frac{\left(1 - POG_{m_i}\right)\left(r_{m_i} - d_{a_{m_i}}\right)}{r_{m_i} - \left(1 - POG_{m_i}\right) g_{m_i} X_{m_i}} \qquad (24)$$

$$d_{a_{m_i}} = 0.5\left(1.47 S_{R_{m_i}}\right)\left(\frac{1}{r_{a_{m_i}}} + \frac{1}{r_{d_{m_i}}}\right) \qquad (25)$$

where:

r_{m_i}= effective red duration ($CL^i - g_{m_i}$) for movement *m* of intersection i (*sec*),

q_{m_i}= volume during cycle for movement *m* of intersection i (*veh*),

X_{m_i}= volume-to-capacity ratio ($= q_{m_i} \frac{CL^i}{s_{m_i} g_{m_i}}$) for movement *m* of intersection i,

s_{m_i}= saturation flow rate for movement *m* of intersection i (*veh/h* or *veh/s*),

$d_{a_{m_i}}$= deceleration-acceleration delay for movement *m* of intersection i (*sec*),

$r_{a_{m_i}}, r_{d_{m_i}}$= acceleration, deceleration rate for movement *m* of intersection i (ft/s^2),

$S_{R_{m_i}}$ = running speed for movement *m* of intersection i (*mph*).

For this reason, our revised formulation of *EcoPI* (Eq. 7) now consists of equations 1-2 and equations 4-6.

We evaluated *EcoPI* estimates (from analytical models) against ground truth from the microsimulation model (which represents virtual reality). We arbitrarily selected intersection in the downtown area of the examined network (i.e., Martin Luther Blvd and Market Street), and

estimated *EcoPI*s on a cycle-by-cycle basis for specific protected movements (e.g. through flows) or permitted (or protected/permitted) traffic movements (e.g., left-turn flows). It needs to be stated that estimation of *EcoPI*s for protected/permissive movements relies on similar models for delays and number of stops as shown previously. However, slight modifications of analytical models exist due to the specifics of traffic operations in protected/permissive phases and can be found elsewhere (*2*). Obtained results are presented in Figure 10. In general, estimations of *EcoPIs* for the high-traffic through movements (observe part *a)* and *b)* of Figure 10) are reliable and they have resulted in high correlations with the ground truth values (obtained from simulation). However, when one observes analytical estimates for protected/permissive left-turn movements (see part *c)* and *d)* of Figure 10), it is found that the two data sets are not equally well correlated.

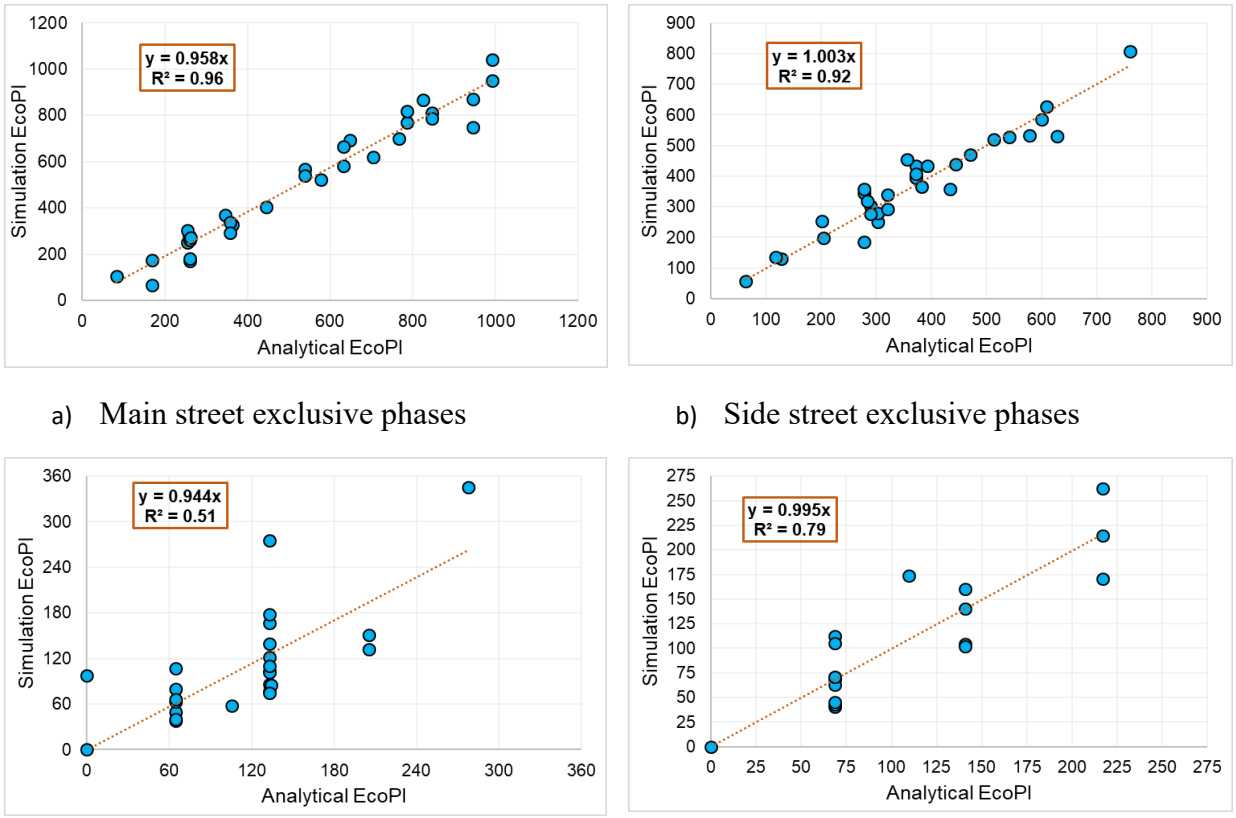

a) Main street exclusive phases

b) Side street exclusive phases

c) Main street in protected/permitted phases

d) Side street protected/permitted phases

Fig. 10: Comparison between analytically derived and ground truth EcoPI

Overall, we find that the *EcoPIs* estimated by using one of the proposed analytical models are acceptable for three reasons: 1. Major movements of the network are those served with exclusive phases (e.g., through coordinated movements) and for those movements, the *EcoPI*s estimates are reliable; 2. Although the accuracy of analytical models for estimation of *EcoPI*s for protected/permitted movements is lower, a general trend between two datasets still exists; 3. Amount of traffic for protected/permitted phases contributes much less (in the overall intersection

EcoPI) than those of the protected. In the later stages of research, analytical models will be calibrated based on real-world data to further improve their accuracy. For current research efforts, we recommend using the existing analytical models.

4.2.1 Evaluation of Framework for Development of Constraints for Local/Global Optimization

Development of constraints for local/global optimization starts by determining the minimum cycle length (CL^i_{min}) that ensures enough green time to service previously stopped vehicles, i.e., vehicles that arrived on red (AoR). Previously proposed formula for CL^i_{min} (Equation 11) was evaluated, and some inconsistencies were found.

$$CL^i_{min} = \frac{L}{1 - \frac{\sum AoR_{m_{i_{critical}}}}{0.5 \times CL^i_{previous}}} \qquad (11)$$

Therefore, we replaced Equation 11 with Equation 12 as the new one better ensures that queued vehicles are always served with a given CL^i_{min}.

$$CL^i_{min} = L_i + \left(AoR_{\phi 1} + AoR_{\phi 2} + AoR_{\phi 3} + AoR_{\phi 4}\right) * h_{sat} \qquad (12)$$

where:

CL^i_{min}= minimum cycle length (*s*),

L_i= total lost time per cycle per intersection (*i*) (*s*):

$$L_i = \sum_{m'} L_{\phi_{m'}} \qquad (13)$$

$$L_{\phi_{m'}} = \left(l_{1_{m'}} + y_{m'} + ar_{m'} - e_{m'}\right) \qquad (14)$$

where:

$L_{\phi_{m'}}$= lost time per phase ϕ that serves specific movement group (m') (*s*),

$l_{1_{m'}}$= start-up lost time (usually, $l_{1_{m'}} = 2s$) (*s*),

$y_{m'}$= yellow (*s*),

$ar_{m'}$= all red (*s*),

$e_{m'}$= used time during yellow and all-red (usually, $e_{m'} = 2s$) (*s*),

h_{sat}= saturation headway (*s*),

$AoR_{\phi_{m'}}$= maximum arrivals on red for phase ϕ that controls movement group m'(vehicles per lane):

$$AoR_{\phi_{m'}} = \left\{AoR_{\phi 1_{m'}}, \ldots, AoR_{\phi 4_{m'}}\right\} \qquad (15)$$

where:

$AoR_{\phi 1-4_{m'}}$= arrivals on red for each movement m in movement group m' associated with phase ϕ (vehicles per lane).

Based on the Equation 16, the minimum green time required to accommodate vehicles of a particular movement group are calculated as:

$$g_{min_{\phi_{m'}}} = L_{\phi_{m'}} + AoR_{\phi_{m'}} * h_{sat} \qquad (16)$$

It needs to be stated here that in the cases when calculated $g_{min_{\phi_{m'}}}$ is lower than recommended (currently deployed) minimum green time in the signal controller, the value from signal controller should be adopted for safety purposes.

To calculate upcoming cycle length and corresponding green times for each intersection in the network, we use Equations 17 and 18. Further, we select maximum of minimum cycle lengths for each intersection to determine the minimum cycle length for the entire group (or network) (CL_{min}^{group}).

$$CL_{min}^{group} = \left(CL_{min}^{i}\right) \qquad (17)$$

For each intersection where a group CL_{min}^{group} is supposed to be operational, we evaluate 60 cycle lengths with incremental increase of CL_{min}^{group} for Δ (where Δ = [1, … ,60]) to find most appropriate (from the perspective of *EcoPI*) minimum cycle length for the entire group/network ($CL_{min_{EcoPI}}^{group}$). Although a wide range of cycles was evaluated, the implementation of appropriate cycle time for the upcoming cycle will depend on the value of the cycle time in the previous cycle.

Calculated $CL_{min_{EcoPI}}^{group}$ is supposed to allow proper coordination of all intersections within the same group, and represents a minimum *CL* for local/global optimization procedures. While increasing $CL_{min_{EcoPI}}^{group}$, the difference between the minimum $CL_{min_{EcoPI}}^{group}$ and increased $CL_{min_{EcoPI}}^{group} + \Delta$ is used to distribute extra green times according to a number of vehicles arriving on red, stop penalty factor (*K*) and total volumes during cycle as shown in Equation 18:

$$g_{extension1-4} = \left((CL_{min_{EcoPI}}^{group} + \Delta) - CL_{min_{EcoPI}}^{group}\right) \times \frac{AoR_{m_i} * K_{m_i} * q_{m_i} \; for \; \phi_{1-4}}{\sum AoR_{m_i} * K_{m_i} * q_{m_i}} \qquad (18)$$

Such green times ($g_{extension1-4}$) are added to minimum green times previously computed by using the Equation 16. Finally, to determine network cycle length that will be used as $CL_{min_{EcoPI}^{*}}^{group}$ for local/global optimization purposes, we calculate *EcoPI* for each $CL_{min_{EcoPI}}^{group} + \Delta$ and each

intersection in the network on the cyclical level. Since traffic distribution at each intersection can be quite distinctive, and therefore *EcoPIs* can be different too, we define $CL^{group}_{min^{*}_{EcoPI}}$ as a *CL* that results in the lowest total *EcoPI* for multiple intersections.

Figure 8 illustrates how *EcoPI* change with each $CL^{group}_{min_{EcoPI}} + \Delta$, when two intersections are observed. We restrict our focus on two characteristic intersections in the network to illustrate how values of *EcoPI* change for $CL^{group}_{min_{EcoPI}} + \Delta$ at one non-critical and one critical intersection, which are intersections of Martin Luther King Blvd and Broad Street and Martin Luther King Blvd. and Market Street, labeled as intersections 2 and 3 in Figure 8, respectively. Intersection 2 is non-critical, its volumes are relatively low and thus the optimum conditions (on a local level) might exist for values of cycle length lower than $CL^{group}_{min_{EcoPI}}$. However, Intersection 3, which represents a critical intersection, has a CL^{i}_{min}, which is, in most cycles, selected as a $CL^{group}_{min_{EcoPI}}$. Thus, any increase in $CL^{group}_{min_{EcoPI}}$ by Δ, will improve *EcoPI* at intersection 3, up to a certain point (see gray lines in fig. 11). Therefore, by increasing *CL*, intersection 2 usually does not benefit in terms of *EcoPI* (observe orange lines in fig. 11). Such a trend can be explained by the fact that higher cycle lengths tend to increase delay, which is one component of the *EcoPI*). Finally, when *EcoPI*s of both intersections are added together, one can observe that the resulting $CL^{group}_{min^{*}_{EcoPI}}$ is a compromise solution between best-performing cycle lengths from both intersections (see part *a)* of fig. 11). In this way, $CL^{group}_{min^{*}_{EcoPI}}$ is determined as an input for other optimization procedures. Green times associated with the $CL^{group}_{min^{*}_{EcoPI}}$ are already allocated, within each intersection, as discussed previously.

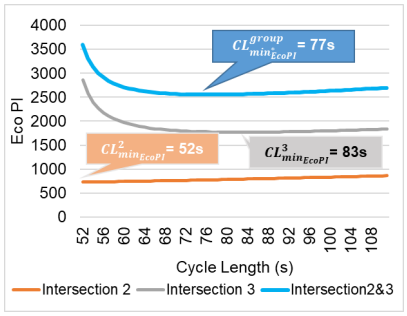

a) Cycle 1

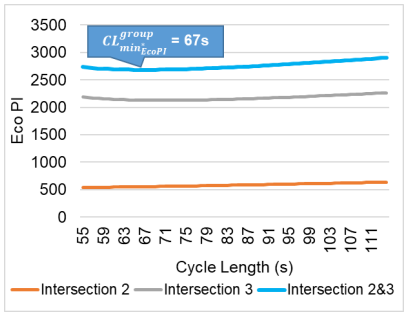

b) Cycle 2

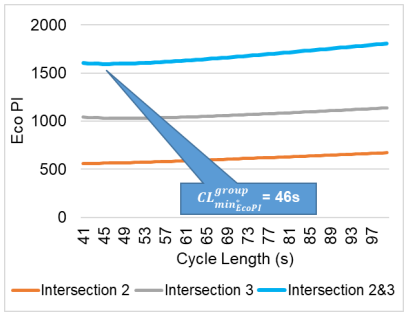

c) Cycle 3

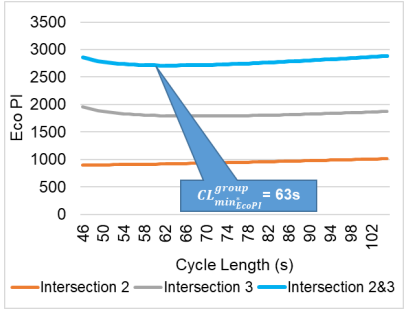

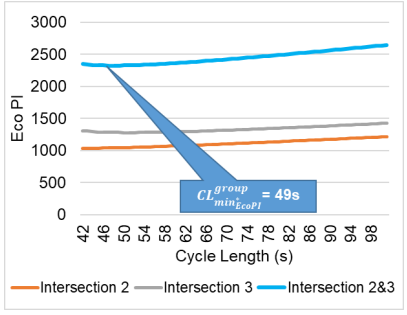

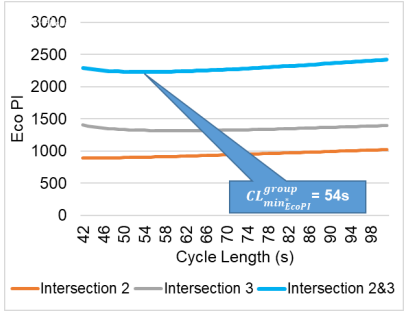

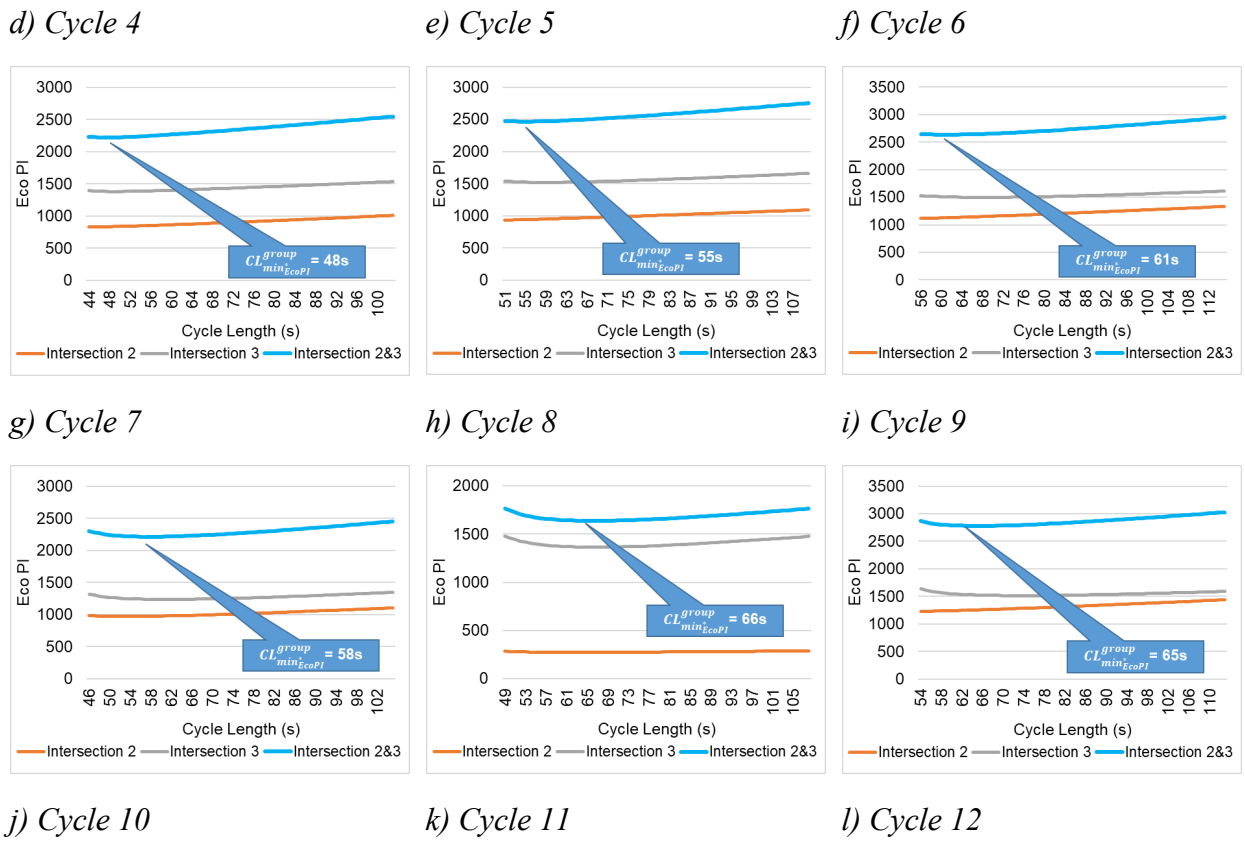

Fig. 11: Impact of non-critical and critical intersection CLs on minimum group CLs

3.7 Local Optimization

Adaptive traffic control systems (ATCSs) have been in use since 1970s but have only received significant attention in the U.S. within the last ten years. In that period, the number of deployed systems increased by 600% (*13*). The two main factors contributing to such trends are the emergence of ATCSs brands customized for the U.S. market and the promotion of these systems' benefits within the research and traffic signal community (*14*). In essence, ATCSs adjust signal timings to accommodate spatial and temporal changes in traffic flow in a real-time manner. So far, there are more than 20 commercially available ATCSs brands around the world. Each system is slightly different in its internal logic that governs the decision-making process of these real-time traffic signal controllers. Traffic signal performance measures (TSPMs) represent feedback between ATCSs operations (or provided capacity) and vehicular arrival patterns (demand). The operational objective of ATCSs (e.g., smooth traffic flow, balanced capacity, etc.) highly depends on the performance measures (e.g., delay, queue profiles, degree of saturation, etc.) that are used by the algorithm to develop new signal timing elements. So far, ATCSs were developed with an explicit focus on mobility-related performance measures (*15-19*). A limited number of

studies focused on the development of signal timing parameters that will consider the impact on the environment in the offline signal retiming procedures (*20-21*). Few attempts were made to develop online (real-time) ATCSs that are ecologically aware (*22*). However, such systems were tested in a simulation environment at a single intersection level without considering realistic constraints imposed by real-world networks (i.e., coordination of multiple intersections, various road users, etc.). Thus, ecologically-aware ATCSs were not developed for field implementation purposes so far. Also, part of the problem lies in the fact that analytical fuel consumption and emissions performance measurements were lacking (until recently (*23*)). Objective of this project task is to develop an ecological Adaptive Traffic Control System (Eco-ATCS) based on the Eco-Performance Index (Eco-PI) that will be ready for field deployments.

The first stage of developing, validating, and fine-tuning Eco-ATCS will be carried out in a high-fidelity micro-simulation tool Vissim (*24*). The simulation approach consists of three main components: 1) A reliable (properly calibrated and validated) microsimulation model of the real-world network (MLK Boulevard in Chattanooga, TN), 2) An adaptive signal control logic that minimizes Eco-PI, and 3) Vissim's Component Object Model (COM) that allows communication between items 1 and 2. Such a simulation approach is a viable tool for testing various adaptive signal control logic strategies and has been used in previous research (*25-27*). The use of a high-fidelity microsimulation environment will allow for the development of solutions that are ready for field deployment.

The typical ATCSs architecture consists of local and global-level signal timing optimizers (*28*). At the local (or intersection) level, ATCSs seek to find a local optimum solution, whereas, on the global (network) level, the system seeks to find a global optimum that coordinates multiple intersections. In other words, local signal timing parameters (e.g., cycle lengths, splits) are initially optimized for each intersection individually. Once a local optimum is found for each intersection, the global optimizer seeks to find values for those signal timing parameters (i.e., offsets, phase sequences) that will result in optimum signal performance (i.e., minimum Eco-PI) on the network level. Within each optimization stage, it is necessary to define optimization constraints (e.g., minimum and maximum allowable units of time to serve particular movements). The following section provides details of the process to determine local control constraints.

3.7.1 Constraints for Local Optimization

The development of constraints for local optimization consists of two modules: 1) initialization and 2) real-time module. Within the initialization, it is imagined that the ATCS does not operate in a fully adaptive mode and, therefore, signal timing parameters that will be deployed in the field should provide enough time to effectively clear the queues at the local intersection level. Another important aspect of the initialization module is that it should provide a good basis for the estimation of cyclical TSPMs before the real-time module is activated. Specifically, if signals were set to operate in a free actuated mode (no cycle length imposed) in the Initialization module, estimation of cyclical TSPMs would not be viable. The transition between initialization and real-time module can occur either based on predefined rules (e.g., traffic volumes reach a certain level) or preset agency requirements (e.g., adaptive regime starts operating at a specific time of the day). The Initialization procedure is outlined in the left part of the chart flow presented in fig. 12.

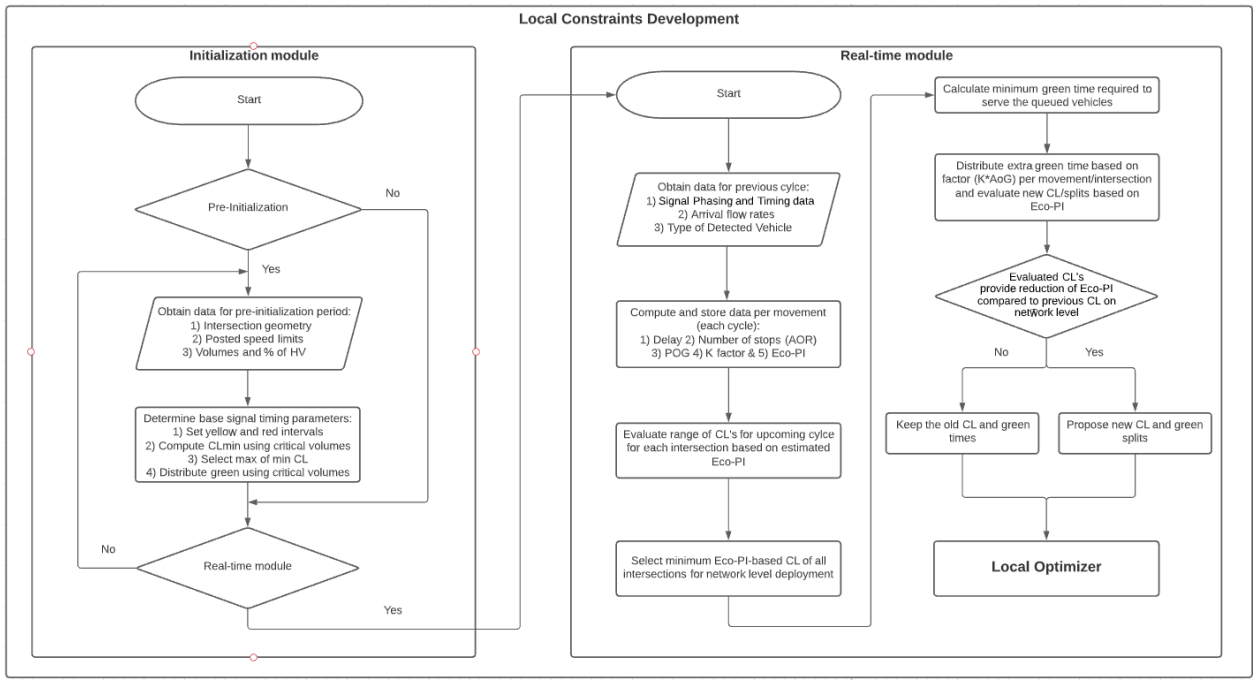

Fig. 12: Framework for Local Constraints Development

Once the Real-time module is initiated, data from the previous cycle from each intersection in the network are collected. These data contain signal phasing and timing data as well as information about arrival flow rates and composition of the traffic flows (as illustrated in the right part of the chart flow in fig. 12). Based on such data (obtained for each intersection

movement), the main performance measures (which are used for derivation of the Eco-PI can be calculated by using the Equations 19-22).

$$EcoPI_{total}^{i} = \sum_{m=1}^{8} d_{m_i} + K_{m_i} * N_{m_i} \qquad (19)$$

$$d_{m_i} = \frac{0.38 * CL^i\left(1 - g_{m_i}/CL^i\right)^2}{1 - y_{m_i}} * PF_{m_i} \qquad (20)$$

$$PF_{m_i} = \frac{1 - POG_{m_i}}{1 - g_{m_i}/CL^i} * \frac{1 - y_{m_i}}{1 - y_{m_i} * \left(\frac{CL^i}{g_{m_i}}\right) * POG_{m_i}} * \left[1 + y_{m_i} * \frac{1 - POG_{m_i} * CL^i/g_{m_i}}{1 - g_{m_i}/CL^i}\right] \qquad (21)$$

$$N_{m_i} = 0.9 \times \frac{1 - g_{m_i}/CL^i}{1 - y_{m_i}} \qquad (22)$$

Where:
$EcoPI_{total}^{i}$= Eco Performance Index of intersection i,
m= Movement number of the intersection (for standard four-legged intersection m_{max} = 8),
i= Intersection Number,
d_{m_i}= Stopped Delay (sec/veh) at movement m of intersection i,
PF_{m_i}= Progression adjustment factor at movement m of intersection i,
K_{m_i}= Stop Penalty value of movement m of intersection i,
N_{m_i}= Number of Stops at movement m of intersection i,
CL^i = Previous cycle length at intersection i (sec),
g_{m_i}= Green time for movement m of intersection i,
y_{m_i}= Ratio of volume and saturation flow rate at movement m of intersection i,
POG_{m_i}= Percentage of Arrivals on Green at movement m of intersection i.
Further, the Real-time module will utilize 20 candidate cycle length values in a range of $CL^i \pm \Delta$, where Δ represents an integer value between 0 and 10, and CL^i value represents the previous local cycle length. For a range of new cycle lengths, the algorithm will evaluate their performance in terms of the Eco-PI. To compute the green time (g_{m_i}), for each incremental change of cycle length, a distribution of green times (based on K_{m_i}) will be used. Cycle length with the lowest $EcoPI_{total}^{i}$ will give the optimal cycle length of the intersection i (i.e., CL_{EcoPI}^{i}).
Since each intersection might have a different CL_{EcoPI}^{i} it is necessary to select the maximum cycle length from those identified for each intersection, as this approach will provide

accommodation of flows on a critical intersection and ensure proper coordination for later phases of the signal optimization process. Such a maximum cycle length will then represent the minimum cycle length constraint for the local optimization, and it is computed by using equation 23. Such group cycle length should not be confused with cycle length that might result from network optimization, it is only an input which ensures that the cycle length values from network optimization satisfy local requirements.

$$CL_{EcoPI}^{group} = \left(CL_{EcoPI}^{i}\right) \quad (23)$$

After the group cycle length is defined, only "critical" intersection (with the highest CL) that drives the group cycle length CL_{EcoPI}^{group}, will have properly allocated green splits. Therefore, it is necessary to recompute green splits for all other "non-critical" intersections. In particular, the difference between proposed CL_{EcoPI}^{group} and minimum cycle length ($CL_{min_q}^{i}$), that is needed to serve the queued vehicles, will be used to distribute green time among the approaches based on numbers of vehicles arriving on green and their stop penalty. Minimum cycle length to serve queued vehicles is computed by using a modified Webster's formula or equation 24-28:

$$CL_{min_q}^{i} = \frac{Total\ Lost\ Time}{1 - \frac{\sum AOR_{m_{i_{critical}}}}{0.5 \times CL^{i}}} \quad (24)$$

Green time allocation per phase will be based on following set of equations 25-28:

$$g_{min_{q1}} = CL_{min_q}^{i} \times \frac{\left(AOR_{1,5}\right)}{\sum AOR_{m_{i_{critical}}}} \quad (25)$$

$$g_{min_{q2}} = CL_{min_q}^{i} \times \frac{\left(AOR_{2,6}\right)}{\sum AOR_{m_{i_{critical}}}} \quad (26)$$

$$g_{min_{q3}} = CL_{min_q}^{i} \times \frac{\left(AOR_{3,7}\right)}{\sum AOR_{m_{i_{critical}}}} \quad (27)$$

$$g_{min_{q4}} = CL_{min_q}^{i} \times \frac{\left(AOR_{4,8}\right)}{\sum AOR_{m_{i_{critical}}}} \quad (28)$$

Once the minimum green times are calculated, we use the remaining cycle time ($CL_{EcoPI}^{group} - CL_{min_q}^{i}$) to allocate additional green time for each phase. Such process will be based on weighted Arrivals on Green (AoG_{m_i}) and movement stop penalty factor K_{m_i} (i.e., $AoG_{m_i} * K_{m_i}$) that will be computed for each movement. This approach will be applied to estimate which movements cost more (in terms of fuel consumption) if vehicles (which could otherwise arrive on green) are stopped. Based on the calculated measure, critical movements will be identified (but instead of

being based on the volumes such critical movements will be assessed from an Eco-impact perspective). For those movements, additional green time (that will be added to the minimum green times necessary to serve the queues) will be calculated by using equation 29.

$$g_{extension1-4} = \left(CL_{EcoPI}^{group} - CL_{min_q}^{i}\right) \times \frac{critical\ movement\ based\ on\ AoG_{m_i} * K_{m_i}\ for\ phase\ 1-4}{\sum critical\ movement\ based\ on\ K(AoG)} \quad (29)$$

Finally, by using equation 30, the total green for each phase will be calculated.

$$g_{total_{1-4}} = g_{min_{q1-4}} + g_{extension1-4} \quad (30)$$

In such a way, minimum ($g_{min_{q1-4}}$) and maximum green ($g_{total_{q1-4}}$) times and minimum Cycle length (CL_{EcoPI}^{group}) are developed.

3.7.2 Output from Local Constraints Development

The Real-time module will output proposed green times for each intersection, and the network-level EcoPI will be estimated to document whether such a change of cycle will lead to a performance improvement. If yes, new cycle length, and corresponding minimum and maximum green times, will be reported as outputs from the local constraint procedure and provided as input for further fine-tuning within the local and network optimizers. Let us suppose that the newly suggested cycle length and belonging splits do not provide performance improvement on the network level. In that case, outputs from the previous cycle will be reported as desirable values for following optimization steps.

Section 4: Simulation and Testing

4.1 DGMARL Testing

The date used to train the DGMARL model was collected 12/15/2022. The DGMARL model was first trained for 100 episodes with a simulation resolution of 1 second. We then tested the model with 10 random seed values during the PM-peak period and observed an average of 29.88% improvement in Eco-PI over a 3-hour period as shown in Fig. 13. However, the Pine and Peeples intersections exhibited negative performance compared to actuated results as shown in Fig. 14.

When we tested the model with a 24-hour simulation, we observed an overall performance improvement of 44.27%.

Node	Avg. Actuated	Avg. Eco_Pi	Avg. Eco_Pi % Improvement
Pine	22681.66	21303.76	6.07%
Carter	53663.61	30104.53	43.90%
Broad	63145.29	39928.84	36.77%
Market	68661.05	42168.49	38.58%
Georgia	43645.22	37380.67	14.35%
Lindsay	20206.95	12376.34	38.75%
Houston	15349.9	10990.3	28.40%
Douglas	17793.43	11099.54	37.62%
Peeples	1203.596	1079.455	10.31%
Magnolia	4765.637	3555.876	25.39%
Central St	79283.93	63774.6	19.56%
Total	**390400.3**	**273762.4**	**29.88%**

Fig. 13: PM-Peak 3-hour Eco0PI; Data: 12/15/2022
Simulation resolution: 1 second; Random seeds: 12, 25, 45, 41, 32, 37, 27, 44, 29, 22

Seed	Node	Actuated	DGMARL	Eco_Pi %
25	Peeples	1140.254	1266.929	-11.11%
45	Pine	23362.24	23609.16	-1.06%
27	Peeples	1094.578	1320.751	-20.66%
29	Pine	22963.07	23901.18	-4.09%

Fig. 14: Pine and Peeples Eco-PI impact

4.1.1 Sharing DGMARL Packages and Output for Integration Testing

We created actuated Eco-PI calculation and DGMARL model packages and shared them with ORNL team for testing. Additionally, we generated 11 “Signal Timing” output files, one for each intersection, and shared them with the Pitt and Georgia Tech team for testing purposes. The format of the signal timing output file is illustrated in Fig. 15, and it contains details such as simulation timing, random seed value used, version of VISSIM network file used, and the date of the test. A detailed description of the signal timing format can be found in Fig. 16.

Fig. 15: Signal Timing Output

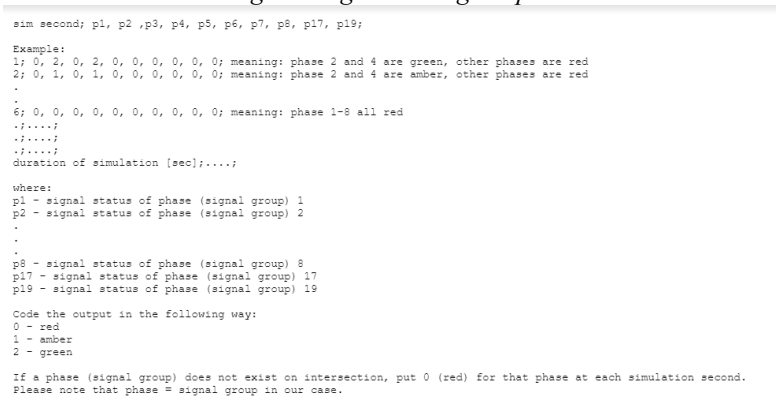

Fig. 16: Signal Timing Output Template

4.1.2 Model Integration Testing

We provided support for integration testing and identified an issue with handling the red phase during signal switching in the DGMARL output of "Signal Timing." While DGMARL was designed to switch signal phases, it did not serve the red phase before switching to green, unlike the VISSIM RBC controller. To address this, we updated DGMARL's signal update function to match VISSIM's yellow and red clearance timings, using a 0.1 second simulation resolution. For example, a 2/4 second red clearance at the Pine intersection was accurately replicated. Additionally, we addressed differences in protected-permissive left signals between the actuated VISSIM file and field configurations.

- Red Phase: changing the simulation resolution significantly impacts the Eco-PI formula, as the stop delay component must align with the new resolution. This modification affects the reward calculation in the reinforcement learning algorithm, requiring the DGMARL model to be retrained. Additionally, incorporating the red phase before switching to green has a notable effect on Eco-PI performance, necessitating further retraining to improve the model's understanding of the environment and its decision-making process.

4.2 Digital Twin: VISSIM Model Verification, Validation, and Calibration

Verification - Verification confirms that the built model operates as intended. This requires stepping through the model in detail to ensure its construction and operation is as expected. Verification of the simulation construction is conducted primarily within Tier 1. Verifications in

Tier 2 and Tier 3 relate to the integration of the dynamic data streams. A detailed checklist of the items considered when verifying a model may be found in *(1)*.

As a data verification example for the MLK model, volume balance checks were conducted for a typical PM Peak period (May 11, 2021) to identify any errors in the detector data received, or the Vissim model network. Identification of any significantly erroneous data points and implementation of the necessary corrections is critical to attaining simulation behavior and output that is an accurate reflection of the field conditions. For the MLK case study, the volume balance verification check involved confirming the equality between the intersection field detector volumes at each approach and the expected volumes as computed from the exit counts of the immediate upstream intersection. For a few intersections, up to a 20% difference in these volumes were observed. The reason for these differences were tracked to mid-block sources and sinks that were not initially included in the model, as well as some detector issues that were subsequently addressed.

Validation and Calibration - Validation seeks to confirm the validity of the model (e.g., how well key field and simulated performance measures agree) while calibration seeks to adjust underlying simulation parameters to achieve a valid model *(1)*. For example, in the MLK case study, one parameter considered for validation and calibration was the headway distributions at exit detectors, determined using archived per vehicle record data. Headway distributions for the field versus simulation were compared, as this parameter significantly influences the number of vehicles that may be processed at an intersection approach. Fig. 17 plots show this comparison at two detectors for two intersections on the MLK Smart Corridor. In these figures, the overlap of histograms (blue and orange) is shown in gray.

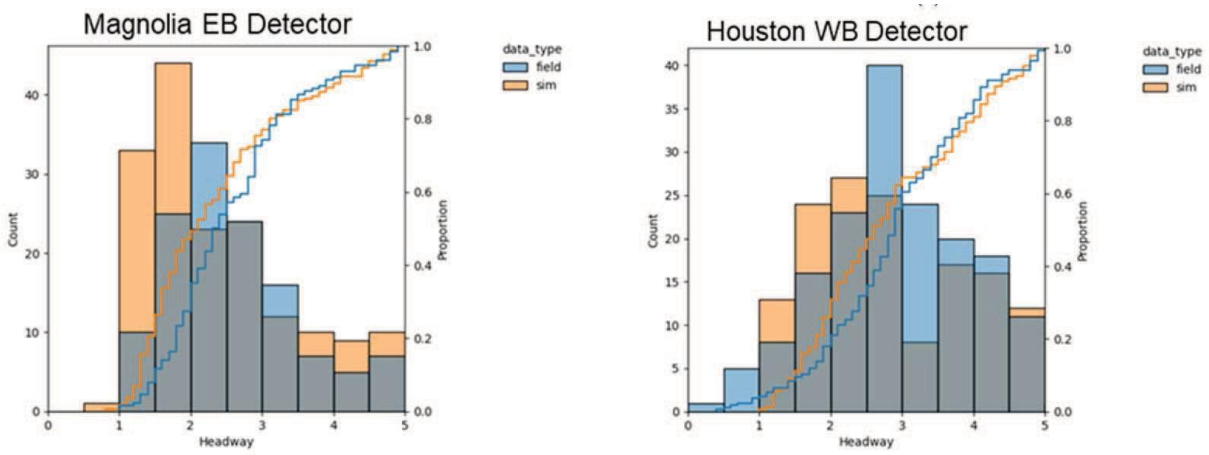

(a) (b)

Fig. 17: Saturation headway distribution comparison - field vs simulation plots at (a) MLK @ Magnolia Eastbound approach detector, and (b) MLK @ Houston Westbound approach detector.

The plots serve as an initial check of the model's departure headway calibration and a demonstration that the model is operational. The field and Vissim generated headway distributions are observed to be similar, but there are some differences in the shape of the

distributions, which indicate the potential for improvements with further calibration of the Vissim saturation headway parameters. Other parameters included in the validation and calibration were related to the vehicle speed distributions and critical route travel times. Additional information on calibration and validation for Vissim simulation may be found in Hunter 2021 (*1*).

4.3 Software-in-the-Loop (SIL) Simulation

The PITTS team connected all 11 intersections on the MLK corridor in Vissim to SEPAC m60 controllers. For each controller, port numbers are assigned, and necessary files are created. First, 11 virtual controllers were connected with default signal timing plans to verify the established connection. Once the connection was established through assigned port numbers. The PITTS team used software called TACTICS to upload field signal timing plans for all 11 intersections from the MLK corridor. In fig. 18, one can see all 11 virtual machines representing field controllers working with the help of the management system of SEPAC TACTICS.

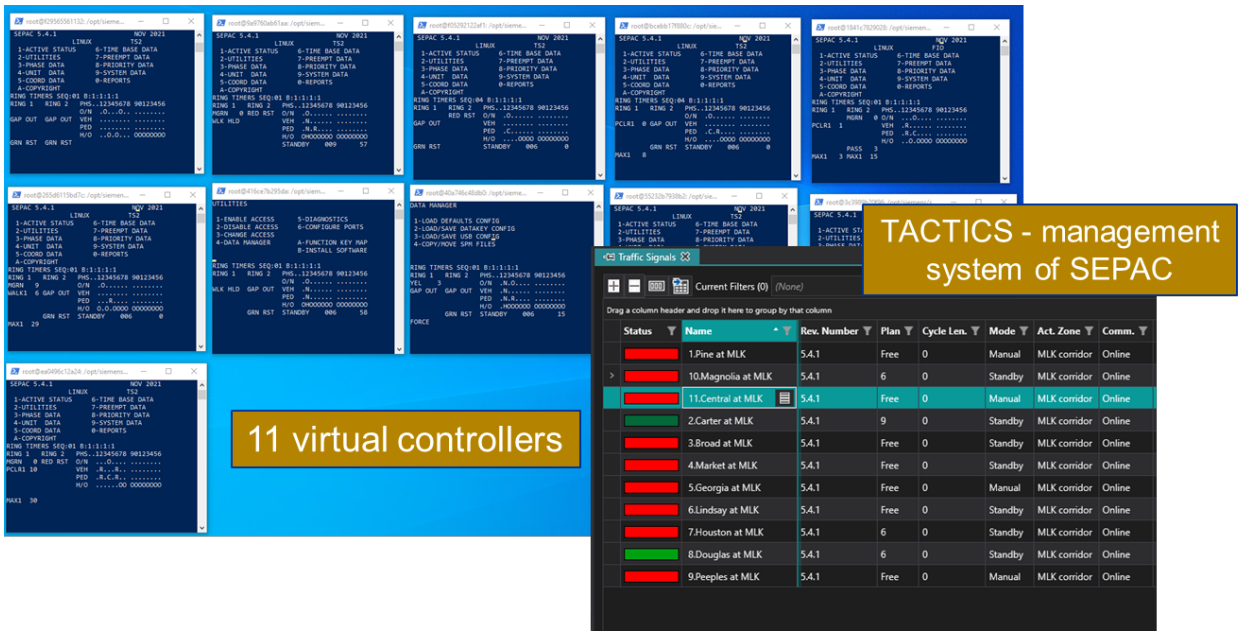

Fig. 18: View of Siemens SEPAC SILS

In fig. 19 it can be observed that the signal status is the same in both platforms meaning that the communication is established properly. In addition, the EB approach has two vehicles placing a call and that vehicle call can also be observed in TACTICS.

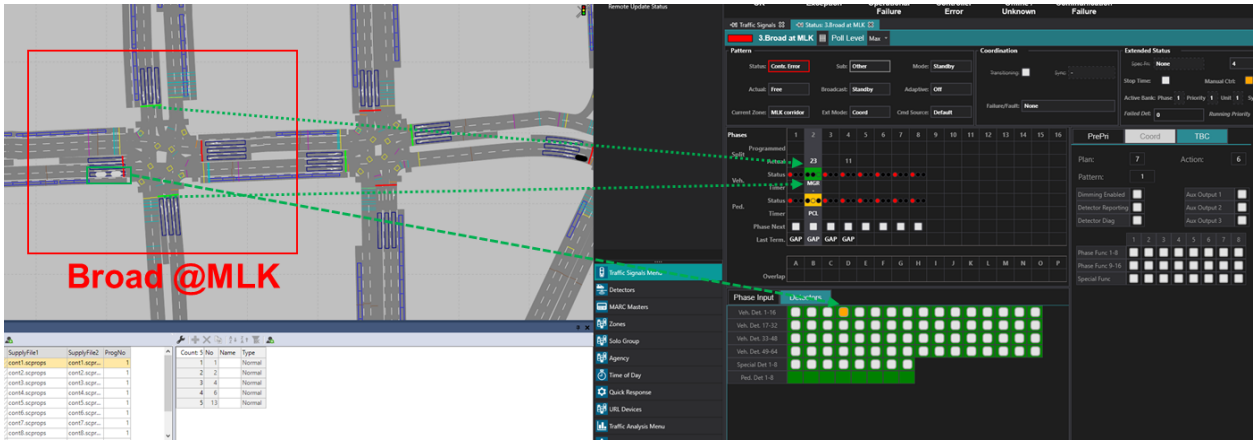

Fig. 19: Field signal timing plans operating in SILS environment at Broad @MLK

To test different implementation methods using the developed ATCS module, the authors used an 11-intersection corridor along MLK Blvd, in Chattanooga, Tennessee (fig. 20). The software used for this study, Vissim, was chosen because it is a widely used tool to model various traffic operations. Vissim simulation model of this network has been properly calibrated, validated, and used in some of the previous studies.

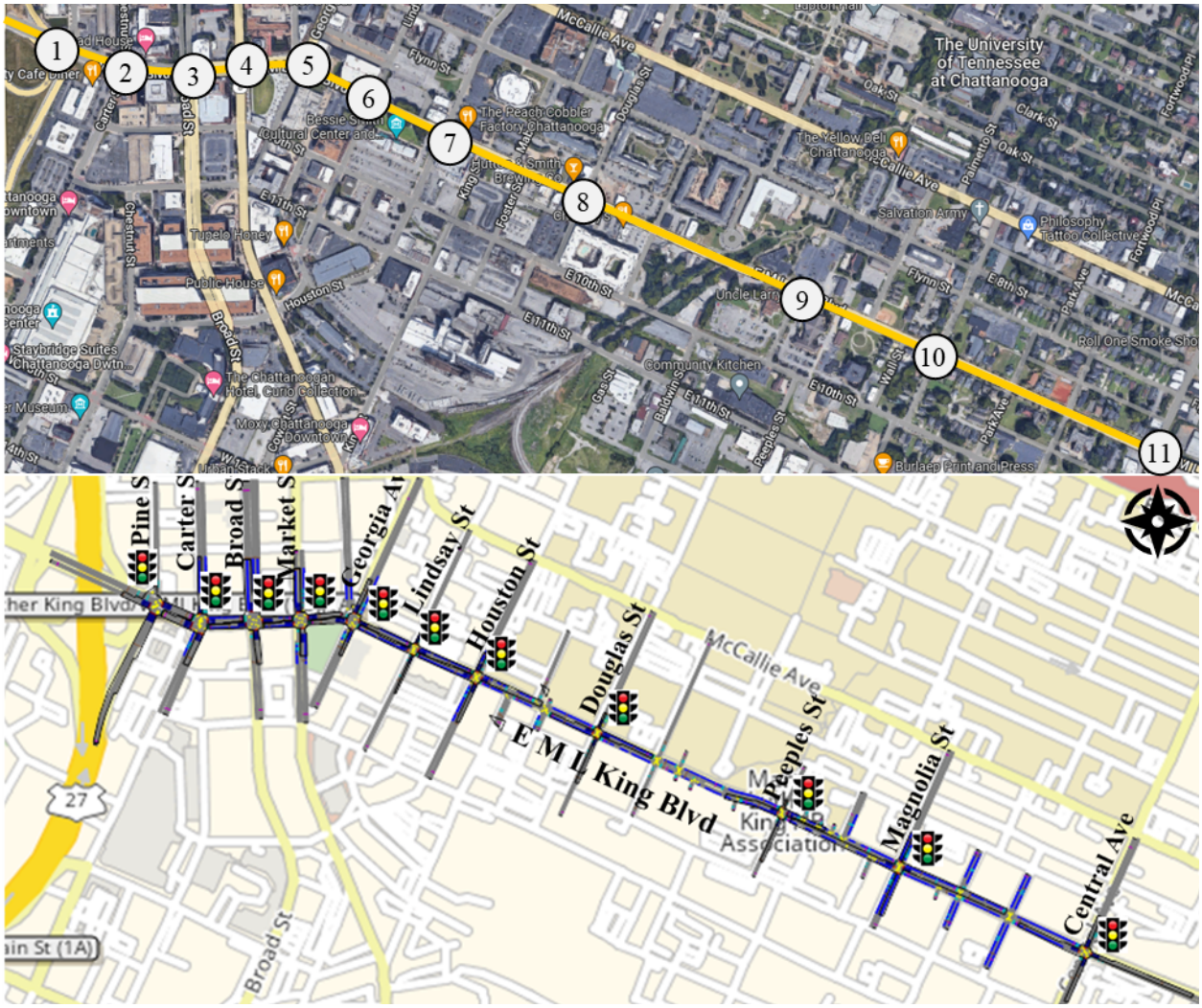

Fig. 20: Test-bed network

Intersections in the corridor of interest are equipped with Siemens m60 controllers. Each controller has SEPAC 5.40 software and as such is created as a virtual machine and connected to Vissim. At each update interval, the ATCS module collects data from Vissim through the COM interface and calculates new signal timing parameters as explained in one of the previous subsections. Then, the NTCIP software, which acts as a translator between Vissim and SEPAC, creates the necessary messages to modify the dynamic objects, such as current pattern, cycle length, offset, splits, of the SEPAC software (Fig. 21). Note that NTCIP software maintains constant connection between SEPAC and Vissim even when no signal timing modifications are needed.

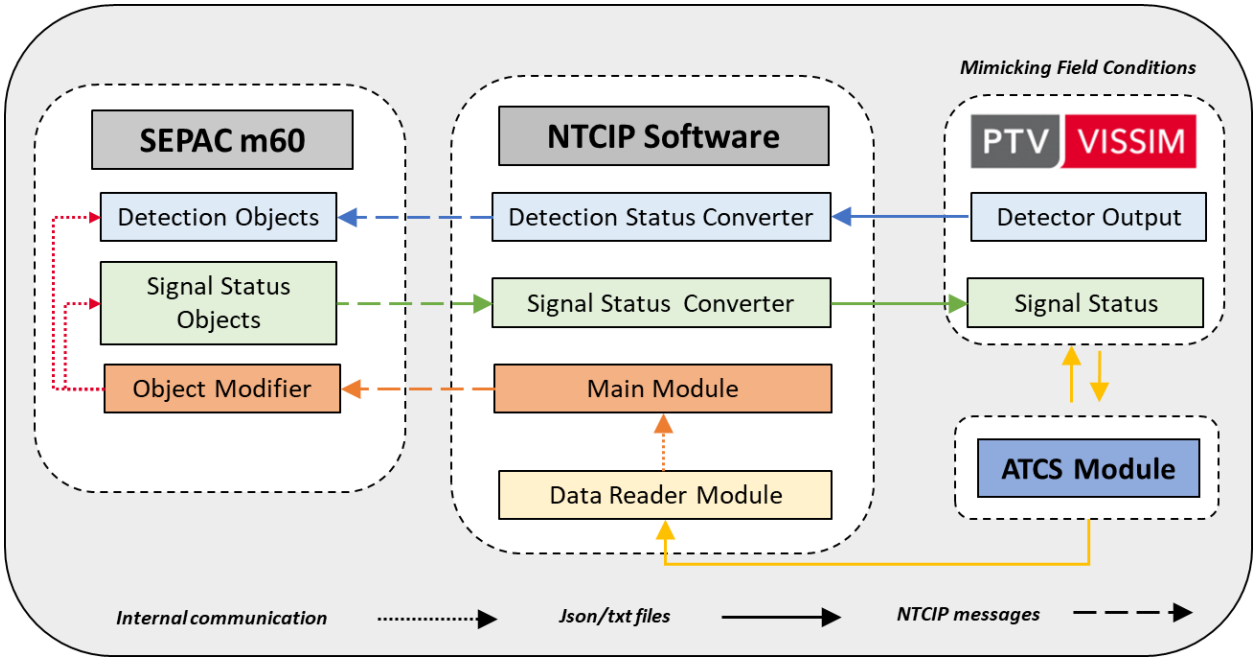

Fig. 21: Architecture of SILS

4.3.1 Experimental Design

To assess different methods for implementing ATCS in the field, numerous scenarios can be created. However, the authors focused on three major criteria, as illustrated in Figure 22. Firstly, vehicular demand varied between low, medium, and high levels. Each vehicular demand was modeled to maintain the average volume-to-capacity ratio (v/c ratio) within specific bounds, as indicated in Figure 22. The purpose of such a modeling approach was to avoid oversaturated conditions, which could hinder the benefits of any adaptive traffic control logic. Secondly, the different update intervals were tested. Both PM and DC methods were tested for all update intervals. However, it was not feasible to implement the PC method on a cycle-by-cycle basis, and thus, it was not tested with such an update rate; instead, the pattern was changed every 5 or 10 min. Thirdly, the PC method was coupled with three transition logics (Dwell, Shortway2, Shortway+) as described previously.

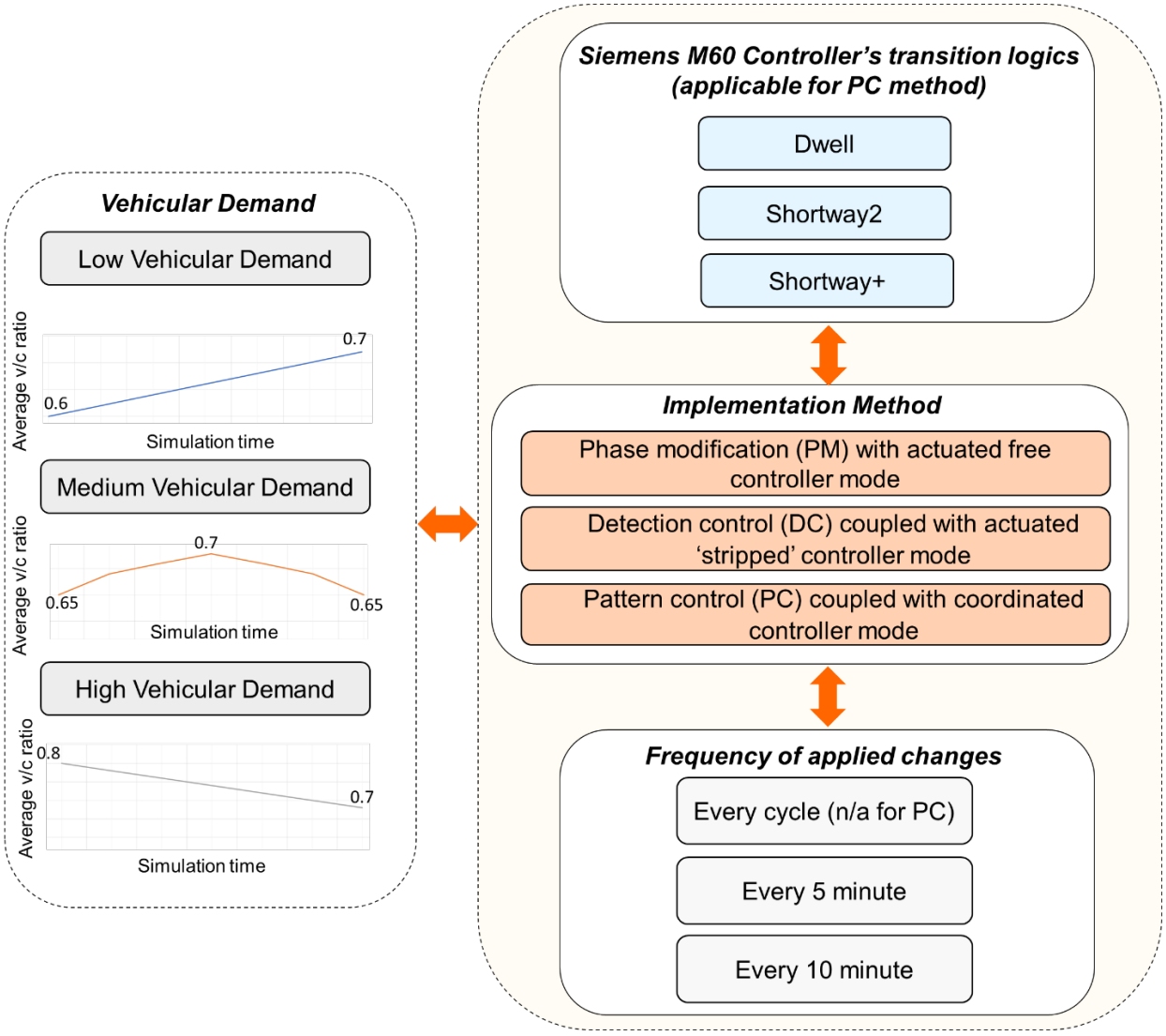

Fig. 22: Experimental design

In total, 36 VISSIM simulation models were prepared and tested, with 9 models (3 demand levels x 3 update intervals) for each of the PM and DC methods (18 in total), and 18 models for the PC method (3 demand levels x 2 update intervals x 3 transition logics). The analysis for each scenario used 1h of data collected after a 20-minute warm-up period for each scenario.

4.3.2 Total Network Delay and Total Number of Stops

Fig. 23 shows comparison of various methods and update intervals for the entire network. The results indicate that frequent signal timing changes, such as cycle-by-cycle updates, lead to a significant increase in total delay across all of the analyzed traffic demands.

For low-demand scenarios, total delay remains relatively similar across all implementation methods except for PC-Shortway+-5min and DC-10-min methods. When considering medium demand, the PM-10-min performs the best. Among the PC methods, Shortway+-10min outperforms the others for medium demand. It is important to note that, in all scenarios, the PM-10 min method consistently performs the best.

As for PC methods, PC-Dwell-10min slightly outperforms Shortway+-10min for both low and high-demand scenarios.

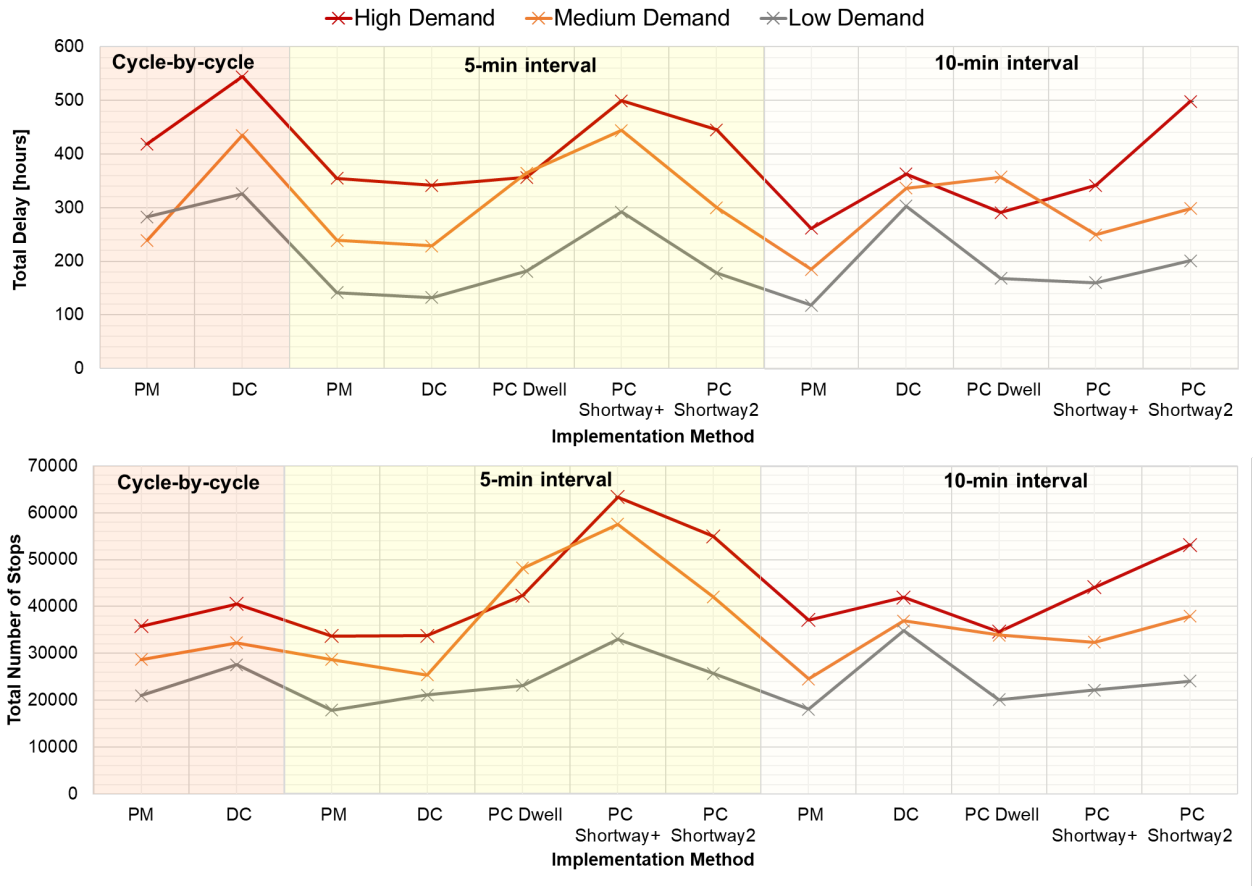

Fig. 23: Total delay and number of stops in the network

4.3.3 Implementation of Adaptive Logic to the SILS Environment

Before field deployment of Eco-ATCS, it is necessary to ensure that all the constraints are met and that the Eco-ATCS performs as expected. Having developed a fully operating SILS environment, the PITT team started exploring the possibilities of implementing Eco-ATCS to field controllers. First, PITT identified three ways of implementing various optimization logics to the actual field controller:

1. Changing Time-of-day (TOD) plans
2. Manipulation of vehicle calls
3. Using holds, omits and force-off.

The first approach had several unfavorable aspects, including its high memory requirement and limited flexibility compared to the other two approaches. As a result, it was determined that the first approach is unsuitable for implementation.

To implement Eco-ATCS, or in other words optimization output, to an actual controller NTCIP software must be used. Through NTCIP software NTCIP messages are sent to controller in form of hold/omit/force offs or “manipulated’ detection calls. The controller then relays the phase status

back to the NTCIP software, which converts it to a .json file and transmits it back to the Vissim microsimulation environment. It is worth noting that once Eco-ATCS is deployed in the field, there will be no messages sent back to the Vissim digital twin. Furthermore, the digital twin will solely rely on detection input from the field sensors.

In Fig. 24, the framework for offline Eco-ATCS implementation is explained. First, the output from the UTC server is obtained in the form of a text file. DGMARL output is then converted to a file readable to NTCIP in the data reader module. The converted output contains second by second phase statuses. As such, information from the text file is sent to the main NTCIP module and then in the form of a NTCIP message it is sent to SEPAC m60. It is important to note that, in this offline implementation, the SEPAC m60 receives detection output from Vissim, while Vissim receives signal status directly from the SEPAC m60 (which is provided by the DGMARL output). Additionally, the NTCIP software acts as a mediator between Vissim and the SEPAC m60 by transmitting messages that are readable to both Vissim (.json files) and the SEPAC m60 (NTCIP messages).

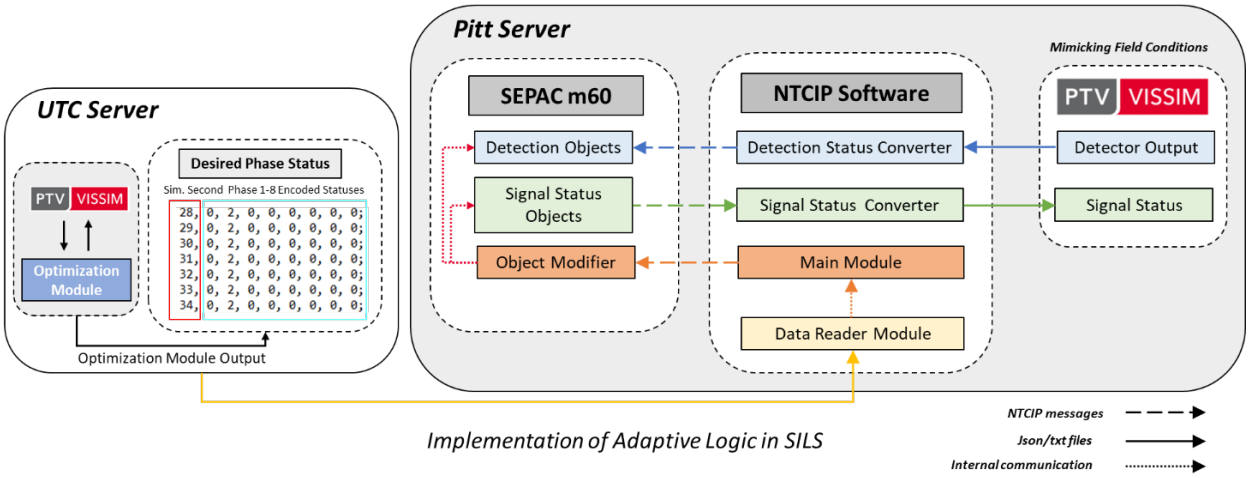

Fig. 24: Framework for Offline Adaptive Logic Implementation

4.4 Hardware-in-the-Loop (HIL) Simulation

4.4.1 Integration of Communication Model in Hardware-in-the-Loop Architecture

To test and account for the effects of communications in the HIL environment, ORNL tested the CAVE lab and the RealSim toolchain to architect the HIL environment. Fig. 25 shows how the communication model is integrated in the CAVE lab HIL architecture.

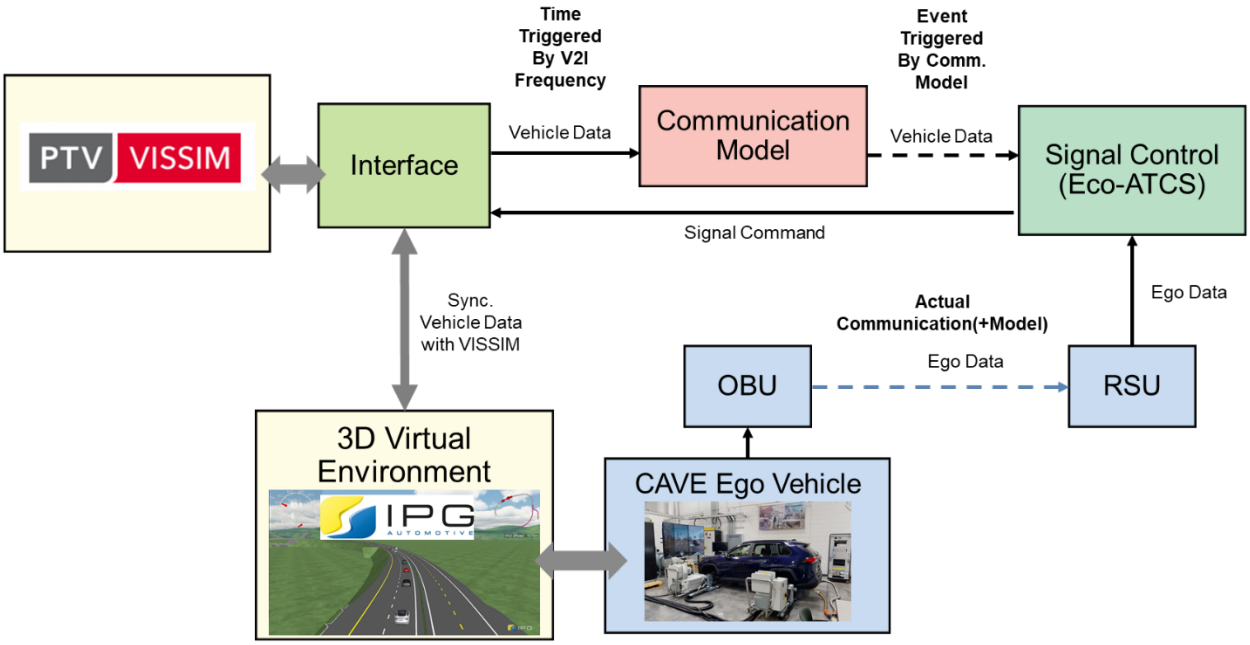

Fig. 25: CAVE lab HIL architecture including communication model

A similar HIL architecture (using SUMO instead of VISSIM) was applied to another project in the CAVE lab to quantify the effect of communication latencies on a lane merging coordination algorithms application (Fig. 26).

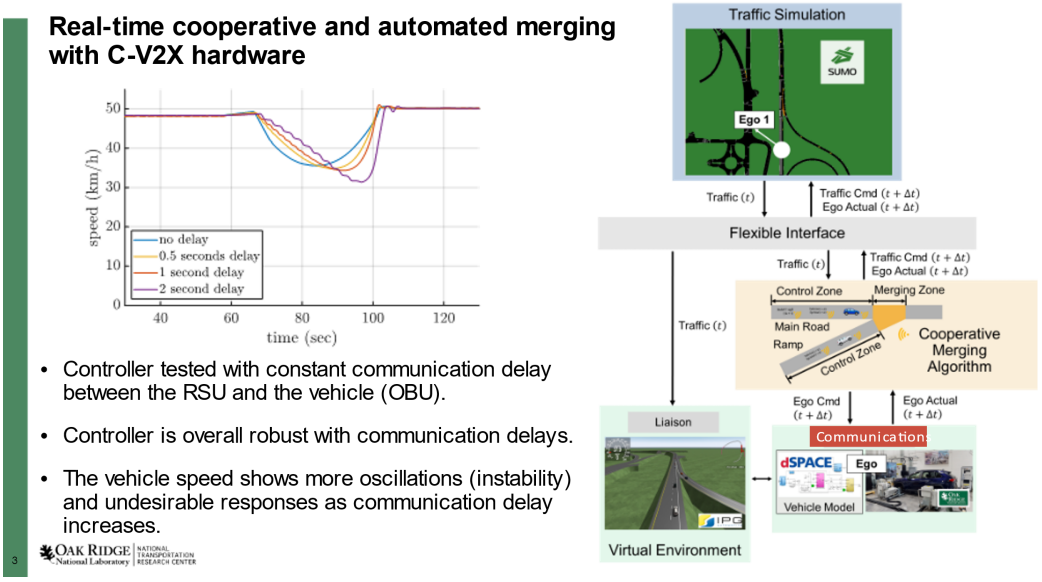

Fig. 26: Example of CAVE lab application quantifying the effect of communications on connected vehicles during traffic merging optimization

The plan was to use the same HIL architecture except for the use of VISSIM instead of SUMO for this project. However, the VEINS VANET simulator used in the project was found to be very complex and it did not run real time which is a prerequisite for HIL applications.

Communications models used in the CAVE lab HIL environment are typically statistical models

as they run faster than real time and yet they can capture some of the complexity of the physical systems. Hence, the next step was to convert the VEINS VANET model into a real time statistical model that can be imported into the ORNL HIL architecture.

4.4.2 Vehicle Hardware-in-the-Loop Architecture

In this project one key goal was to conduct hardware in the loop testing of a real vehicle in ORNL's CAVE lab subjected to virtual road load and traffic conditions. The ORNL CAVE Lab HIL architecture is shown in Figure 27. It comprises the real vehicle under test, the VISSIM environment for traffic simulation, IPG CarMaker for the virtual vehicle environment, the HIL system to interact between the models and the vehicle actuators, and an external traffic controller coordinating the various road network components.

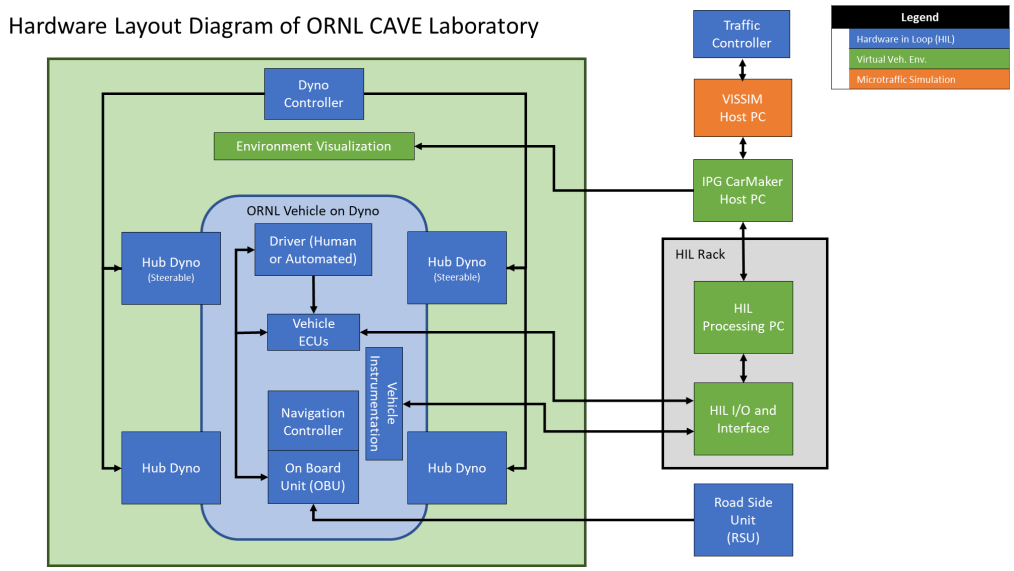

Figure 27: CAVE lab HIL architecture diagram

The digital twin model of MLK Smart Corridor in Chattanooga developed using the VISSIM (2022) was integrated into the CAVE lab using the IPG CarMaker-VISSIM interface.

Software-in-the-loop simulation (SILS) Mode Test: To reach the goal of conducting experiment with real vehicle in the loop in the realistic traffic scenario of MLK Smart Corridor simulated in VISSIM, first the architecture implementation was tested in Software-in-loop simulation (SILS) mode without an actual vehicle. Figure 28 shows a real-time simulation of the HIL environment running on the dSPACE system, but without the real vehicle in the loop. The road network and traffic simulation are modeled in VISSIM, the road load estimation, driver model and 3D visualization are handled by CarMaker, the dSPACE software and hardware interacts with the real vehicle under test.

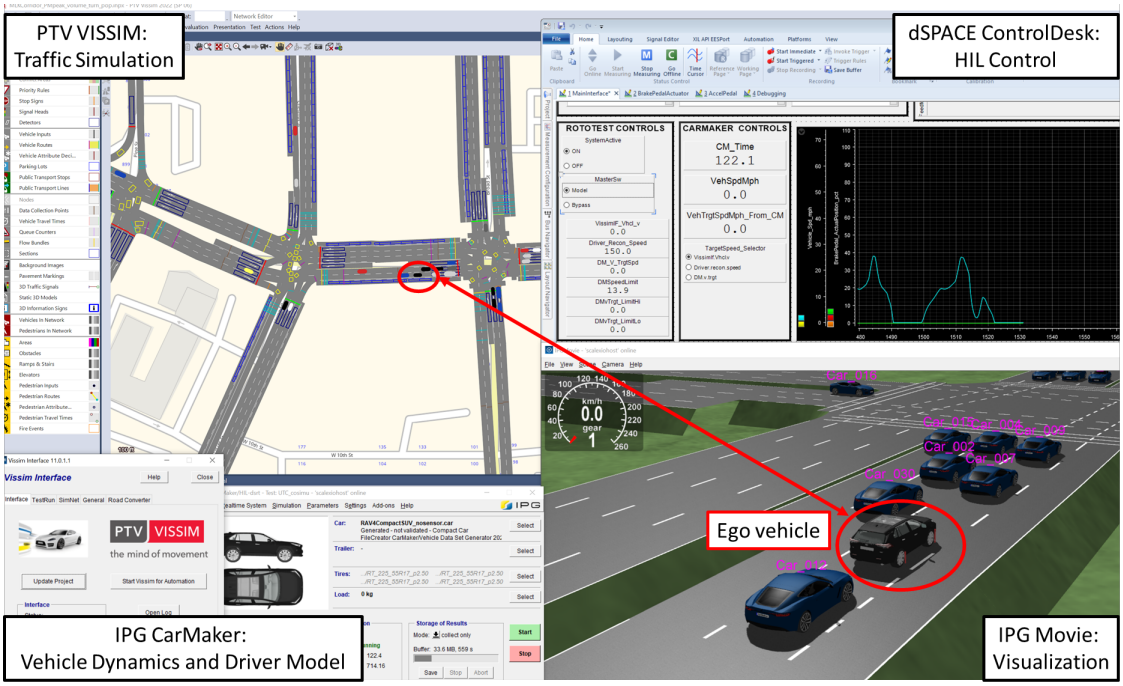

Figure 28: HIL architecture demonstration with VISSIM in the CAVE lab

In this configuration (CarMaker and VISSIM), the Carmaker driver model must be used to control vehicle speed as it calculates target speed and corresponding accelerator, and pedal position based on traffic information from VISSIM. VISSIM does not provide a target speed for the EGO vehicle, so the CarMaker driver model cannot be bypassed. Initially, issues with the CarMaker driver model prevented running a closed loop with the actual vehicle in the CAVE lab as the CarMaker driver tends to request maximum acceleration pedal during cruise operation though it regulates speed properly in all other conditions. After fixing some of these issues, a proof-of-concept experiment using an actual vehicle was conducted as described in the next section.

Proof of concept of HIL integration using Ford Mach E: A proof of concept Hardware-in-the-loop (HIL) architecture set up with Ford Mach E was accomplished. This included integration and synchronization on software end using the Real Sim interface - latest Vissim MLK model, IPG Carmaker for vehicle dynamics, dSpace to connect to the physical vehicle and control the Rototest dyno in CAVE lab. Figure 29 shows the skeleton of the HIL architecture integration with the physical vehicle in the CAVE lab. For this integration, at the hardware level, real-time vehicle CAN bus data is retrieved and recorded on the dSPACE box.

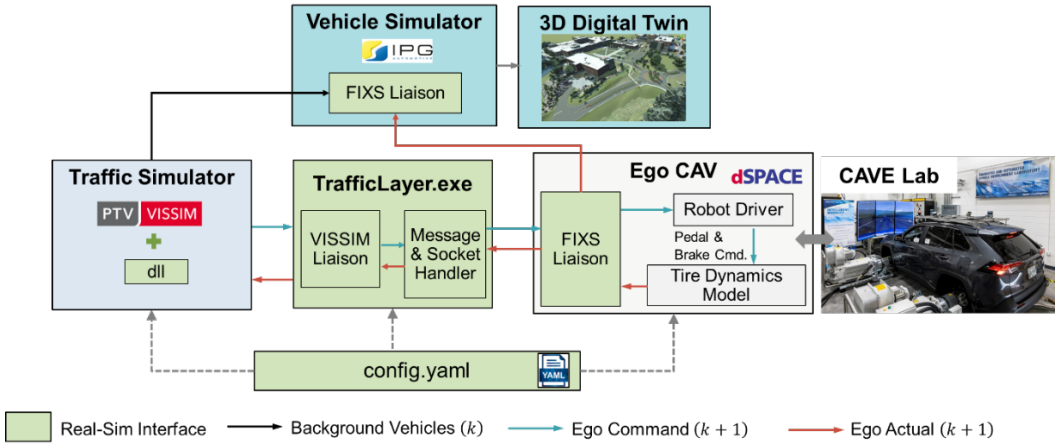

Figure 29: HIL architecture integrating Vissim MLK model with Ford Mach E

A preliminary experiment was conducted as a proof of concept to test the appropriateness of the HIL set up. The ego vehicle was run for ~1.95 miles of the entire corridor. The current and voltage of the battery were collected using vehicle CAN bus data along with the vehicle speed. Figure 30 shows the cumulative power consumption (primary axis) and speed of vehicle (secondary axis) with progress in simulation time. The total energy consumed is: ~0.651 kWh which estimated the MPGe =~102.

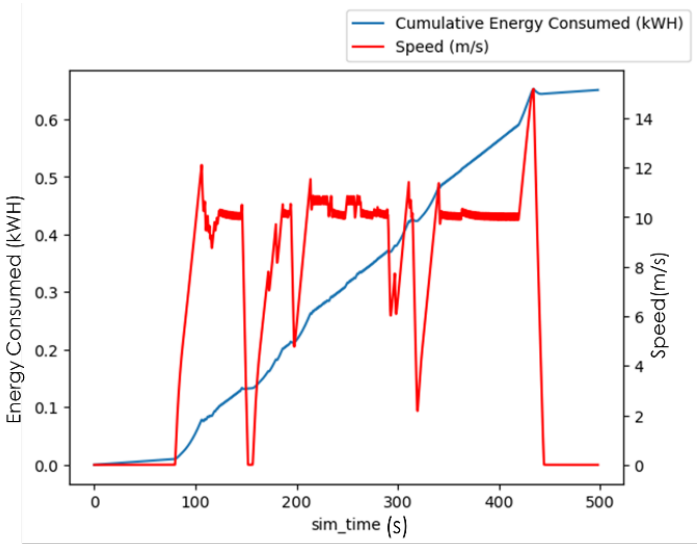

Figure 30: Power consumption and speed of ego vehicle in the MLK Vissim simulation for a single run across the corridor in Eastbound direction.

Proof of concept of HIL integration where signal control is driven externally using DGMARL: For the experiment, CarMaker in-built vehicle model was used while the car tire dynamics and car body were updated to represent Ford MachE. The carmaker following parameters were updated/tuned for realizing ego vehicle following behavior. For the comparison of vehicle energy consumption while driving on the corridor for two cases when the 1) corridor has

actuated signal timing plan, versus 2) corridor has DGMARL signal timing implementation. For the experiment, in the two scenarios, the same ego vehicle entry location, time, and Vissim traffic demand input was used. To implement DGMARL signal implementation in the developed HIL architecture, IPG "Start with Automation" feature was used. This was implemented for DGMARL driven co-simulation. Figure 31 and Figure 32 show the ego vehicle energy consumption and ego vehicle speed (mph) during the simulation run for the two scenarios. This provided a baseline test of differences in vehicle energy consumption with different signal plan implementation. This was not an exhaustive test to particularly determine that one plan works better than the other in all cases. It was learned during this process that it will take effort and time to conduct several tests if we use CAVE experiments to evaluate the impact of signal timing plan of vehicle fuel consumption.

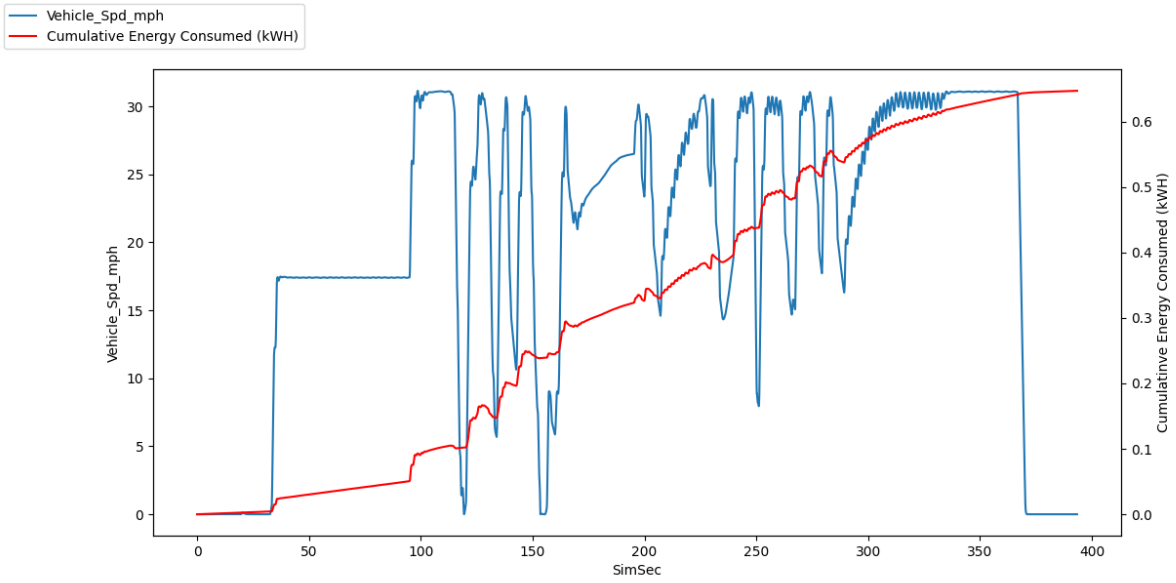

Figure 31: Actuated signal controls Ego vehicle speed and cumulative energy consumption – Mach E

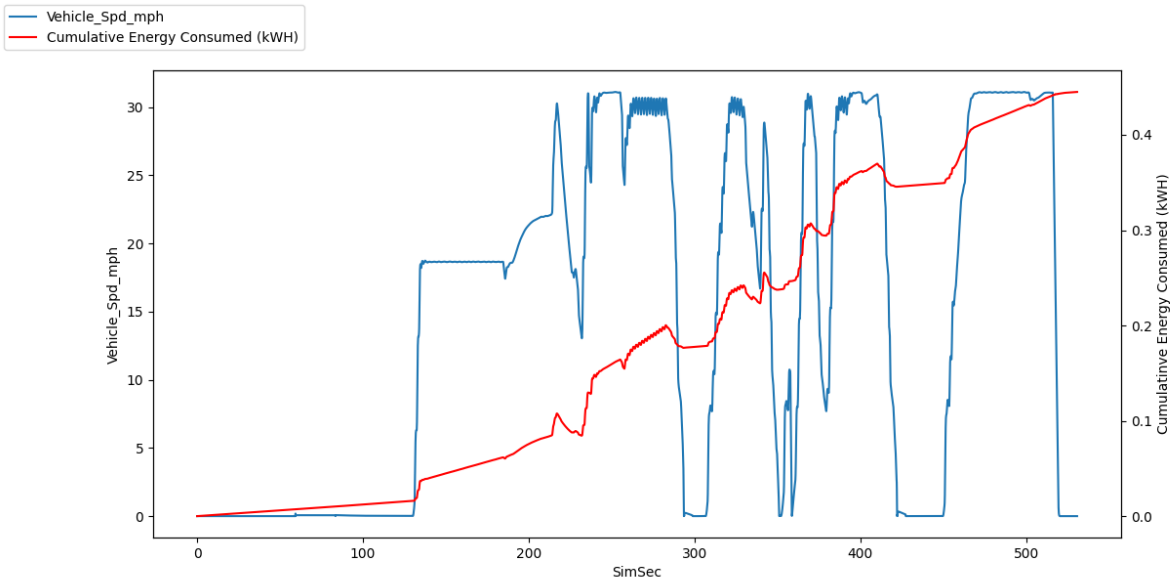

Figure 32: DGMARL signal controls Ego vehicle speed and cumulative energy consumption – Mach E

Lastly, AVL Plutron Fuel Flow Meter (FFM) was purchased and installed on a Toyota RAV4 in the CAVE laboratory with an intention to test the actual fuel consumption on the vehicle. Figure 33 shows the installed FFM on RAV 4. The CAN configuration to measure FFM readings was also completed and tested using short vehicle runs without it being on the MLK corridor (Vissim). However, it was realized that due to recent changes in software compatibility between IPG, Vissim, and dSpace, the ego vehicle with FFM HIL experiment will take more effort than expected. We expect to solve the compatibility issues as part of the Real-Sim effort.

Figure 33: AVL Plutron Fuel Flow Meter installed on RAV4 in CAVE Laboratory

Section 5: Findings and Results

5.1 DGMARL Testing Outcomes

Training existing DGMARL model with 105 episodes. Performed multiple tests to validate the results. Pine, Georgia, Peeples, and Magnolia intersections are having their performance impacted as shown in Fig. XX

- Test Scenarios
  - 1 Hour Simulation:
    - Overall Eco-PI improved by 16.63%
    - Overall stop delay improved by 43.80%
    - Number of stops reduced by 15.13%
  - 3 Hour Simulation
    - Overall Eco-PI improved by 15.29%
    - Overall stop delay improved by 43.96%
    - Number of stops reduced by 10.05%

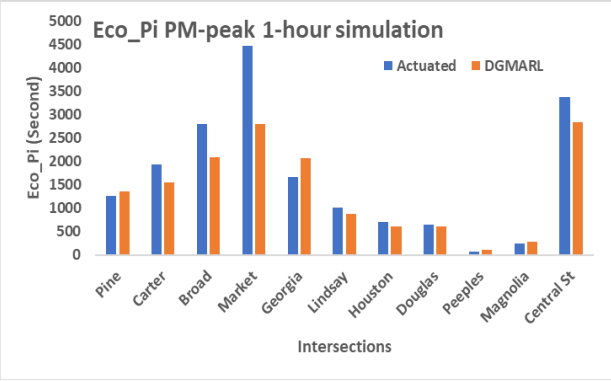

Node	Actuated	DGMARL	%
Pine	1264.765704	1360.566	-7.57%
Carter	1938.054917	1549.567	20.05%
Broad	2806.981228	2083.691	25.77%
Market	4466.239603	2809.791	37.09%
Georgia	1664.027442	2078.297	-24.90%
Lindsay	1019.277417	873.994	14.25%
Houston	704.1671827	610.716	13.27%
Douglas	652.0101882	604.659	7.26%
Peeples	77.02113721	107.426	-39.48%
Magnolia	252.5771327	285.469	-13.02%
Central St	3385.80875	2834.15	16.29%
Total	**18230.9307**	**15198.326**	**16.63%**

Fig. 34: PM-peak 1 Hour Simulation Test Results

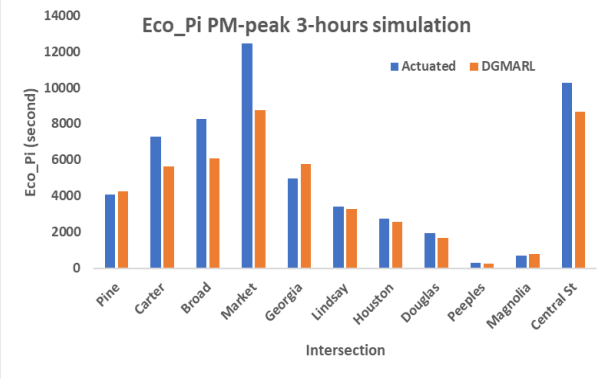

Node	Actuated	DGMARL	%
Pine	4089.825891	4240.674	-3.69%
Carter	7304.622662	5631.773	22.90%
Broad	8252.061816	6076.327	26.37%
Market	12434.08111	8737.537	29.73%
Georgia	4957.651198	5769.946	-16.38%
Lindsay	3431.395635	3284.548	4.28%
Houston	2734.583124	2591.272	5.24%
Douglas	1936.988007	1703.281	12.07%
Peeples	291.1535964	261.231	10.28%
Magnolia	693.0480542	807.524	-16.52%
Central St	10266.42646	8665.133	15.60%
Total	**56391.83755**	**47769.246**	**15.29%**

Fig. 35: PM-peak 3 Hour Simulation Test Results

After DGMARL fine tuning to account for LDVs and HDVs

Tables 7-11

Total Eco_PI – 5% HDV
Test - 80007

	Actuated	DGMARL	%
Pine	26991.12	30428.89	-12.74%
Carter	57094.26	46794.52	18.04%
Broad	64535.16	51103.28	20.81%
Market	95568.8	68690.66	28.12%
Georgia	34127.16	41003.34	-20.15%
Lindsay	25395.81	22719.74	10.54%
Houston	21812.12	16759.19	23.17%
Douglas	24803.67	34139.17	-37.64%
Peeples	1957.362	2421.52	-23.71%
Magnolia	4593.444	4420.578	3.76%
Central St	78523.56	48949.88	37.66%
	435402.5	**367430.8**	**15.61%**

Total Eco_PI – 4% HDV
Test - 80008

	Actuated	DGMARL	%
Pine	24956.75	27515.2	-10.25%
Carter	55420.46	46314.24	16.43%
Broad	62387.07	51228.14	17.89%
Market	93576.75	60697.98	35.14%
Georgia	32370.87	38559.85	-19.12%
Lindsay	24614.08	20679.51	15.99%
Houston	21726.01	16187.48	25.49%
Douglas	22691.93	32832.43	-44.69%
Peeples	2156.546	1811.461	16.00%
Magnolia	4685.571	4880.236	-4.15%
Central St	73120.13	43622.82	40.34%
	417706.2	**344329.3**	**17.57%**

Total Eco_PI – 3% HDV
Test - 80009

	Actuated	DGMARL	%
Pine	26876.46	26576.07	1.12%
Carter	56642.02	45916.48	18.94%
Broad	64473.02	49426.02	23.34%
Market	82221.34	58018.87	29.44%
Georgia	35025.02	37918.21	-8.26%
Lindsay	24921.98	20094.77	19.37%
Houston	20555.69	14239.56	30.73%
Douglas	25899.19	32822.78	-26.73%
Peeples	1422.154	1830.014	-28.68%
Magnolia	4618.953	5516.213	-19.43%
Central St	72600.75	42307.93	41.73%
	415256.6	**334666.9**	**19.41%**

Total Eco_PI – 2% HDV
Test - 80010

	Actuated	DGMARL	%
Pine	24081.56	24793.27	-2.96%
Carter	50174.58	45763.32	8.79%
Broad	58851.8	46836.02	20.42%
Market	75300.72	53083.14	29.51%
Georgia	31339.99	34086.17	-8.76%
Lindsay	22369.66	18513.47	17.24%
Houston	21062.65	14610.07	30.64%
Douglas	21579.61	31090.11	-44.07%
Peeples	1672.345	1751.771	-4.75%
Magnolia	4023.593	4327.326	-7.55%
Central St	68926.94	42560.51	38.25%
	379383.5	**317415.2**	**16.33%**

Total Eco_PI – 1% HDV
Test - 80011

	Actuated	DGMARL	%
Pine	22414.17	24861.13	-10.92%
Carter	48304.07	38906.22	19.46%
Broad	56874.65	41201.3	27.56%
Market	85438.29	54420.59	36.30%
Georgia	29541.67	33941.8	-14.89%
Lindsay	21951.49	17900.08	18.46%
Houston	19898.14	14551.83	26.87%
Douglas	21451.33	31266.32	-45.75%
Peeples	1587.332	1881.436	-18.53%
Magnolia	3861.027	4327.243	-12.07%
Central St	66225.3	38970.97	41.15%
	377547.5	**302228.9**	**19.95%**

5.1.1 Fine Tuning DGMARL

The DGMARL model was fine-tuned to address red clearance using a simulation resolution of 0.1 seconds. This adjustment also included resolving protected-permissive left signal issues. The Eco-PI function was updated to accommodate the 0.1 second time step, and stop penalty calculations were corrected. Following these updates, testing was conducted using both 3-hour and 24-hour scenarios, with the results shared with the larger team for integration testing. The

DGMARL execution time was improved by implementing multi-threading techniques, which also enhanced the Actuated COM solution for Eco-PI observation. The primary sources of slowness in DGMARL were the signal state updates in VISSIM through COM and additional validations before switching the signal state. However, in the field, DGMARL is expected to run faster since it won't perform signal state updates. Future work will test whether reducing the frequency of Eco-PI observations to 1 second can further enhance execution speed.

Table 12

Model	Simulation Hour(s)	Original Timing	Improved Timing	Output(s)
Actuated	1-hour	2 hours, 34 minutes	23 minutes, 59 seconds	Eco_PI, Vehicles in Net, Signal State
	3-hours	Around 5 hours	1 hour, 4 minutes	
DGMARL	1-hour	3 hours, 38 minutes	1 hour, 36 minutes	Eco_PI, Vehicles in Net, Signal State, Node State and other details
	3-hours	Around 12 hours	4 hours, 55 minutes	

A maximum green constraint was added to DGMARL to handle pedestrian and minimum recall times. Additionally, vehicle count and speed-related inputs were removed from the model, and it was retrained and tested based on these changes. Then DGMARL model was trained by integrating Light Duty Vehicle (LDV) and Heavy Duty Vehicle (HDV) formulas into the Eco-PI function. The model was then tested with varying percentages of HDVs at 5%, 4%, 3%, and 1%. The test configurations included a simulation resolution of 0.1 seconds, Version 5 of the VISSIM network, 3 hour simulations, and a random seed of 21.

Additional Fine-Tuning to DGMARL:

- Vehicle Count Input Enhancement: the vehicle count input feature was reintroduced due to the availability of a computer vision module in the field, allowing vehicle count data to be included in the input features for DGMARL
- Intersection Coordination Validation: validation of intersection coordination was conducted, and preliminary testing indicated a slightly higher Eco-PI improvement without message passing compared to with message passing, as shown in the figures below.
- Message Passing Enhancement: the input to the DMGARL neural networks was enhanced by aggregating traffic states direction-wise, along with neighboring states, resulting in a 24.72% improvement in Eco-PI during one hour simulation.
- Visualization of Intersection Coordination: Vehicle trajectory reports were developed for both eastbound and westbound directions. Since DGMARL optimizes Eco-PI by considering traffic from both main and side streets, achieving a green wave is not always possible, as the model adjusts green lights based on traffic from all approaches.
- Reports for Unique Vehicles: Reports were developed to track unique vehicles at intersections during green and red signals, as well as AOR/AOG. While the reports showed differences between Actuate and DGMARL, they didn't fully capture coordination

- Change in Vehicle Stop State Consideration: The vehicle stop state was redefined as a speed less than or equal to 3 mph, instead of 0. This adjustment resulted in a slight decrease in Eco-PI to 21.37% during one-hour simulation testing shown in Table 13.

Table 13

Without Message Passing			
1-hr sim	Actuated	DGMARL	%
Pine	8532.522	9078.161	-6.39%
Carter	15010.87	10692.89	28.77%
Broad	22306.46	14976.2	32.86%
Market	29651.8	24204.07	18.37%
Georgia	13007.5	12652.69	2.73%
Lindsay	7422.028	7334.966	1.17%
Houston	5200.612	3425.311	34.14%
Douglas	9298.906	10600.68	-14.00%
Peeples	520.0162	926.8122	-78.23%
Magnolia	1783.23	1488.852	16.51%
Central St	25359.28	15550.25	38.68%
	138093.2	**110930.9**	**19.67%**

Previous approach – With Message Passing			
1-hr sim	Actuated	DGMARL	%
Pine	8532.522	8832.619	-3.52%
Carter	15010.87	10918.25	27.26%
Broad	22306.46	15447.74	30.75%
Market	29651.8	23137.99	21.97%
Georgia	13007.5	13723.71	-5.51%
Lindsay	7422.028	6644.614	10.47%
Houston	5200.612	3930.351	24.43%
Douglas	9298.906	11076.56	-19.12%
Peeples	520.0162	850.8524	-63.62%
Magnolia	1783.23	1624.885	8.88%
Central St	25359.28	16730.18	34.03%
	138093.2	**112917.8**	**18.23%**

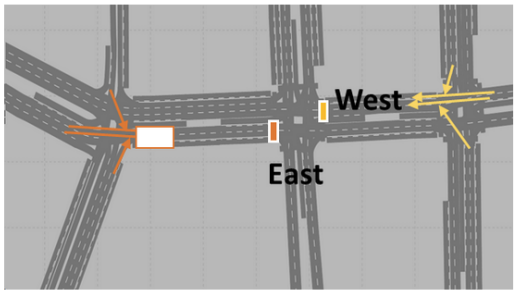

NEW - With Message Passing			
1-hr	Actuated	DGMARL	%
Pine	6956.699	6963.358	-0.10%
Carter	12658.01	8579.315	32.22%
Broad	18768.45	12117.76	35.44%
Market	25233.92	17294.65	31.46%
Georgia	10705.41	10331.45	3.49%
Lindsay	5786.092	4716.866	18.48%
Houston	5362.982	3488.379	34.95%
Douglas	7093.474	9352.383	-31.84%
Peeples	356.3135	612.2733	-71.84%
Magnolia	1459.848	1867.387	-27.92%
Central St	22217.69	12457.45	43.93%
	116598.9	**87781.28**	**24.72%**

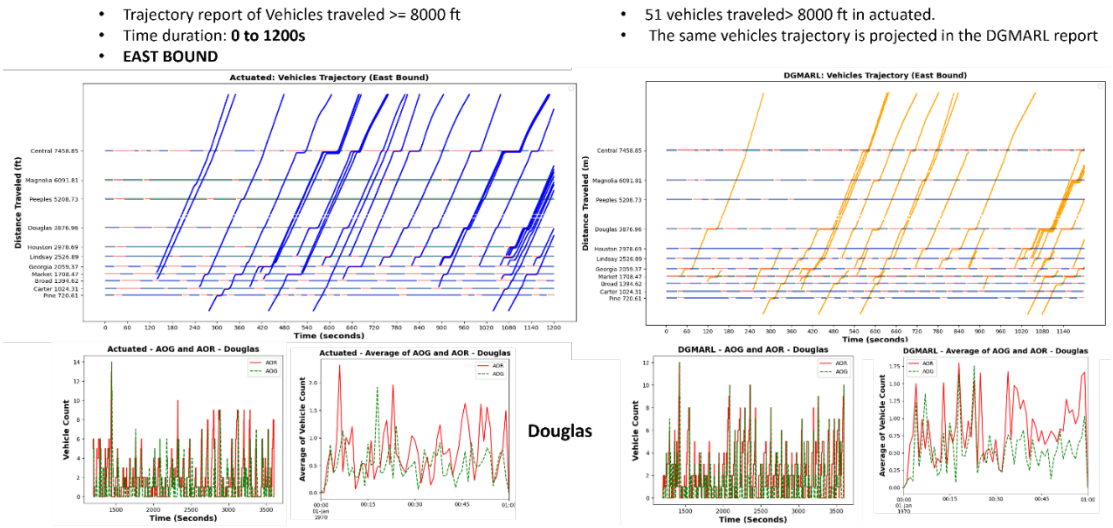

Fig 36: Eastbound: Trajectory report of vehicles traveled >= 8000ft

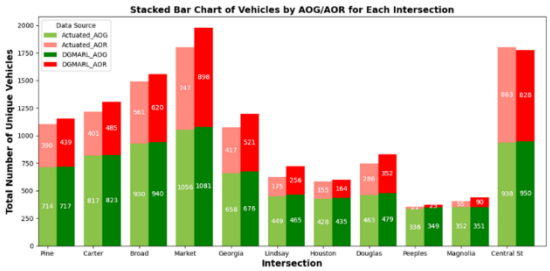

Fig.37: Arrival on green and arrival on red

Stopped vehicles speed <=3mph			
1-hr	Actuated	DGMARL	%
Pine	8206.608	8684.976	-5.83%
Carter	14024.69	9850.864	29.76%
Broad	20510.14	14065.34	31.42%
Market	25329.8	19325.07	23.71%
Georgia	12172.99	12002.76	1.40%
Lindsay	6382.125	5499.636	13.83%
Houston	5902.847	3450.75	41.54%
Douglas	8050.33	10011.97	-24.37%
Peeples	487.9753	822.1571	-68.48%
Magnolia	1607.838	2164.154	-34.60%
Central St	24768.92	14336.55	42.12%
	127444.3	**100214.2**	**21.37%**

Fig. 38: Overall Eco-PI in 1 hour simulation

- **Vehicles Speed ≤ 3 MPH Considered as Stopped: The DGMARL model and Eco-PI formula were updated to classify vehicles as stopped when their speed is ≤** 3 MPH. This change impacted the previously observed Eco-PI, reducing it from approximately 24% to 20% as shown in Fig. 38.
- Improving Intersection Coordination: Intersection coordination was improved by increasing attention to oncoming traffic by two hops, leading to an increase in Eco-PI from 20.89% to an average of 26.52%. The number of stops was reduced by 17.91%

while the stop delay decreased from 44.04% to 33.49% as shown in Fig. XX and XX. The increase in stops occurred as the model adjusted green time for high upcoming traffic, reducing acceleration and deceleration, which in turn, impacts fuel consumption positively. This model was trained and tested using five runs with a random seed value of 21, yielding consistent improvements in Eco-PI, stops, and delays.

Table 14: DGMARL–Improved Intersections Coordination and Average Eco-PI: 26.52%

	Actuated	Previous Alg.		New Alg. Test 1		New Alg. Test 2		New Alg. Test 3		New Alg. Test 4		New Alg. Test 5	
Pine	8185.241	8684.976	-6.11%	7979.621	2.51%	7116.527	13.06%	6990.358	14.60%	6896.521	15.74%	7154.246	12.60%
Carter	13902.52	9850.864	29.14%	13424.57	3.44%	13761.67	1.01%	13776.82	0.90%	14400.02	-3.58%	13914.22	-0.08%
Broad	20382.28	14065.34	30.99%	13822.61	32.18%	14478.4	28.97%	14857.32	27.11%	14301.52	29.83%	13946.63	31.57%
Market	25006.75	19325.07	22.72%	18557.74	25.79%	18310.03	26.78%	17891.16	28.45%	17042.08	31.85%	17959.51	28.18%
Georgia	12131.55	12002.76	1.06%	11204.29	7.64%	12203.93	-0.60%	12497.34	-3.02%	12278.29	-1.21%	11561.31	4.70%
Lindsay	6376.639	5499.636	13.75%	4274.406	32.97%	4912.883	22.95%	4447.026	30.26%	4352.152	31.75%	4581.422	28.15%
Houston	5871.748	3450.75	41.23%	3893.175	33.70%	3520.334	40.05%	3275.001	44.22%	2794.201	52.41%	3913.558	33.35%
Douglas	8050.33	10011.97	-24.37%	5327.777	33.82%	5357.547	33.45%	5453.206	32.26%	6156.63	23.52%	5732.179	28.80%
Peeples	487.9753	822.1571	-68.48%	308.687	36.74%	305.2768	37.44%	278.1765	42.99%	330.3526	32.30%	321.9541	34.02%
Magnolia	1597.224	2164.154	-35.49%	1451.924	9.10%	1386.026	13.22%	1293.778	19.00%	1224.132	23.36%	1300.444	18.58%
Central St	24678.95	14336.55	41.91%	12856.28	47.91%	12287	50.21%	12419.58	49.68%	12208.88	50.53%	13097.94	46.93%
	126671.2	**100214.2**	**20.89%**	**93101.09**	**26.50%**	**93639.63**	**26.08%**	**93179.76**	**26.44%**	**91984.79**	**27.38%**	**93483.41**	**26.20%**

Table 15: DGMARL–Improved Intersections Coordination and Average STOPS: 17.91%

	Actuated	Previous Alg.		New Alg. Test 1		New Alg. Test 2		New Alg. Test 3		New Alg. Test 4		New Alg. Test 5	
Pine	285	313	-9.82%	194	31.93%	192	32.63%	182	36.14%	191	32.98%	181	36.49%
Carter	339	371	-9.44%	291	14.16%	289	14.75%	297	12.39%	284	16.22%	304	10.32%
Broad	455	490	-7.69%	387	14.95%	412	9.45%	403	11.43%	417	8.35%	396	12.97%
Market	598	643	-7.53%	582	2.68%	563	5.85%	557	6.86%	522	12.71%	546	8.70%
Georgia	355	404	-13.80%	373	-5.07%	394	-10.99%	395	-11.27%	397	-11.83%	380	-7.04%
Lindsay	171	214	-25.15%	130	23.98%	142	16.96%	141	17.54%	141	17.54%	143	16.37%
Houston	155	130	16.13%	110	29.03%	110	29.03%	98	36.77%	86	44.52%	113	27.10%
Douglas	232	287	-23.71%	156	32.76%	145	37.50%	146	37.07%	179	22.84%	159	31.47%
Peeples	24	33	-37.50%	16	33.33%	16	33.33%	15	37.50%	17	29.17%	16	33.33%
Magnolia	45	76	-68.89%	27	40.00%	29	35.56%	27	40.00%	29	35.56%	26	42.22%
Central St	633	542	14.38%	433	31.60%	425	32.86%	426	32.70%	425	32.86%	457	27.80%
	3292	**3503**	**-6.41%**	**2699**	**18.01%**	**2717**	**17.47%**	**2687**	**18.38%**	**2688**	**18.35%**	**2721**	**17.35%**

Table 16: DGMARL–Imrpoved Intersections Coordination and Average DELAY: 33.49%

	Actuated	Previous Alg.		New Alg. Test 1		New Alg. Test 2		New Alg. Test 3		New Alg. Test 4		New Alg. Test 5	
Pine	2954.1	2995.5	-1.40%	4601.7	-55.77%	3771.2	-27.66%	3875.8	-31.20%	3556.3	-20.39%	4025.7	-36.28%
Carter	8156.6	3308.1	59.44%	8628.8	-5.79%	8996.8	-10.30%	8847.7	-8.47%	9655.2	-18.37%	8942.4	-9.63%
Broad	13416.9	6256.6	53.37%	7598.4	43.37%	7862.9	41.40%	8310.2	38.06%	7723.3	42.44%	7746.3	42.26%
Market	15011.7	8389.2	44.12%	8537.3	43.13%	8367	44.26%	8296.3	44.73%	7956.9	47.00%	8523.2	43.22%
Georgia	6234.1	5310.7	14.81%	5133	17.66%	5630	9.69%	5706	8.47%	5394.2	13.47%	5300.3	14.98%
Lindsay	3451.8	1668.8	51.65%	2059.9	40.32%	2415.8	30.01%	2077.5	39.81%	1952.9	43.42%	2126.2	38.40%
Houston	3096.8	1101.9	64.42%	1889.1	39.00%	1595.3	48.49%	1554.7	49.80%	1303.5	57.91%	1894.7	38.82%
Douglas	3542.7	4593	-29.65%	2425.3	31.54%	2705.2	23.64%	2726.2	23.05%	2845.9	19.67%	2800.5	20.95%
Peeples	113.1	217.3	-92.13%	46.9	58.53%	45.1	60.12%	41.4	63.40%	57.5	49.16%	51.5	54.47%
Magnolia	689.1	494.9	28.18%	897.9	-30.30%	816.9	-18.55%	779.8	-13.16%	659.4	4.31%	802.5	-16.46%
Central St	14033.1	5226.2	62.76%	5274.2	62.42%	4957.3	64.67%	5122.8	63.49%	4880.9	65.22%	5311.2	62.15%
	70700	**39562.2**	**44.04%**	**47092.5**	**33.39%**	**47163.5**	**33.29%**	**47338.4**	**33.04%**	**45986**	**34.96%**	**47524.5**	**32.78%**

- Visualization–Heatmap Analysis for Stops and Delays: Developed heatmaps to analyze stops and delays observed in the DGMARL. With the previous version of the model, the analysis indicated that while DGMARL effectively reduces delays, it also leads to an increase in the number of stops. After improving the model with the coordination, one of the test results is shown in fig. 39, comparing stop reduction between Actuated and DGMARL. Fig. 40 shows the delay reduction comparison, and Fig. 41 illustrates the difference in stops and delays between DGMARL and Actuated. The color shading indicates the increase or decrease in DGMARL performance.

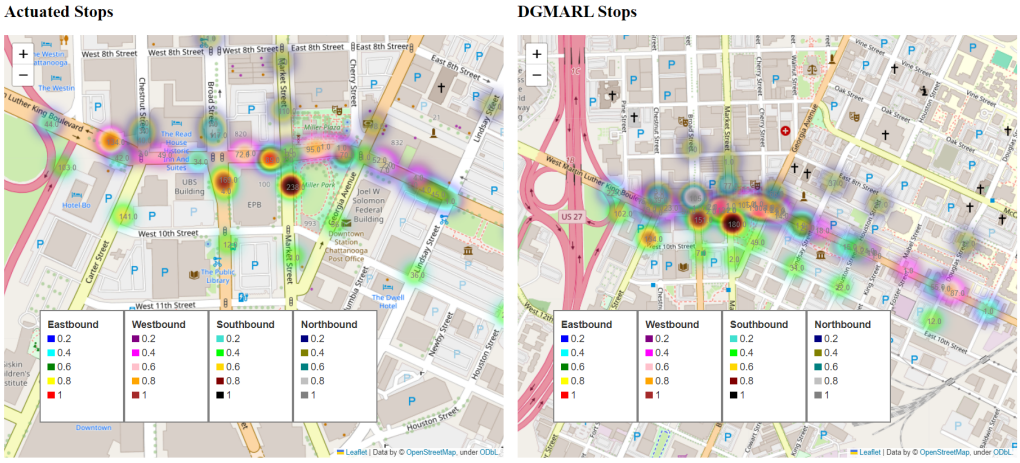

Note: Approach links are mapped based on latitude and longitude values obtained from VISSIM

Fig 39: Actuated vs DGMARL–Stops Reduced by 17.35%

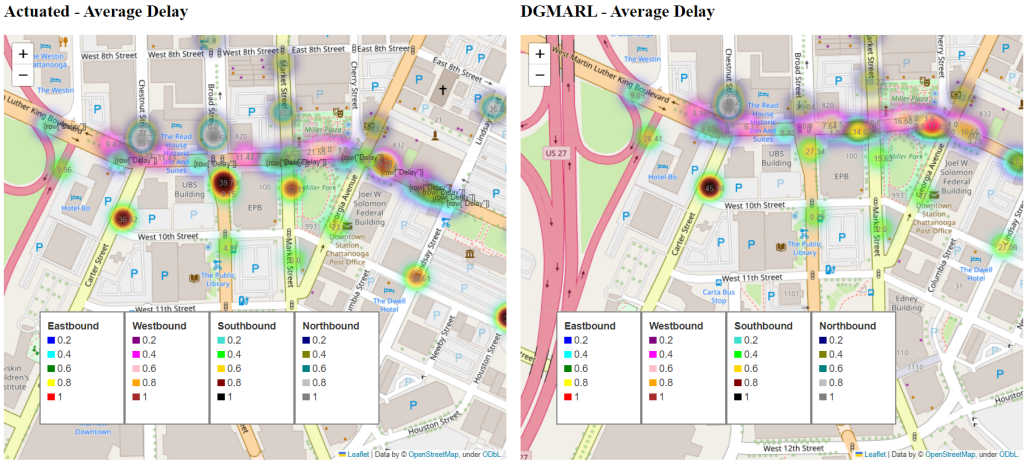

Note: Approach links are mapped based on latitude and longitude values obtained from VISSIM

Fig. 40: Actuated vs DGMARL–Delay Reduced by 32.78%

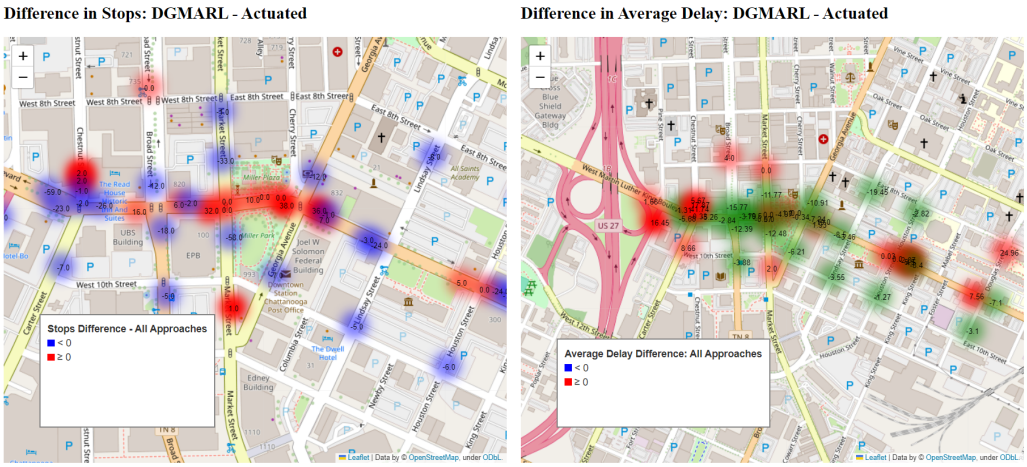

Note: Approach links are mapped based on latitude and longitude values obtained from VISSIM

Fig. 41: Difference in Stops and Delays (DGMARL minus Actuated)

- Model Development: a new version of the DGMARL model was developed to reduce pedestrian and driver waiting times. Comparative analysis was conducted using three scenarios: pedestrian recall, automated pedestrian detection, and push-button requests. The automated pedestrian detection with dynamic signal timing showed significant performance improvements over the traditional pedestrian recall system
- Model Overview: the model, titled Optimizing Traffic Signal Control to Enhance Transportation Efficiency and Maximize Pedestrian Benefits in the Road Network, uses an objective function that considers vehicle Eco-PI, driver delays, and pedestrian waiting times. Inputs include vehicle presence, count, average speed, signal state, pedestrian volume, and waiting time. The output determines whether to switch or stay in the current phase, with the phase sequence being free but prioritized by the highest occupancy (vehicles or pedestrians). Key constraints enforced include minimum green time, pedestrian recall, and yellow and red clearance times.
- Comparative Analysis: The model compared real-time signal timing configurations, automated pedestrian detection, and phase activation based on traffic demand. Additionally, it dynamically adjusted the pedestrian signal timing based on traffic demand. The effectiveness of automated detection and dynamic timing was evaluated alongside push-button requests, showing significant performance improvements in all metrics.

- Data: vehicle data and signal timing were based on real-time observations from December 15, 2022. Pedestrian data were randomly generated, with the same volumes applied to both actuated and DGMARL models for consistency.
- Experiment: The experiment was conducted during a PM-peak hour simulation involving 458 pedestrians and 2825 vehicles. Notably, this test was performed before the coordination improvements, so the issue of increased vehicle stops still existed. Eco-PI was measured per second, and the test revealed that DGMARL with dynamic pedestrian signal timing adhered to minimum serving time constraints efficiently.
- Scenario Comparisons: In the scenario comparisons, DGMARL with automated detection and dynamic timing, including push-button activation, improved vehicle Eco-PI 27.14%, reduced delay by 58.73%, and decreased pedestrian waiting time by 60.62% on average compared to actuated signal timing with pedestrian recall. Vehicle stops increased by 4.67% with pedestrian recall, while it was only 0.97% with automated detection and dynamic timing as shown in Fig. 43.
- Pedestrian Serving Time and Stop Delay: DGMARL with automated pedestrian detection and dynamic timing reduced pedestrian waiting time by 60.55% compared to actuated signal timing with pedestrian recall, and by 48.46%

Performance Measurement	Value
Total no. of pedestrians arrived	458
Total no. of vehicles traveled	2825
Actuated: Avg. of peds. serving time	22.51s
DGMARL PedRecal: Avg. of peds. serving time	22.51s
DGMARL Automated: Avg. of peds serving time	21.84s

Fig. 42: Overall Traffic and Serving State

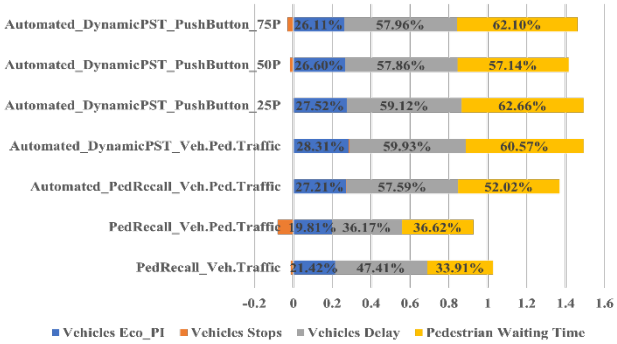

Fig. 43: Automated pedestrian traffic detection with dynamic pedestrian signal timing performance improvements compared to pedestrian recall.

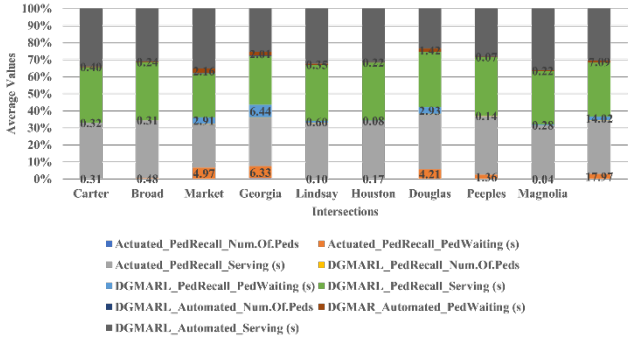

Fig. 44: Pedestrian traffic, waiting time, and serving time comparison.

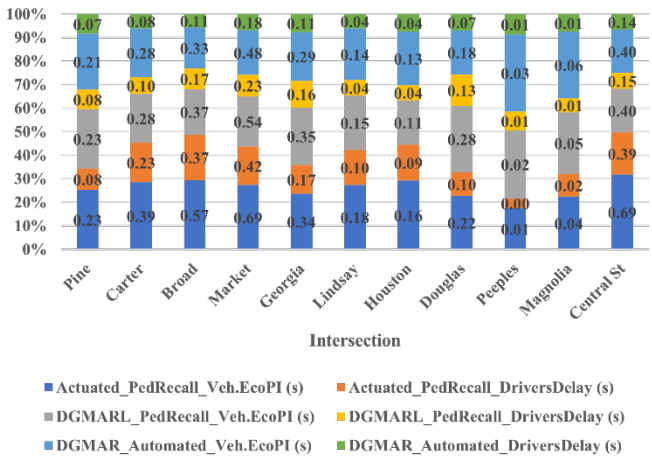

Fig. 45:(23) Vehicles Eco-PI and drivers waiting time comparison

5.2 Comparing Fuel Consumption and Emissions in DGMARL and RBCs

Both the optimization model DGMARL and the ring barrier controller (RBC) were simulated in VISSIM and CMEM to investigate their individual impacts on FC and various emissions. For this particular analysis, we focused on evaluating FC and emissions of light-duty vehicles. As depicted in fig. 46, we extracted vehicle trajectories from the VISSIM model and then prepared the data for the CMEM emissions model using Python scripting. Subsequently, the results were obtained in g/mile.

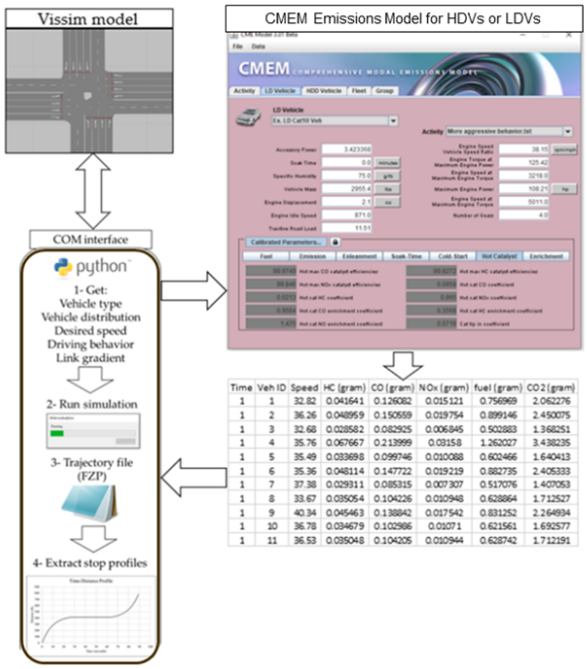

Fig. 46: Processing trajectories in CMEM emissions model

In Table 17, the values for fuel consumption (FC) and emissions for the entire network are presented. It is evident that DGMARL effectively reduces all emissions, except for NOx, which shows a slight increase of 2.93%. On average, other emissions and FC are reduced by approximately 5%. It is important to note that DGMARL optimizes traffic signals specifically to

decrease Eco-PI (footprint at signalized intersections due to traffic signal control). Therefore, to fully comprehend the benefits of DGMARL, it becomes necessary to investigate FC and emissions at the intersection level, which will be discussed in the latter part of this report.

Table 17: CMEM results – MLK corridor

	RBC	DGMARL	Difference (%)
Hydrocarbons (g/mile)	11.81	11.21	-5.04%
Carbon Monoxide (g/mile)	94.57	90.33	-4.48%
Nitrogen Oxides (g/mile)	1.51	1.55	2.93%
Carbon Dioxide (g/mile)	249.59	237.41	-4.88%
Fuel Consumption (g/mile)	603.20	573.25	-4.97%

Furthermore, the Pitt team investigated how fuel consumption (FC) and various emissions changed over the simulation period by calculating their values every minute. However, as depicted in fig. 47, not many conclusions could be drawn from the data presented.

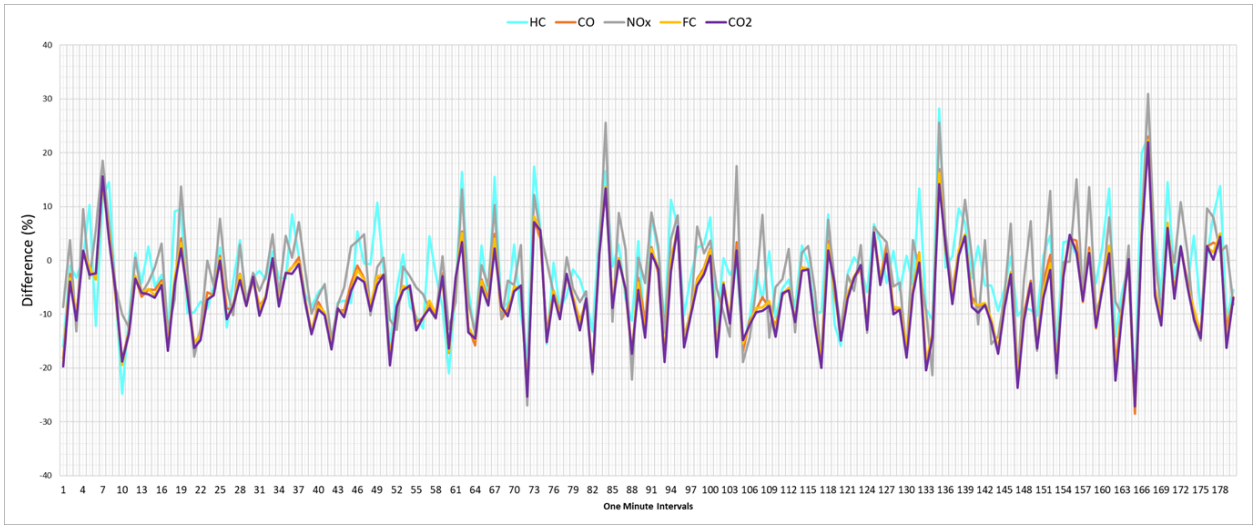

Fig. 47: CMEM results per minute – MLK corridor

To gain a comprehensive understanding of the changes occurring throughout the simulation period (1 hour), the Pitt team developed fig. 48 illustrating the cumulative fuel consumption (FC) and emissions per minute. The graph clearly demonstrates that DGMARL optimization leads to significant reductions in CO2 emissions and fuel consumption. These findings highlight the positive impact of the DGMARL module on improving environmental impacts and fuel consumption.

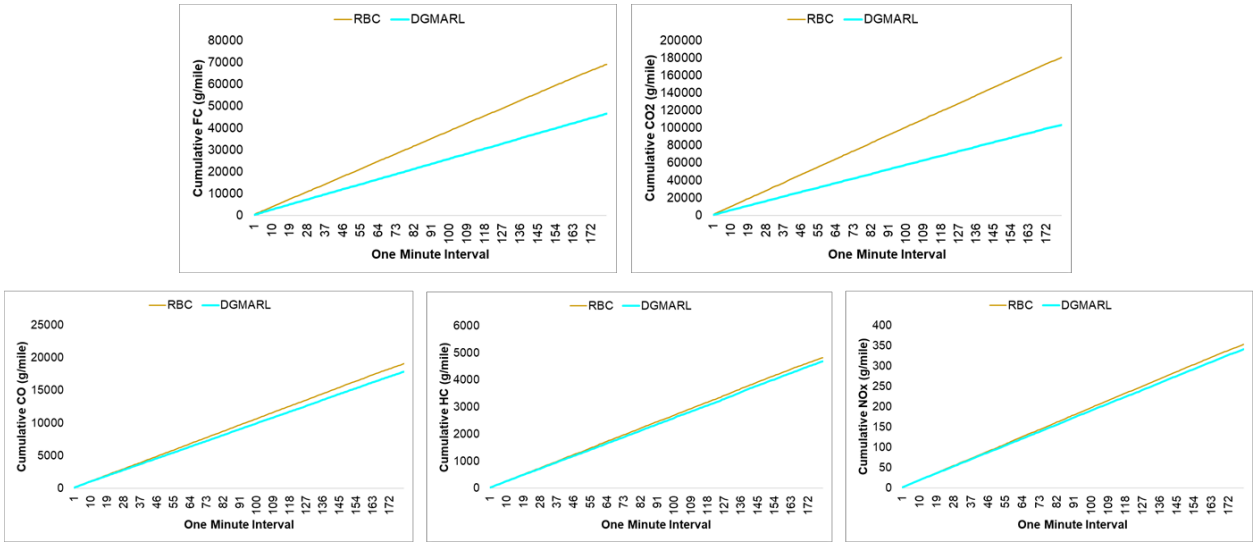

Figure 48: Cumulative emissions and FC

4.2.1 Evaluating FC and Emissions per Intersection

To delve into the fuel consumption (FC) and emissions per intersection, the network needed to be divided based on the links that connect to specific intersections. In essence, only links associated with the nodes were utilized for the analysis of emissions and FC at each intersection. The vehicle trajectories were meticulously tracked during the time they were present in the node, as illustrated in fig. 49. This approach allowed for a detailed examination of the emissions and FC at individual intersections.

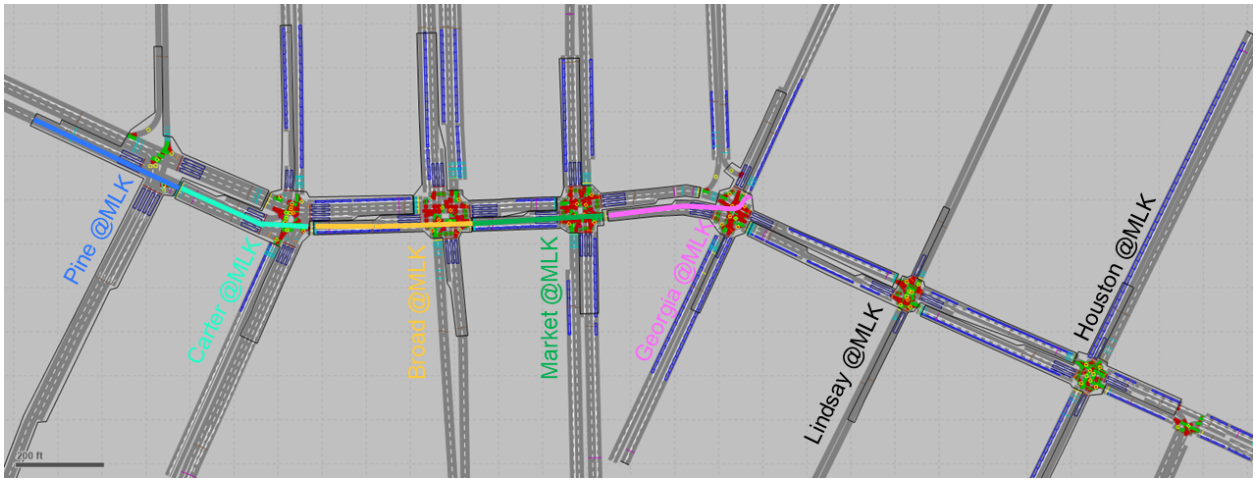

Fig. 49: FC and emissions analysis per intersection

The results from the analysis described earlier are presented in fig. 50. As observed, there is a slight increase in NOx emissions in the DGMARL model at certain intersections. However, in contrast, the other emissions and fuel consumption (FC) exhibit consistent reductions across almost all intersections. This outcome indicates that the DGMARL approach effectively mitigates environmental impacts and reduces FC in the majority of cases.

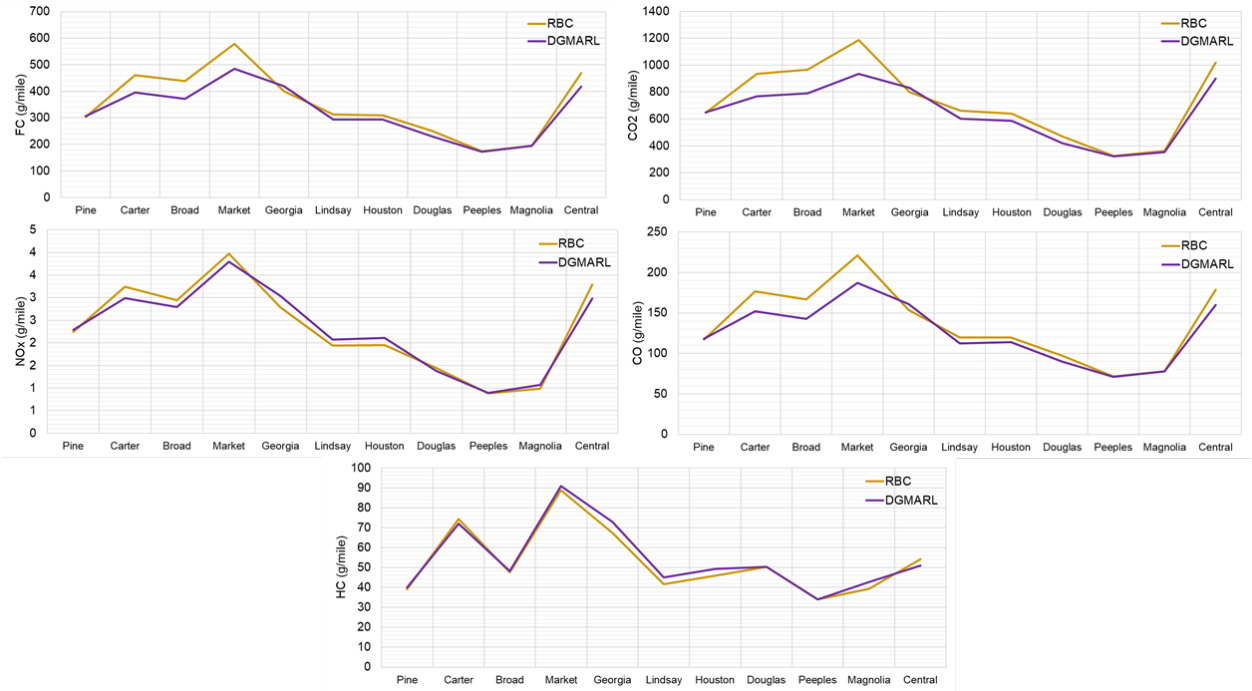

Fig. 50: CMEM results per intersection

Furthermore, the comparison between DGMARL and RBCs is illustrated in fig. 51. It can be observed that there are slight increases in HC and NOx emissions at certain intersections when using DGMARL, while at other intersections, there is a notable reduction in both FC and emissions. Moving forward, the UTC team will conduct a thorough investigation of critical intersections, such as Georgia, Lindsay, Houston, and Magnolia, to gain deeper insights into the performance of the optimization module at these intersections. This analysis will aid in identifying specific areas where further improvements can be made to reduce emissions and FC.

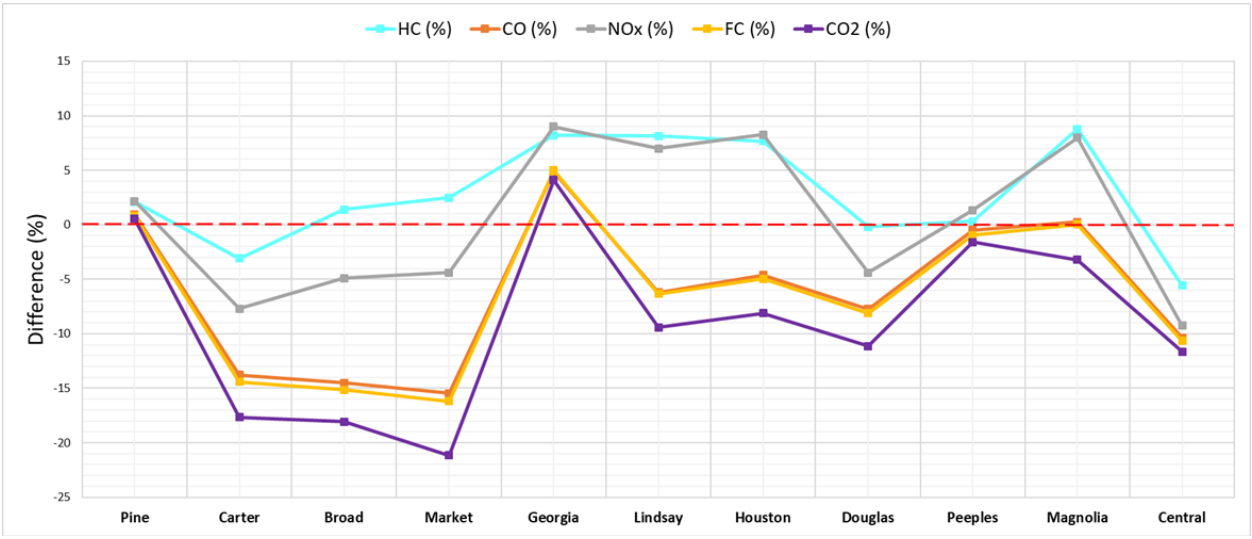

Fig. 51 Difference achieved by DGMARL per intersection

Despite certain intersections experiencing an increase in emissions, the overall environmental footprint at the intersections has been effectively reduced by nearly 10%. It is essential to bear in mind that table 18 encompasses all FC and emissions across the entire network,

whereas Table 18 focuses solely on the results per intersection, where the impact of DGMARL is most apparent. This distinction is crucial as the Eco-PI metric specifically quantifies the footprint generated at intersections due to traffic signal control.

Table 18: Average difference achieved across all intersections

Average Difference (%)				
HC	CO	NO_x	FC	CO_2
2.4%	-7.6%	-1.0%	-8.0%	-10.7%

5.3 Real-World Testing

Field implementation tests were critical to the development and testing of this project. These tests were instrumental in validating the practical functionality and reliability of the Eco-Adaptive Traffic Control System (Eco-ATCS) in field conditions. In fig. 52, the framework for online Eco-ATCS implementation is explained. First, the output from the UTC server is obtained through an API connection. DGMARL output is then converted to a readable version by NTCIP in the data reader module. The converted output contains second by second phase statuses. As such, information is sent to the main NTCIP module and then in the form of NTCIP message it is sent to the SEPAC m60 controller.

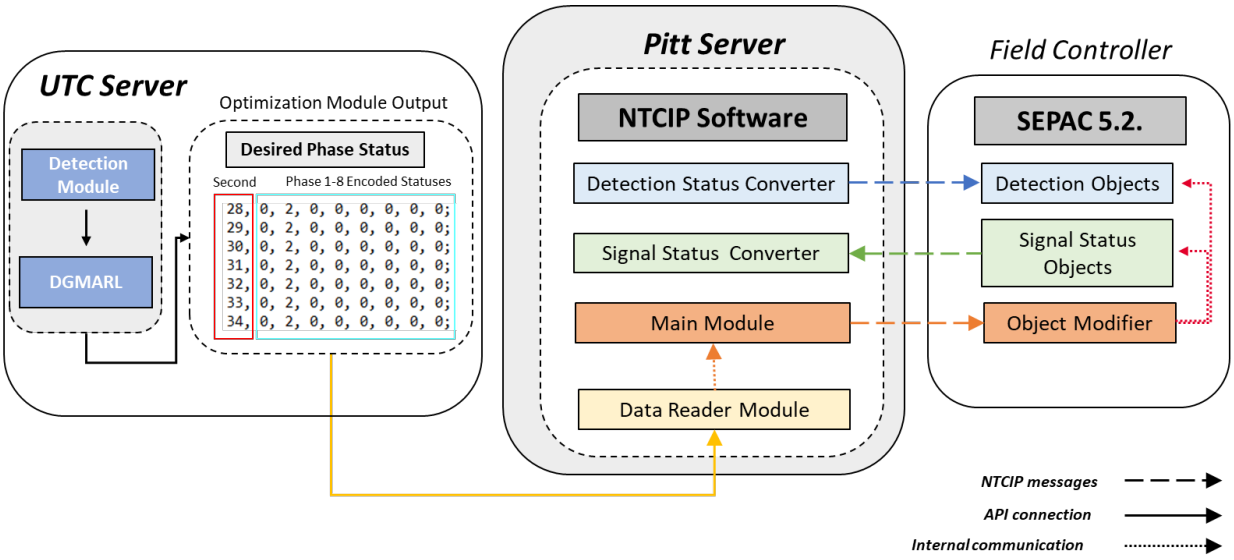

Fig. 52: Framework for Online Adaptive Logic Implementation

5.3.1 Field Testing of DGMARL and Development Updates

Our primary focus has been on field testing and enhancing data integration. Key developments include the creation of an interface to connect and read field inputs, particularly Signal Phase and Timing (SPaT) data and vehicle arrival information. SPaT data retrieved from GridSmart via a custom API developed by the CUIP data collection team, which has been successfully integrated with DGMARL. Vehicle arrivals are observed using Computer Vision, with the data collection team's custom API sending observed vehicle counts per lane to DGMARL to determine traffic

state and occupancy. Since the field testing only provides vehicle counts, DGMARL was updated with custom logic to estimate vehicle occupancy based on arrival patterns. Additionally, DGMARL has been untethered from VISSIM and is now connected to the field's SPaT configurations, incorporating specific parameters such as minimum green, yellow duration, red clearance, and pedestrian serving times. To ensure accurate time measurement for signal durations, DGMARL now uses the field controller's timestamp from the SPaT input.

We also enhanced DGMARL to handle pedestrian push button requests. This involved analyzing GridSmart input fields to determine the phase associated with a push button press. DGMARL was updated to prioritize pedestrian requests over vehicle demand and hold active requests if the current phase already has a green signal. This ensures all phases receive either a minimum green or pedestrian recall serving time.

Field testing, issue resolution, and integration were critical milestones. DGMARL was tested to align with NTCIP module expectations for signal status input. Integration testing involved three modules: Computer Vision for Vehicle Observation, DGMARL, and NTCIP, successfully conducted at the Peeples intersection in the MLK corridor. INitial testing on the LAB_M60 machine, using Georgia intersection signal timing plans, revealed issues like the left phase servicing problems and red flashing lights, which were resolved by adjusting lane index configurations and improving the NTCIP application code.

Following multiple trials on the LAB_M60 machine, testing moved to real intersections, starting with Peeples, where signal timing synchronization was verified. The scope was then expanded to include additional intersections–Peeples, Douglas, Houston, Georgia, Market, and Broad. This phase culminated in a successful demonstration on October 23, 2023, covering Lindsay, Georgia, Market, and Broad intersections, showcasing effective integration and control of real intersections with minimal vehicle queues and efficient pedestrian push button handling.

5.3.2 Tests Conducted in September 2023

The first test, the "Communication test," was conducted to ensure uninterrupted communication with the field controller located at Peeples @ MLK. Upon executing the NTCIP software developed by the Pitt team, we achieved consistent data reception from the controller. This successful test outcome confirmed that the Eco-ATCS was effectively and reliably communicating with the field controller, a pivotal step in the system's real-world deployment.

The second test, known as the "Detection suppression test," aimed to prevent the Gridsmart system from initiating detection calls. Initially, we intended to modify the dynamic value of the detection calls object through NTCIP software, which would normally register as zero when no detection calls were present but would change when a detection call occurred, such as when a car was detected in a specific phase. However, we encountered an obstacle in the form of the City of Chattanooga's SEPAC software version 5.2, which did not support this object. In our lab tests, we had used SEPAC 5.3, which did include this functionality. Consequently, the Gridsmart system was able to place calls during this field test, resulting in an unsuccessful outcome. For subsequent tests in September 2023, we manually disconnected Gridsmart by adjusting the port settings of the controller.

The third test involved the "use of commands," where our objective was to ensure the successful placement of "Hold," "Call," and "Force Off" commands to field controller through NTCIP software. During this test, we executed these commands without any issues, marking it as a successful test. This successful validation of command execution is crucial as it demonstrates the NTCIP software's capability to respond to DGMARL instructions effectively and implement those instructions in the field controller.

Finally, the actual implementation test was conducted with the main objective of ensuring that the integration of the DGMARL and NTCIP software could effectively control an intersection. Initially, the plan was to facilitate the integration of DGMARL and NTCIP through a common file. This file was intended to be created and written by DGMARL, and then read by NTCIP software. However, during the field test, a simple issue arose when both DGMARL and NTCIP software attempted to access the file. As a result, an API was developed to facilitate information exchange between DGMARL and NTCIP software. In this API setup, DGMARL employs the 'SET' command to specify the desired phase status, while NTCIP software uses the 'GET' command to read this desired phase status. The desired phase status defined by DGMARL comprises four statuses: red, yellow, green, and the next green. The NTCIP software successfully matched the phase status in the controller with the desired phase statuses identified by DGMARL.

Throughout the tests conducted in September, the objective of controlling an intersection was achieved. The testing process unfolded in several steps. Firstly, we tested the communication between the field controller and the NTCIP software. Once we had confirmed the stability of this

communication, we proceeded with the detection suppression test. The third step involved verifying the successful implementation of commands like “Hold”, “Call”, and “Force Off”. Finally, we conducted the intersection control test, during which it became evident that the integration of NTCIP software and DGMARL was capable of effectively controlling an intersection.

However, it is worth noting that these tests revealed several issues. For instance, the detection suppression test did not yield the desired results. Therefore, we manually disabled the GridSmart system by adjusting the port settings of the controller. Additionally, DGMARL encountered challenges in serving pedestrian demand at intersections lacking pedestrian recalls. Considering these issues, we have scheduled an additional week of testing in October to address and resolve these issues.

5.3.3 Tests Conducted in October, 2023

During the field tests conducted in October, the GridSmart detection system was manually disabled to suppress detection calls. The primary goal was to automate this process, as well as to enable the automatic activation of the GridSmart detection system when needed. To achieve this, the NTCIP software underwent modifications. The new version of the NTCIP software was initially tested at PITTS Lab using the Siemens m60 controller with SEPAC 5.3. Subsequently, it underwent testing at the UTC research center, this time with a Siemens m60 controller equipped with SEPAC 5.2. In both instances, the modified NTCIP software successfully managed the disabling and enabling of the GridSmart detection system. Following these initial steps, the new version of the NTCIP software was employed for all the tests described below.

The UTC team was tasked with integrating pedestrian push button calls into DGMARL. Once this integration was complete, an initial test was planned using a controller located in the UTC research center. This controller was mimicking the traffic controller at Georgia @ MLK. DGMARL received real-time traffic data throughout the testing process. In addition to real traffic data, pedestrian push button calls were generated using additional equipment attached to the controller, which allowed for the placement of both vehicle and pedestrian calls.

The goal of this test was to ensure that DGMARL could receive information regarding pedestrian push button calls and allocate sufficient green time for pedestrians. During the tests, all pedestrian push button calls were successfully served, indicating the test's success.

The integration of pedestrian push button calls was initially tested at Peeples @ MLK in the field, given its lower pedestrian demand. To confirm the presence of a pedestrian push button call, a UTC lab member initiated a test pedestrian call. The primary objective was to ensure that pedestrian push button calls were effectively serviced. It was observed that DGMARL could provide adequate green time when pedestrians were waiting for service, thus confirming the success of this test. Subsequently, the same test was conducted for the intersections at Houston @ MLK, Douglas @ MLK, and Lindsay @ MLK. In each case, the integration of DGMARL and NTCIP software successfully allocated sufficient green time for pedestrians.

During the field tests, it was observed that if a vehicle call had been placed by GridSmart previously, it was not possible to remove that call. Consequently, DGMARL's desired phase status could differ from the controller's phase status. The phase sequence was not entirely under DGMARL's control due to existing vehicle calls. To address this issue, in addition to Hold, Force Off, and Call commands, the Omit command was introduced. With the implementation of the Omit command, the phase sequence became fully controllable. For example, if a Hold command was issued for a phase, other phases were omitted. When it was necessary to change the active phase, the Omit command was removed for the next phase, and a Call command was placed for that phase. Additionally, a Force Off command was issued for the current running phase. This way, whenever it was necessary to change the running phase, only the next phase, as determined by DGMARL, became available, and the controller was compelled to serve the phase specified by DGMARL.

The modified version of the NTCIP software was initially tested using the controller located at the UTC research center. During this test, it was observed that, even in the presence of calls, the controller followed the phase sequence determined by DGMARL. Consequently, the test was successful.

Following this, the modified NTCIP software was tested at Georgia @ MLK, Broad @ MLK, and Market @ MLK intersections. These intersections were selected because they experience higher vehicle and pedestrian demand compared to others. Therefore, these intersections had calls placed by GridSmart before DGMARL started operating. During these tests, it was confirmed that the phase sequence was controlled by DGMARL, and the integration of DGMARL and NTCIP software successfully managed these intersections individually.

The final test was to control multiple busier intersections. The main goal was to ensure that the integration of DGMARL and NTCIP software could control multiple intersections simultaneously, while also ensuring that pedestrians were being served. In this test, the DGMARL and NTCIP software integration successfully controlled Georgia @ MLK, Broad @ MLK, and Market @ MLK intersections.

Section 6: Conclusion

This project has successfully addressed key challenges associated with optimizing traffic signal control in urban environments. Through the integration of connected vehicle (CV) and connected infrastructure (CI) communication technologies, and leveraging recent advances in AI, optimization, and edge computing, we have developed a sophisticated adaptive traffic signal control system to reduce fuel consumption and improve traffic flow.

The primary accomplishments of this project can be summarized into several achievements, each contributing to the goal of sustainable urban traffic management.

- Advanced System Development: The DGMARL system was developed to formulate the traffic signal control problem as a Multi-Agent Markov Decision Process. The architecture integrated AI technologies such as the Advantage Actor Critic (A2C) reinforcement learning model. This system successfully modeled intersections and coordinated signal timing to minimize environmental impacts, thereby optimizing traffic flow and reducing emissions.
- Development of Fuel Consumption Performance Index (Eco FC-PI): The FC-PI was developed as a critical component for evaluating the system's impact on fuel consumption and emissions. This metric provided a means for understanding the relationship between traffic signal control and the reduction of fuel consumption.
- Extensive Testing and Validation: The system was tested through a series of experiments that included both Software-in-the-Loop (SIL) and Hardware-in-the-Loop (HIL) simulations, followed by real-world testing on the MLK Smart Corridor, an urban corridor managed by the University of Tennessee at Chattanooga (UTC). The system's performance was validated under real-world conditions demonstrating significant improvements in both operational efficiency and environmental metrics.
- Digital Twin Development: A three-tier twin system was developed to enable real-time traffic simulation and optimization. This digital twin framework consisted of pre-populated offline simulations, pseudo-real-time simulations driven with archived data, and real-time simulations using live field data streams. Each tier incrementally increased the complexity and capability of the system, ultimately enabling for a real-time traffic management model

- Real-World Field Deployment: One of the most significant aspects of this research was the field deployment of the developed Eco-Adaptive Traffic Control System (Eco-ATCS). Successful integration with actual traffic controllers, pedestrian systems, and dynamic data streams demonstrated the system's readiness for real-world deployment.

Challenges and Lessons Learned

- Integration Complexity: one of the significant challenges encountered was the integration of the DGMARL model with existing traffic infrastructure. The project required considerable efforts to align various components, such as pedestrian recalls, signal phasing, and adaptive timing. Addressing these integration challenges has provided valuable insights into the requirements for deploying AI-based traffic solutions at scale.
- Pedestrian System Limitations: Initially, pedestrian push-button systems were not effectively integrated,leading to limitation in serving pedestrian demand at intersections without pedestrian recalls. Through multiple testing phases, we were able to develop mechanisms that ensured pedestrian requests were served adequately, but these initial setbacks underscored the importance of comprehensive, cross-system integration.
- Model Training and Real-World Adaptation: The adaptation of the DGMARL model to match the real-world requirements posed challenges in training and retraining, particularly due to differences between simulation environments and the actual physical environment. This highlighted the need for adaptable training methods that incorporate field-specific constraints, such as traffic dynamics, pedestrian movement, and infrastructure variability.

Broader Impacts

The results of this project have implications beyond traffic management and urban mobility. By developing technologies that reduce fuel consumption and emissions, this project aligns with broader efforts to combat climate change and promote sustainability in urban spaces. Furthermore, the deployment of AI-drive systems provides a blueprint for integrating emerging technologies in city infrastructure in many ways beyond traffic management.

Section 7: Future Work

Continued Development of DGMARL and Eco-ATCS

The DGMARL framework demonstrated success in coordinating multiple intersections through a decentralized graph-based, multi-agent reinforcement learning approach. Future work could expand on this by refining integration testing with real-time data and improving adaptability to fluctuating traffic patterns using reinforcement learning adjustments. Additionally, enhancements such as incorporating pedestrian recall, minimum green duration, and improved phase sequence controls were partially implemented and could be expanded to optimize performance in diverse traffic conditions.

Expansion of Fuel Consumption Performance Index (FC-PI)

The development of FC-PI involved significant testing of operational conditions impacting fuel consumption, such as road gradient and vehicle types. Future directions might include expanding the FC-PI to account for additional pollutants like CO2 and PM, and refining regression models to better align with real-world conditions. Additional testing on road gradient and varying fleet compositions may further validate and enhance the FC-PI, particularly in mixed traffic environments

Digital Twin Expansion and Real-Time Testing

Further development of the digital twin model, particularly with integration into ORNL's HIL (Hardware-in-the-Loop) framework, is recommended. The current VISSIM-based model has successfully been tested for compatibility with CarMaker for real-time vehicle simulation, but real-time application has shown limitations due to software compatibility. Future efforts should aim to overcome these limitations and improve the model's real-time adaptability for broader application in connected vehicle environments.

Advanced Field Testing and Scalability

The next steps involve enhancing DGMARL's field testing capabilities by leveraging real-time data from traffic monitoring systems like GRIDSMART and improving the latency in vehicle occupancy data processing. The integration with systems such as Flask-based RESTful API has already shown promise for real-time adaptability, suggesting scalability to larger traffic networks if latency concerns can be mitigated.

Public Engagement and Policy Integration

To ensure the system's success, public engagement and policy considerations will be crucial. The model's data, including fuel consumption and emissions reduction metrics, could be valuable for demonstrating benefits to stakeholders and policymakers. Expanding community outreach and engagement with the city planning departments for further alignment with local and federal energy-conscious traffic management initiatives could also enhance long-term adoption

Section 8: References

[1] M. Hunter, Vissim Simulation Guidance, Final Report, Georgia Department of Transportation, Atlanta, Georgia, 2021. Available: https://rosap.ntl.bts.gov/view/dot/60642

[2] C. S. Bauer, "Some Energy Considerations in Traffic Signal Timing," Traffic Eng., vol. 45, no. 2, pp. 19–25, Feb. 1975.

[3] K. G. Courage and S. M. Parapar, "Delay and fuel consumption at traffic signals," Traffic Eng., vol. 45, no. 11, pp. 23–27, 1975.

[4] D. I. Robertson, C. F. Lucas, and R. T. Baker, Coordinating Traffic Signals to Reduce Fuel Consumption, Report 934, Transport and Road Research Laboratory, Crowthorne, Berkshire, 1980.

[5] S. Reljic, M. Kamhi-Barna, and S. Stojanovic, "Multicriteria signal plan choice at an isolated intersection," in Mathematics in Transport Planning and Control, Cardiff, 1992, pp. 81–93.

[6] McTrans, TRANSYT-7F Users Guide, 2008.

[7] PTV America, PTV VISTRO User Manual, vol. 2, 2014.

[8] D. Husch and J. Albeck, Synchro Studio 7 User Guide, Trafficware, 2006, 522 p.

[9] R. Akcelik, "Fuel efficiency and other objectives in traffic system management," Traffic Eng. Control, vol. 22, no. 2, pp. 54–65, 1981.

[10] D. Ma and H. Nakamura, "Cycle length optimization at isolated signalized intersections from the viewpoint of emission," in Traffic and Transportation Studies 2010, pp. 275–284.

[11] P. J. Claffey, Running Costs of Motor Vehicles as Affected by Road Design and Traffic, National Cooperative Highway Research Program Report 11, 1971.

[12] J. A. Bonneson, M. P. Pratt, and M. A. Vandehey, Predicting the performance of automobile traffic on urban streets, Final Report of NCHRP Project, 3-79, 2008.

[13] N. Dobrota, A. Stevanovic, and N. Mitrovic, "Development of assessment tool and overview of adaptive traffic control deployments in the US," Transp. Res. Rec., vol. 2674, no. 12, pp. 464–480, 2020.

[14] A. Stevanovic, N. Dobrota, and N. Mitrovic, NCHRP 20-07/Task 414: Benefits of Adaptive Traffic Control Deployments-A Review of Evaluation Studies, Technical Report, Final Report, Transportation Research Board of the National Academies, Washington, DC, 2019.

[15] P. B. Hunt, D. I. Robertson, R. D. Bretherton, and R. I. Winton, SCOOT-a traffic responsive method of coordinating signals, LR 1014 Monograph, 1981.

[16] N. H. Gartner, OPAC: A demand-responsive strategy for traffic signal control, Report 906, 1983.

[17] P. R. Lowrie, SCATS, Sydney Coordinated Adaptive Traffic System: A traffic responsive method of controlling urban traffic, 1990.

[18] P. Mirchandani and L. Head, "A real-time traffic signal control system: architecture, algorithms, and analysis," Transp. Res. Part C: Emerging Technol., vol. 9, no. 6, pp. 415–432, 2001.

[19] F. Luyanda, D. Gettman, L. Head, S. Shelby, D. Bullock, and P. Mirchandani, "ACS-Lite algorithmic architecture: applying adaptive control system technology to closed-loop traffic signal control systems," Transp. Res. Rec., vol. 1856, no. 1, pp. 175–184, 2003.

[20] A. Stevanovic, J. Stevanovic, K. Zhang, and S. Batterman, "Optimizing traffic control to reduce fuel consumption and vehicular emissions: Integrated approach with VISSIM, CMEM, and VISGAOST," Transp. Res. Rec., vol. 2128, no. 1, pp. 105–113, 2009.

[21] J. Kwak, B. Park, and J. Lee, "Evaluating the impacts of urban corridor traffic signal optimization on vehicle emissions and fuel consumption," Transp. Plan. Technol., vol. 35, no. 2, pp. 145–160, 2012.

[22] P. Lertworawanich and P. Unhasut, "A CO emission-based adaptive signal control for isolated intersections," J. Air Waste Manag. Assoc., vol. 71, no. 5, pp. 564–585, 2021.

[23] A. Stevanovic, S. A. Shayeb, and S. S. Patra, "Fuel Consumption Intersection Control Performance Index," Transp. Res. Rec., vol. 03611981211004181, 2021.

[24] PTV Group, PTV Vissim 2020 User Manual, 2020.

[25] P. Sa Hosseini and K. Savla, "A comparison study between proportionally fair and max pressure controllers for signalized arterial networks," Transp. Res. Board Ann. Meeting, Paper No. 16-6738, 2016.

[26] S. B. Al Islam, A. Hajbabaie, and H. A. Aziz, "A real-time network-level traffic signal control methodology with partial connected vehicle information," Transp. Res. Part C: Emerging Technol., vol. 121, art. no. 102830, 2020.

[27] X. Sun and Y. Yin, "A simulation study on max pressure control of signalized intersections," Transp. Res. Rec., vol. 2672, no. 18, pp. 117–127, 2018.

[28] A. Stevanovic, Adaptive traffic control systems: domestic and foreign state of practice, 2010.

Section 9: Appendices

Appendix A: Figures

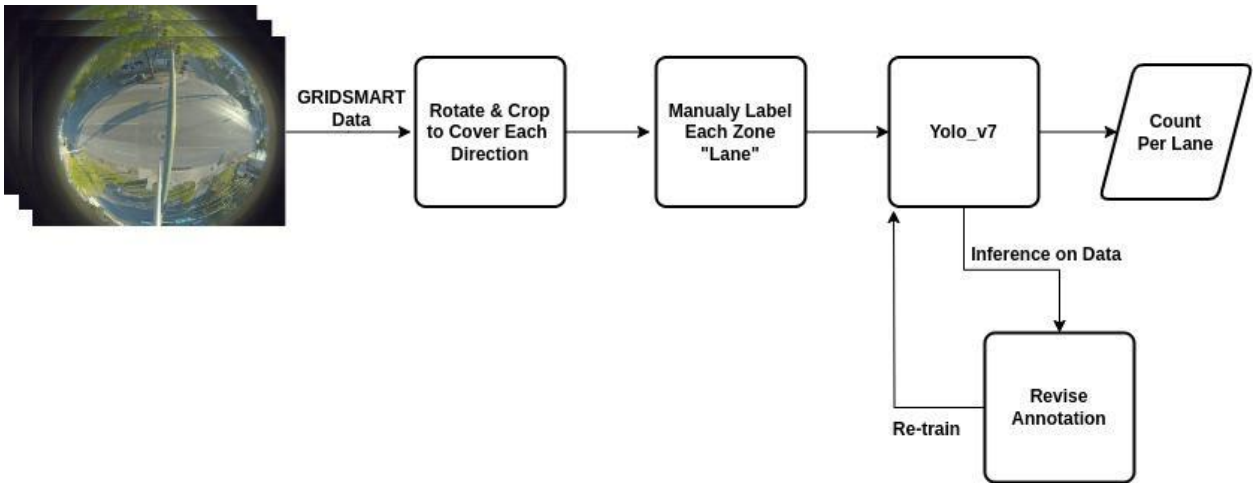

Fig. 1: System Pipeline

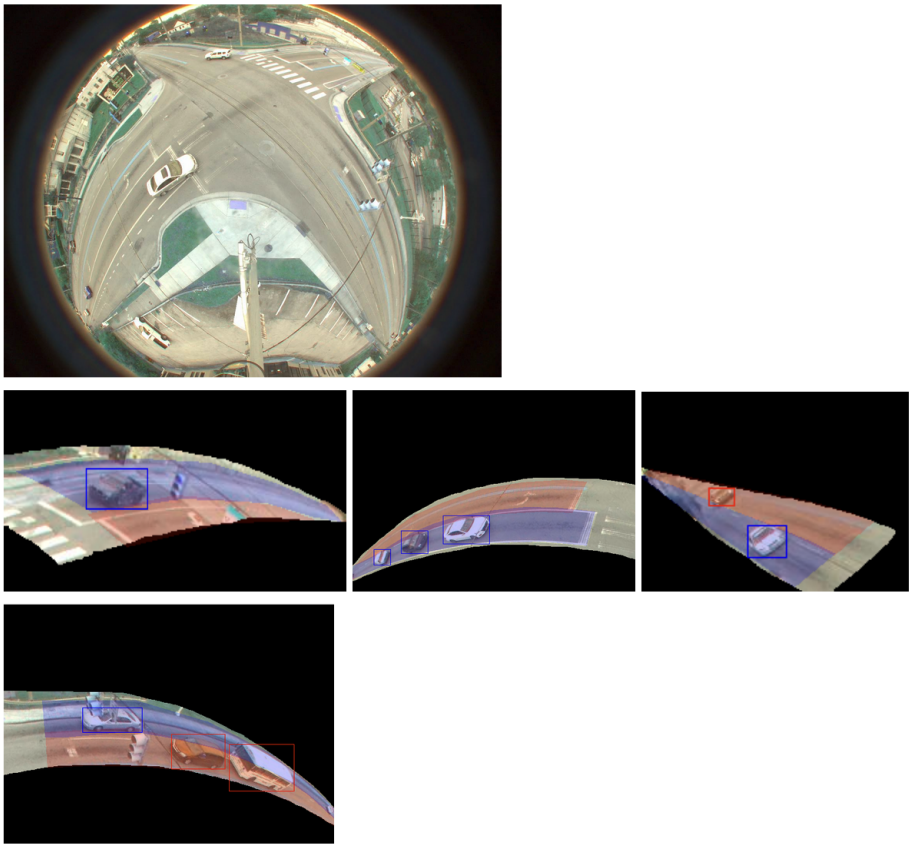

Fig. 2: Intersection at MLK Blvd and Central Ave.

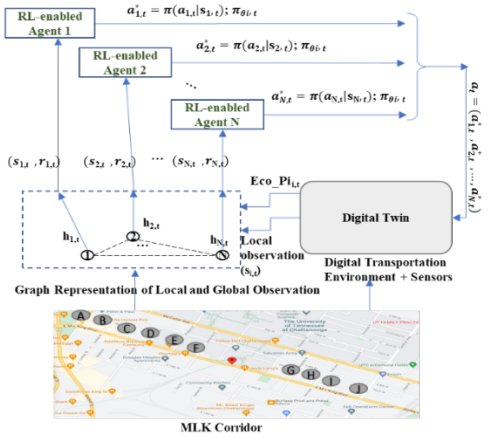

Fig. 3: DGMARL Architecutre

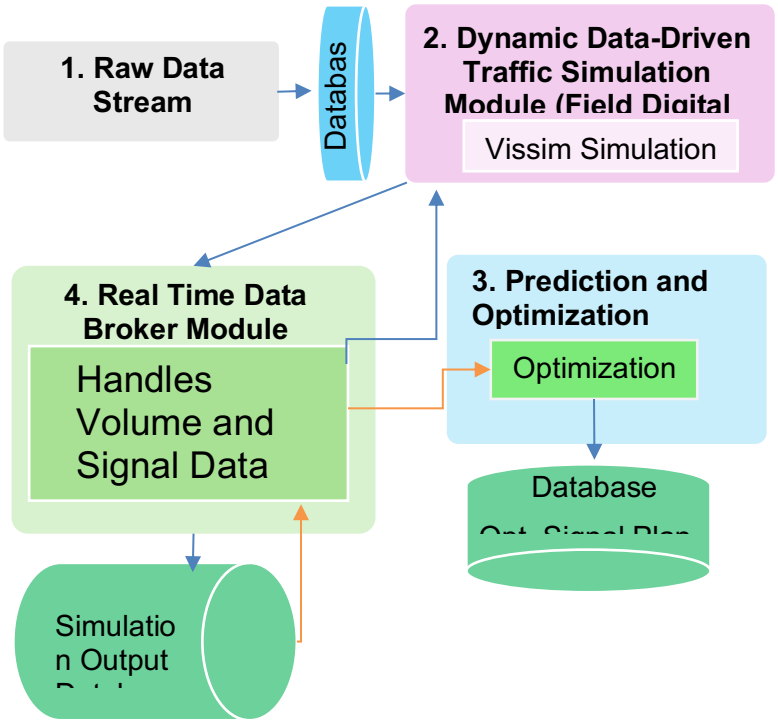

Fig. 4: Digital Twin Architecture

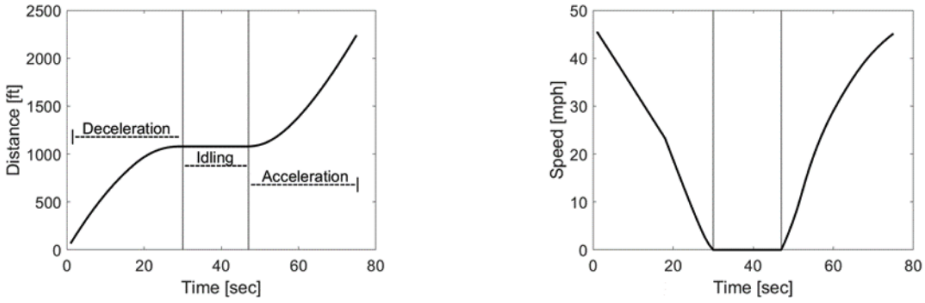

a) Distance-time (stop) profile b) Speed profile

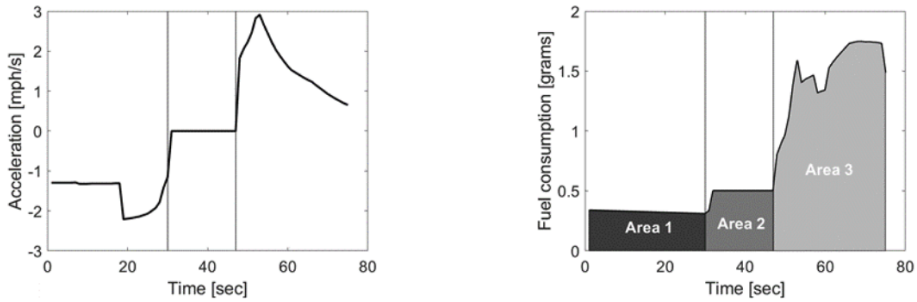

c) Deceleration-acceleration profile d) Fuel consumption profile

Fig. 5: Dynamics and Kinematics of a Stopped Vehicle

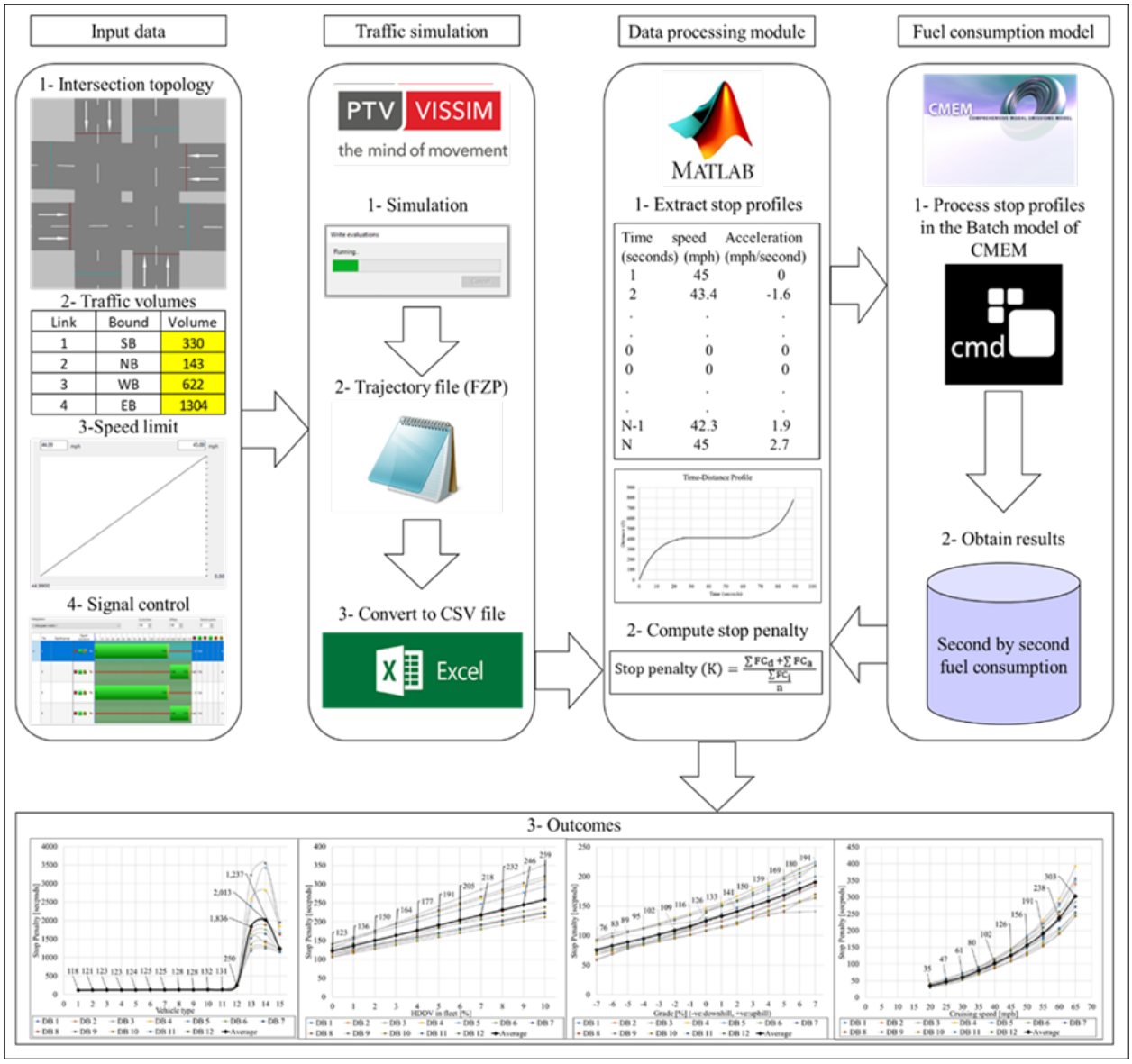

Fig. 6: VISSIM-Matlab-CMEM connection

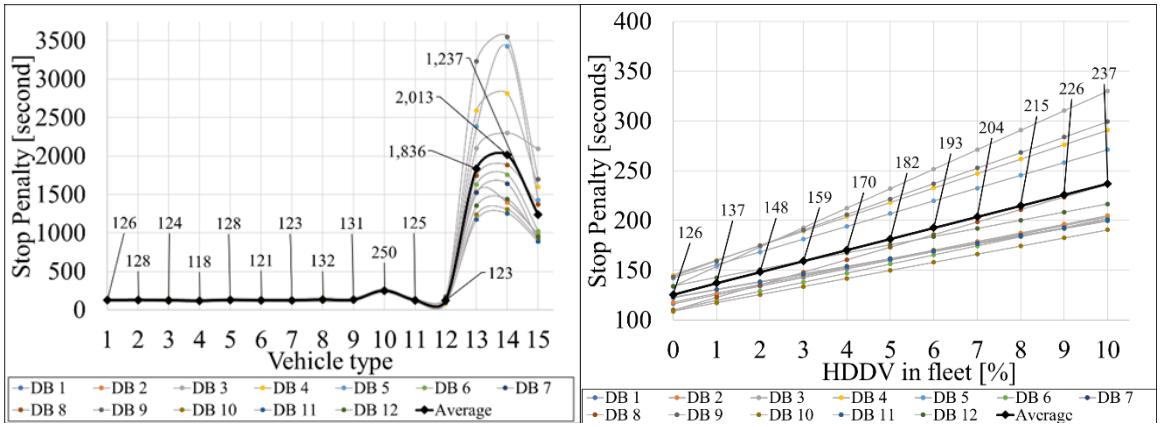

a)vehicle type b) fleet distribution

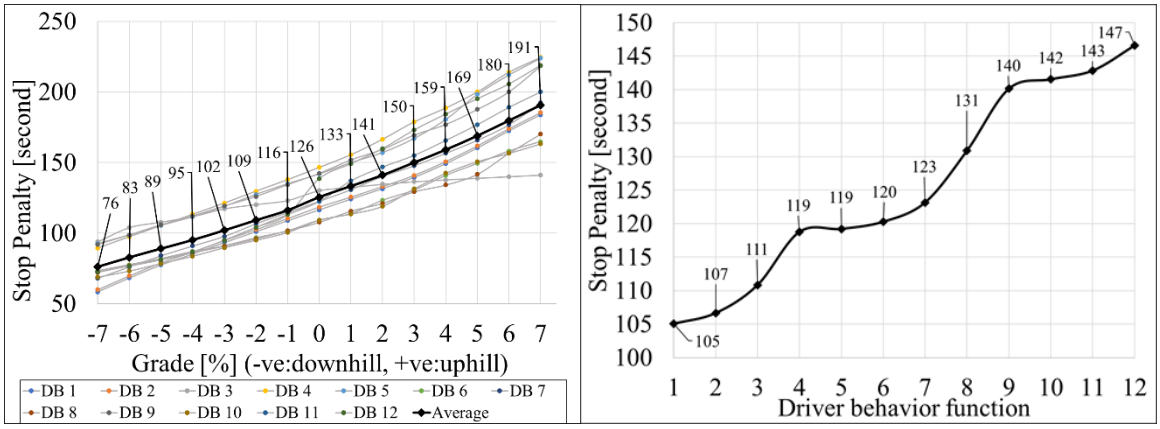

c) road gradient d) driving behavior

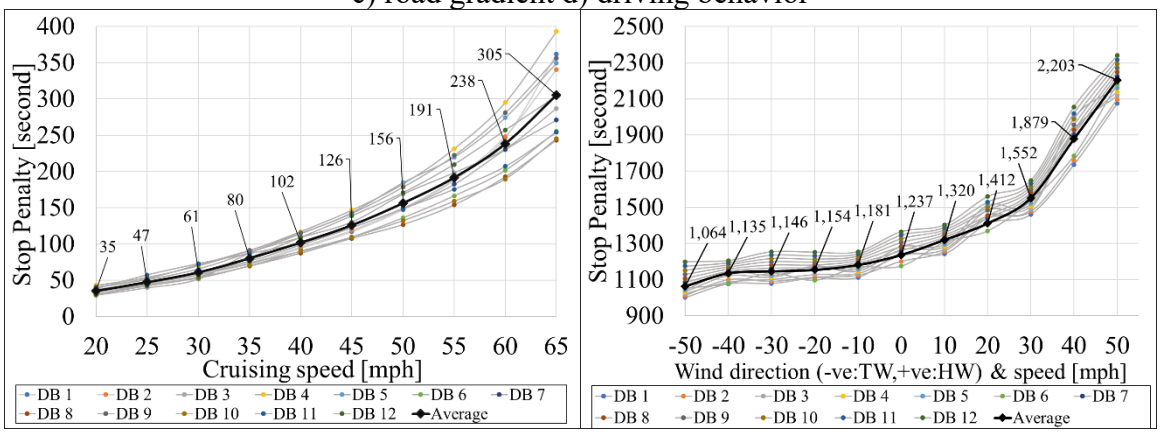

e) cruising speed f) wind effect

Fig.7: Impact of various operational condition on stop penalty (K); DB: driver behavior

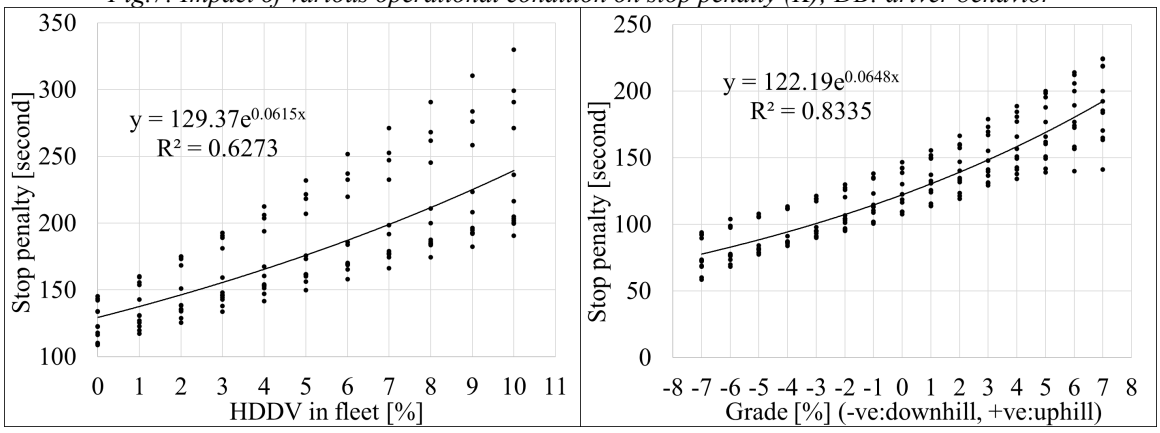

a)percentage of HDDVs in fleet b) slope during acceleration phase

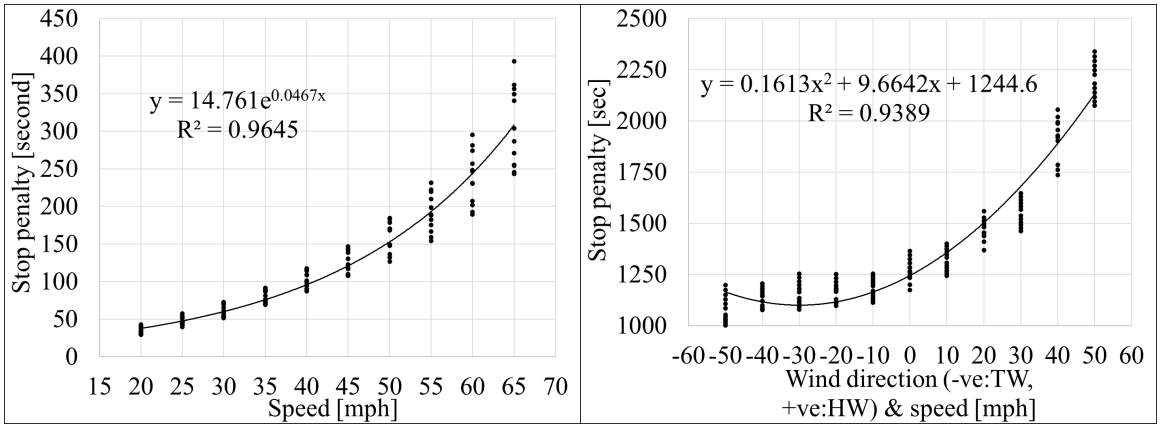

c) cruising speed d) aerodynamic effect of wind speed and direction

Fig. 8: Regression models to computer stop penalty

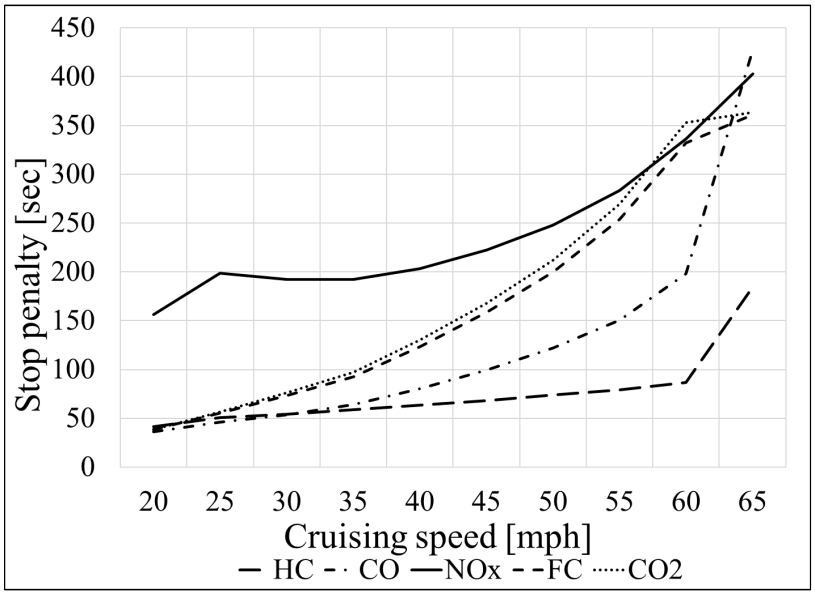

Fig. 9: Impact of a single stop-and-go event of excess emissions

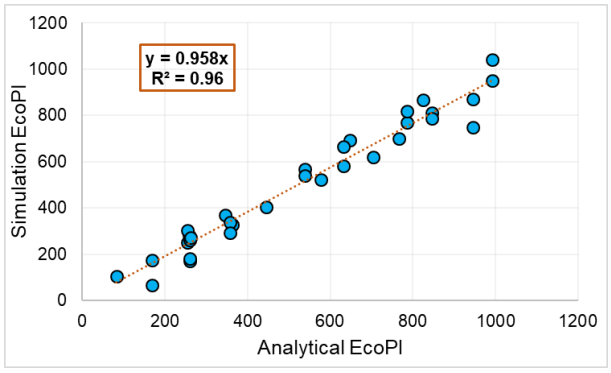

a) Main street exclusive phases

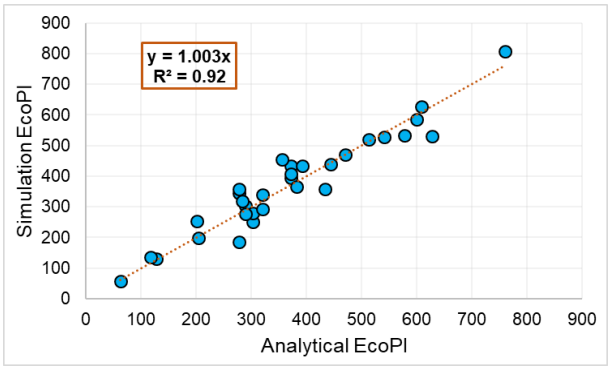

b) Side street exclusive phases

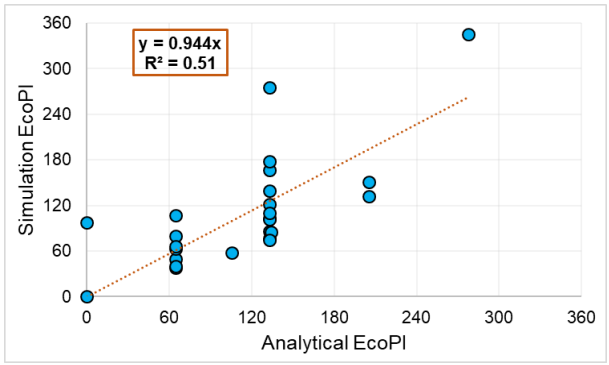

c) Main street in protected/permitted phases

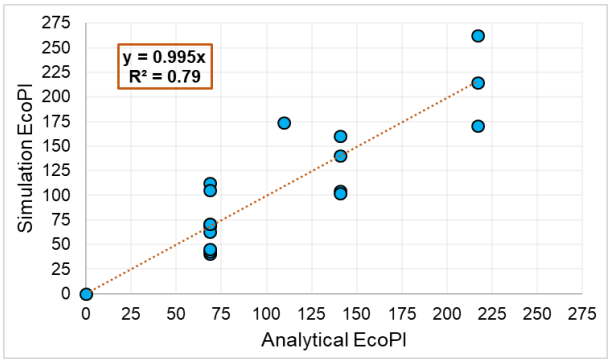

d) Side street protected/permitted phases

Fig. 10: Comparison between analytically derived and ground truth EcoPI

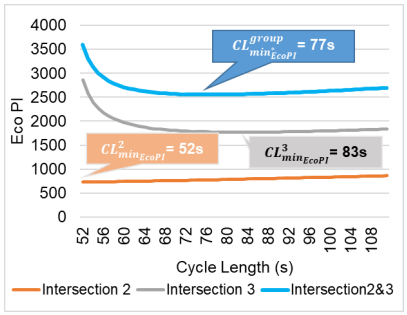

a) Cycle 1

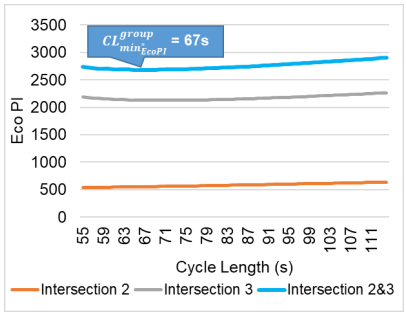

b) Cycle 2

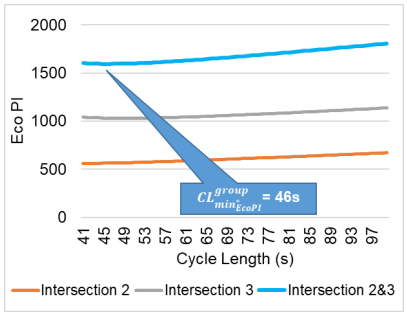

c) Cycle 3

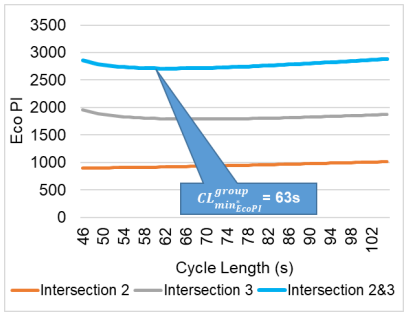

d) Cycle 4

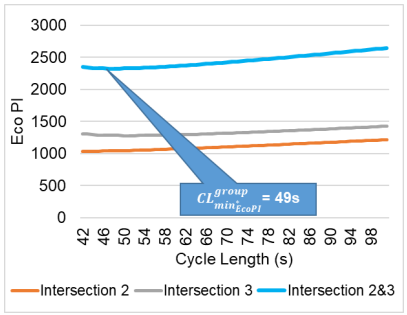

e) Cycle 5

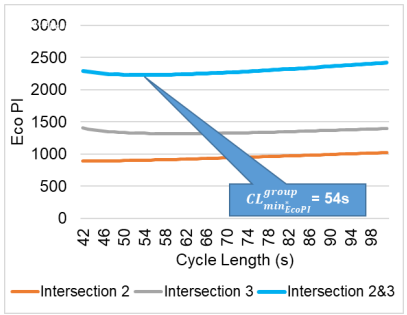

f) Cycle 6

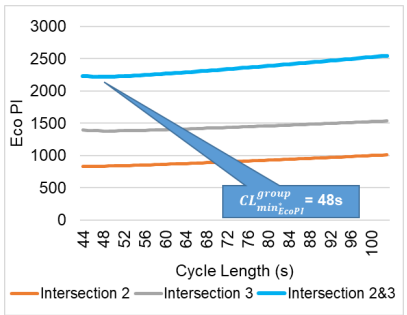

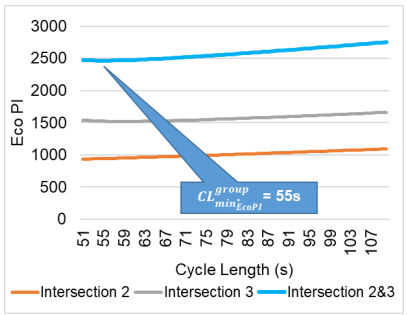

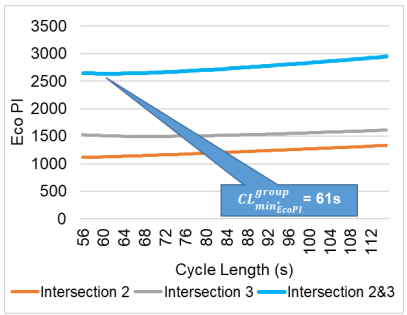

Node	Avg. Actuated	Avg. Eco_Pi	Avg. Eco_Pi % Improvement
Pine	22681.66	21303.76	6.07%
Carter	53663.61	30104.53	43.90%
Broad	63145.29	39928.84	36.77%
Market	68661.05	42168.49	38.58%
Georgia	43645.22	37380.67	14.35%
Lindsay	20206.95	12376.34	38.75%
Houston	15349.9	10990.3	28.40%
Douglas	17793.43	11099.54	37.62%
Peeples	1203.596	1079.455	10.31%
Magnolia	4765.637	3555.876	25.39%
Central St	79283.93	63774.6	19.56%
Total	**390400.3**	**273762.4**	**29.88%**

g) Cycle 7 *h) Cycle 8* *i) Cycle 9*

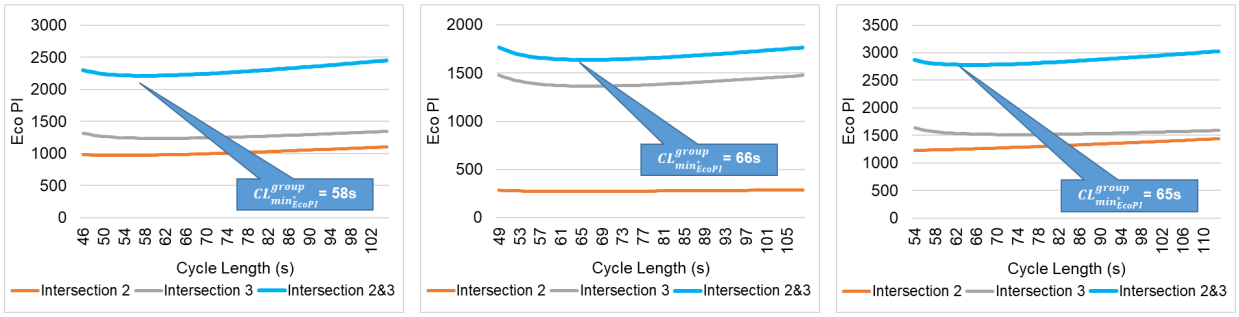

j) Cycle 10 *k) Cycle 11* *l) Cycle 12*

Fig. 11: Impact of non-critical and critical intersection CLs on minimum group CLs

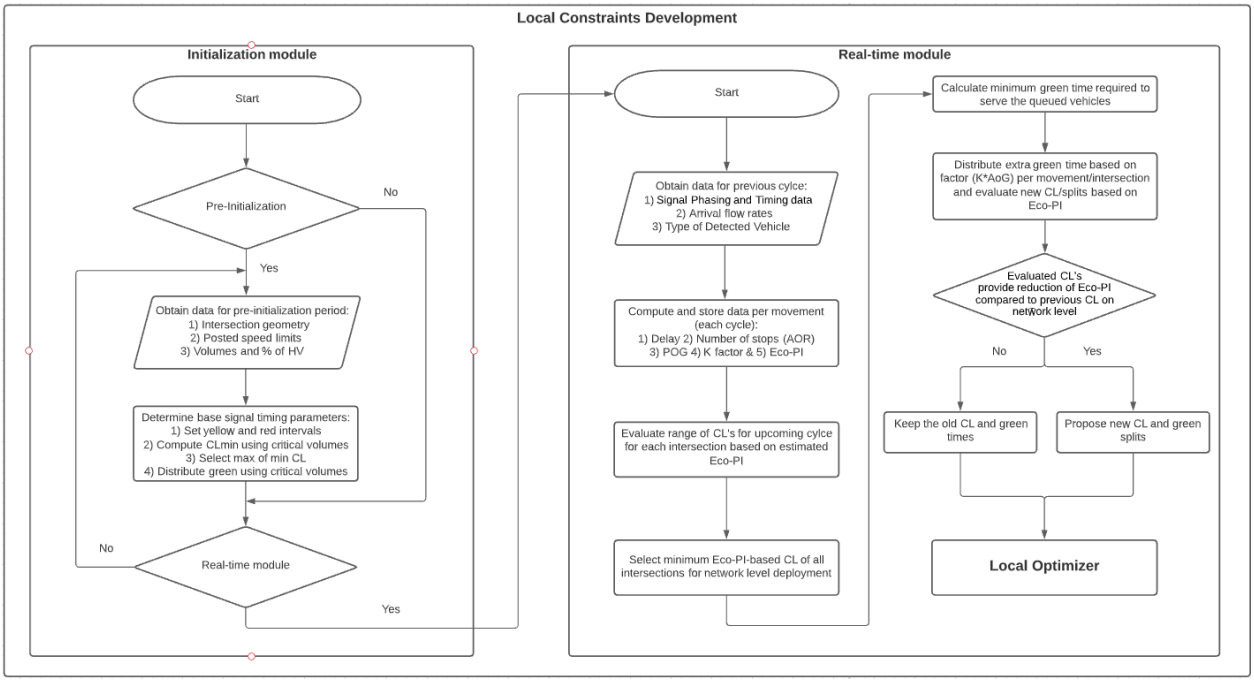

Fig. 12: Framework for Local Constraints Development

Fig. 13: PM-Peak 3-hour Eco0PI; Data: 12/15/2022

Simulation resolution: 1 second; Random seeds: 12, 25, 45, 41, 32, 37, 27, 44, 29, 22

Node	Avg. Actuated	Avg. Eco_Pi	Avg. Eco_Pi % Improvement
Pine	22681.66	21303.76	6.07%
Carter	53663.61	30104.53	43.90%
Broad	63145.29	39928.84	36.77%
Market	68661.05	42168.49	38.58%
Georgia	43645.22	37380.67	14.35%
Lindsay	20206.95	12376.34	38.75%
Houston	15349.9	10990.3	28.40%
Douglas	17793.43	11099.54	37.62%
Peeples	1203.596	1079.455	10.31%
Magnolia	4765.637	3555.876	25.39%
Central St	79283.93	63774.6	19.56%
Total	390400.3	273762.4	29.88%

Seed	Node	Actuated	DGMARL	Eco_Pi %
25	Peeples	1140.254	1266.929	-11.11%
45	Pine	23362.24	23609.16	-1.06%
27	Peeples	1094.578	1320.751	-20.66%
29	Pine	22963.07	23901.18	-4.09%

Fig. 14: Pine and Peeples Eco-PI impact

dgmarl_signalstatus_9065_test_10800_seed_21_2_1 - Notepad

File Edit Format View Help

```
Signal Status

Date: 2023-04-24 09:35:32.951739
Vissim File: D:\Viji\NEWVissim_December2022\SentBy_Somdut\2023-04-12_PM-peak_Dec15-2022_Model\MLKCorridor_PMpeak_2022-12-15_v5.inpx
Time: 0 - 10800
Seed: 21

Intersection : 2
Signal Groups : 1, 2, 3, 4, 19

0.0, 0, 0, 0, 0, 0, 0, 0, 0, 0, 0;
0.1, 0, 0, 0, 0, 0, 0, 0, 0, 0, 0;
0.1, 0, 0, 0, 0, 0, 0, 0, 0, 0, 0;
0.2, 0, 0, 0, 0, 0, 0, 0, 0, 0, 0;
0.2, 0, 0, 0, 0, 0, 0, 0, 0, 0, 0;
0.3, 0, 0, 0, 0, 0, 0, 0, 0, 0, 0;
0.3, 0, 0, 0, 0, 0, 0, 0, 0, 0, 0;
0.4, 0, 0, 0, 0, 0, 0, 0, 0, 0, 0;
0.4, 0, 0, 0, 0, 0, 0, 0, 0, 0, 0;
0.5, 0, 0, 0, 0, 0, 0, 0, 0, 0, 0;
0.5, 0, 0, 0, 0, 0, 0, 0, 0, 0, 0;
0.6, 0, 0, 0, 0, 0, 0, 0, 0, 0, 0;
0.6, 0, 0, 0, 0, 0, 0, 0, 0, 0, 0;
```

Fig. 15: Signal Timing Output

```
sim second; p1, p2 ,p3, p4, p5, p6, p7, p8, p17, p19;

Example:
1; 0, 2, 0, 2, 0, 0, 0, 0, 0, 0; meaning: phase 2 and 4 are green, other phases are red
2; 0, 1, 0, 1, 0, 0, 0, 0, 0, 0; meaning: phase 2 and 4 are amber, other phases are red
.
.
6; 0, 0, 0, 0, 0, 0, 0, 0, 0, 0; meaning: phase 1-8 all red
.;....;
.;....;
.;....;
duration of simulation [sec];....;

where:
p1 - signal status of phase (signal group) 1
p2 - signal status of phase (signal group) 2
.
.
.
p8 - signal status of phase (signal group) 8
p17 - signal status of phase (signal group) 17
p19 - signal status of phase (signal group) 19

Code the output in the following way:
0 - red
1 - amber
2 - green

If a phase (signal group) does not exist on intersection, put 0 (red) for that phase at each simulation second.
Please note that phase = signal group in our case.
```

Fig. 16: Signal Timing Output Template

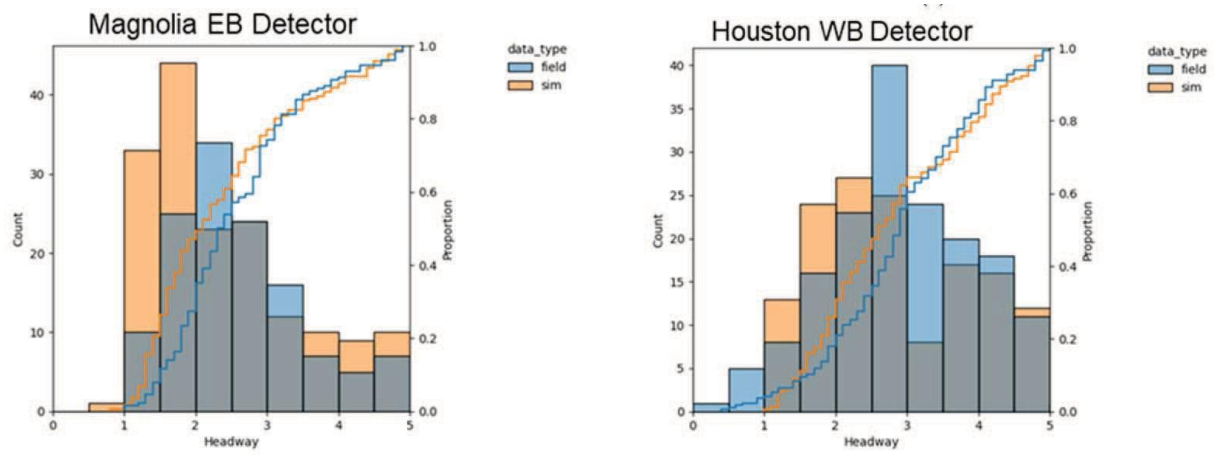

Fig. 17: Saturation headway distribution comparison - field vs simulation plots at (a) MLK @ Magnolia Eastbound approach detector, and (b) MLK @ Houston Westbound approach detector.

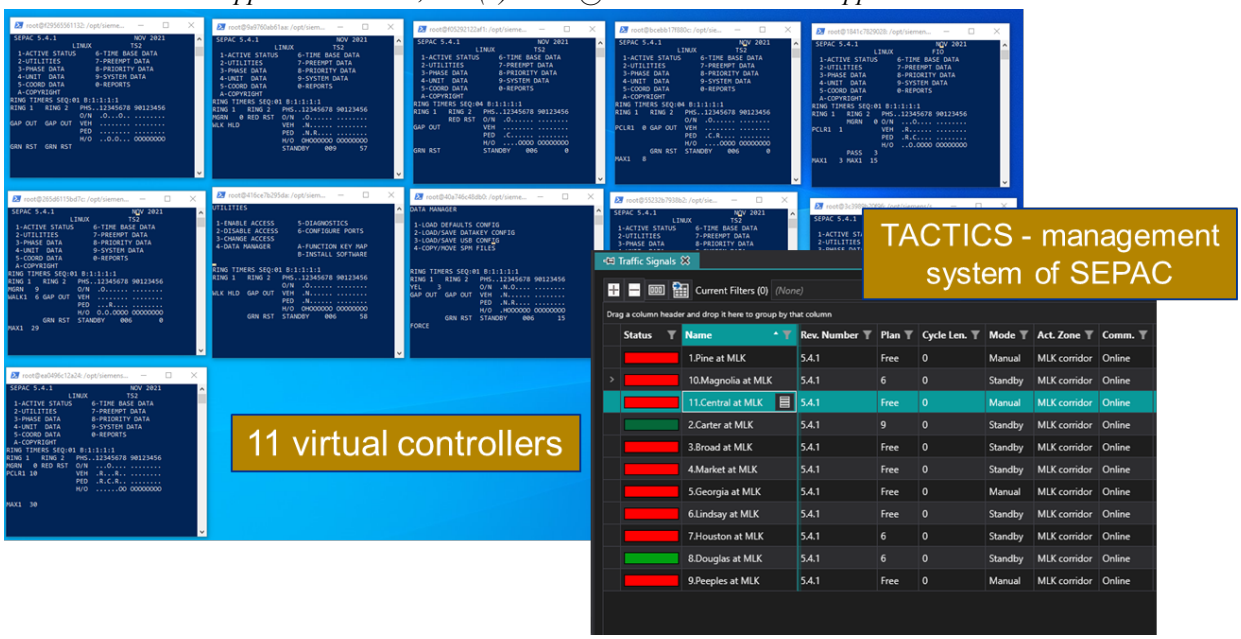

Fig. 18: View of Siemens SEPAC SILS

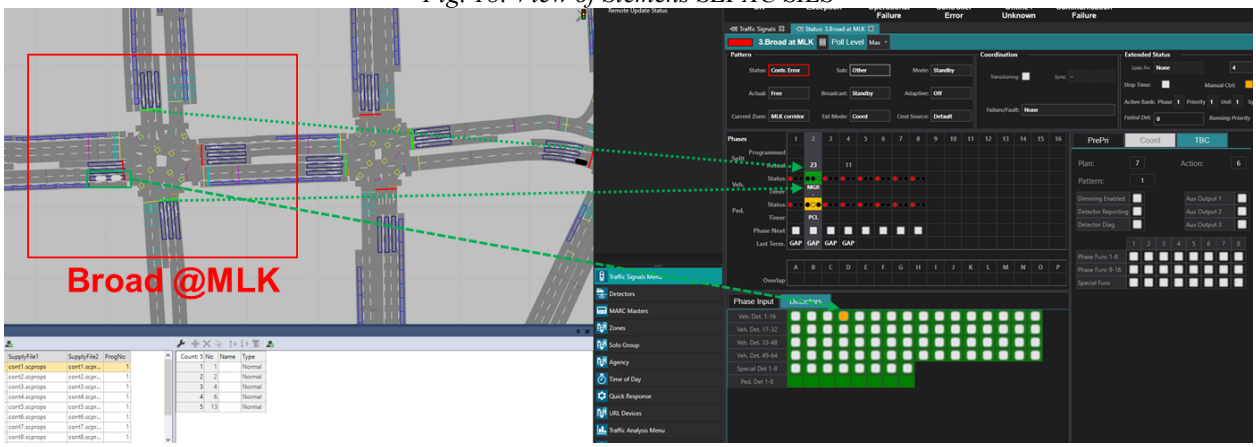

Fig. 19: Field signal timing plans operating in SILS environment at Broad @MLK

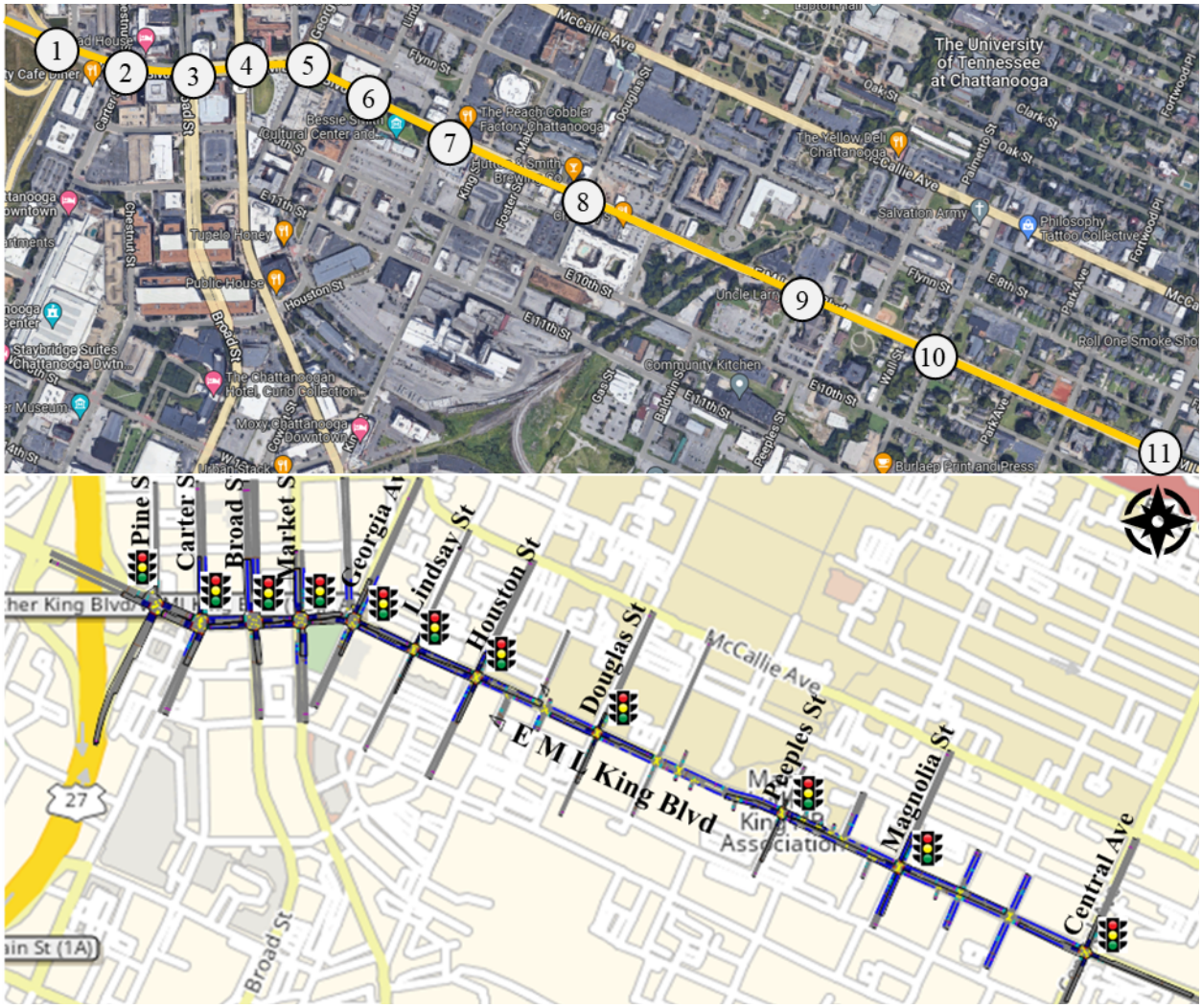

Fig. 20: Test-bed network

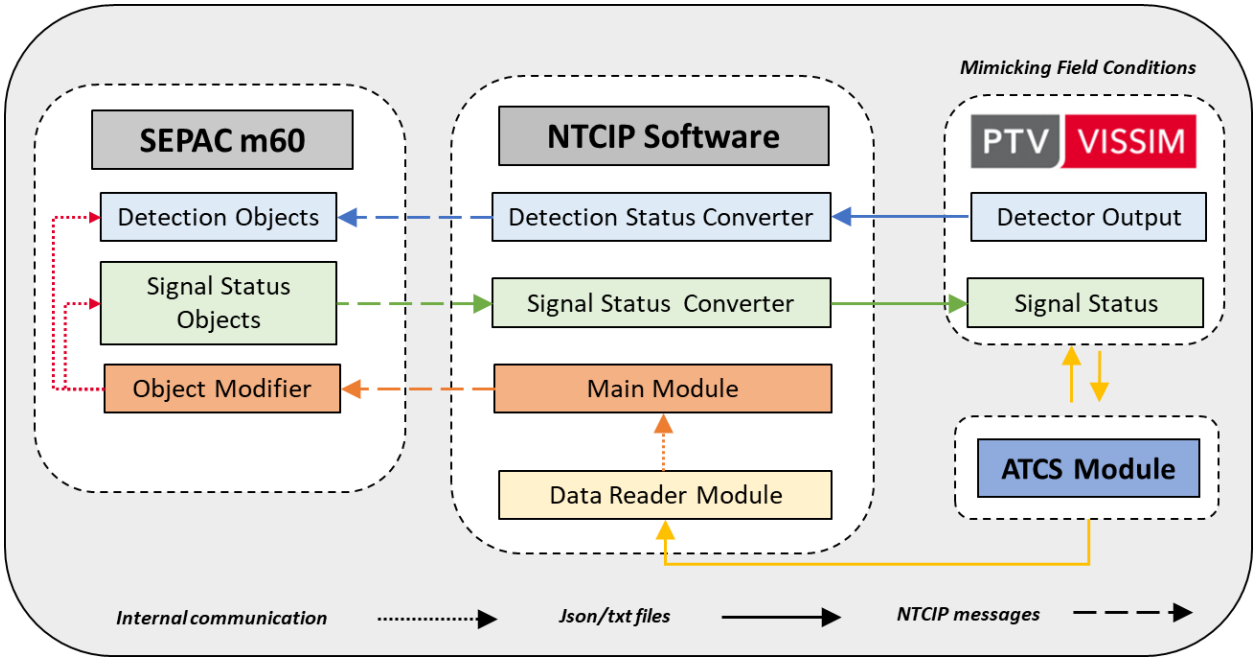

Fig. 21: Architecture of SILS

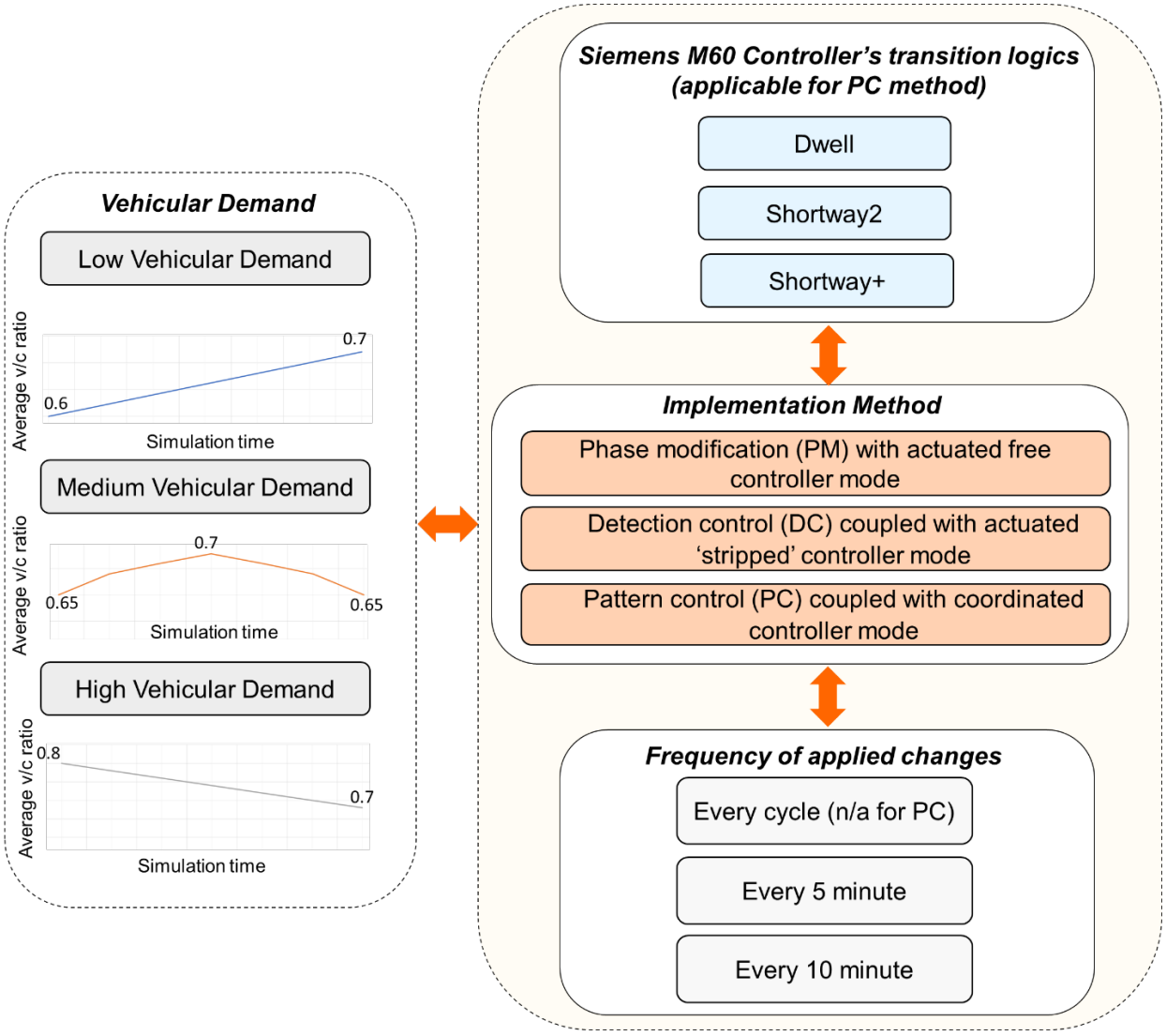

Fig. 22: Experimental design

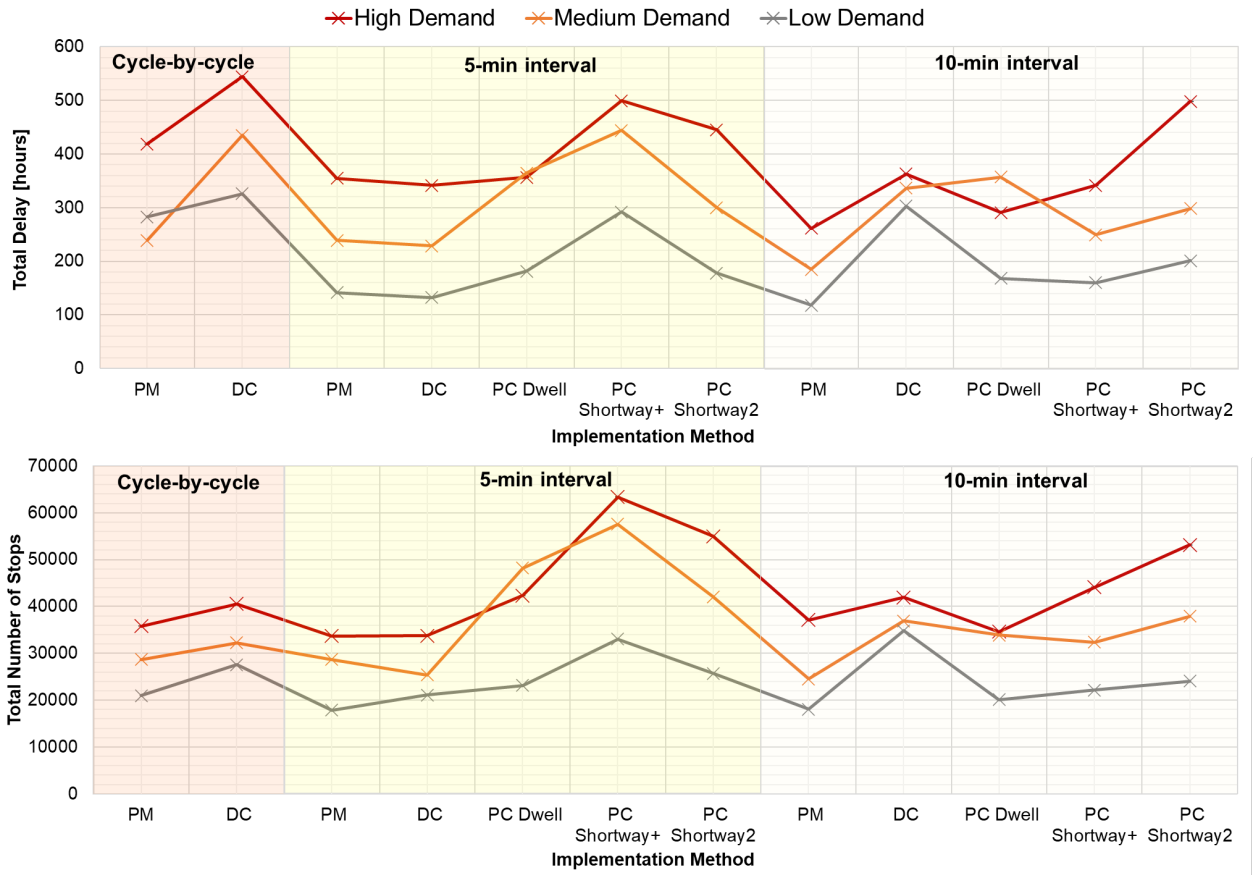

Fig. 23: Total delay and number of stops in the network

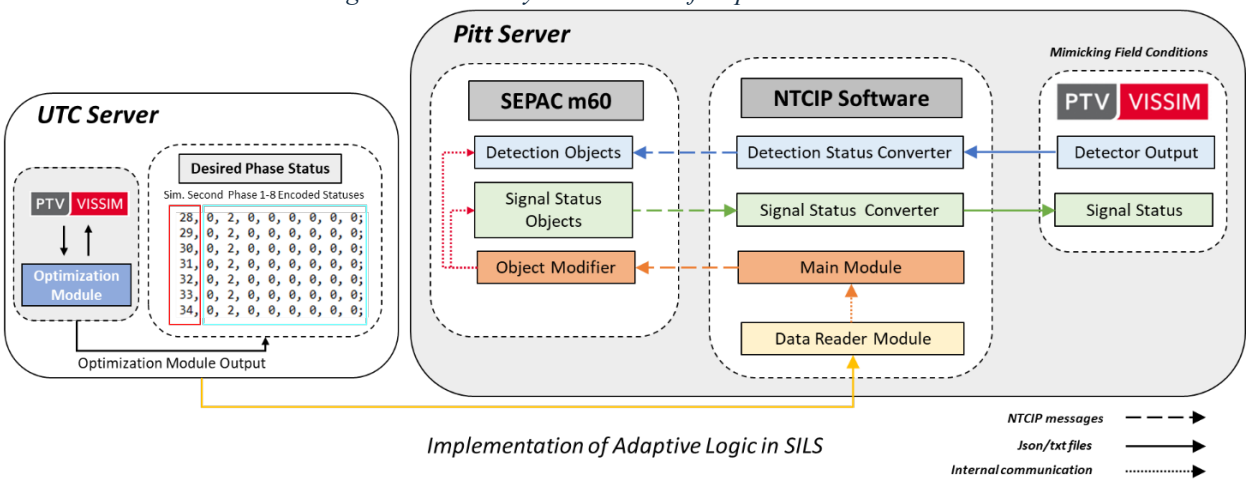

Fig. 24: Framework for Offline Adaptive Logic Implementation

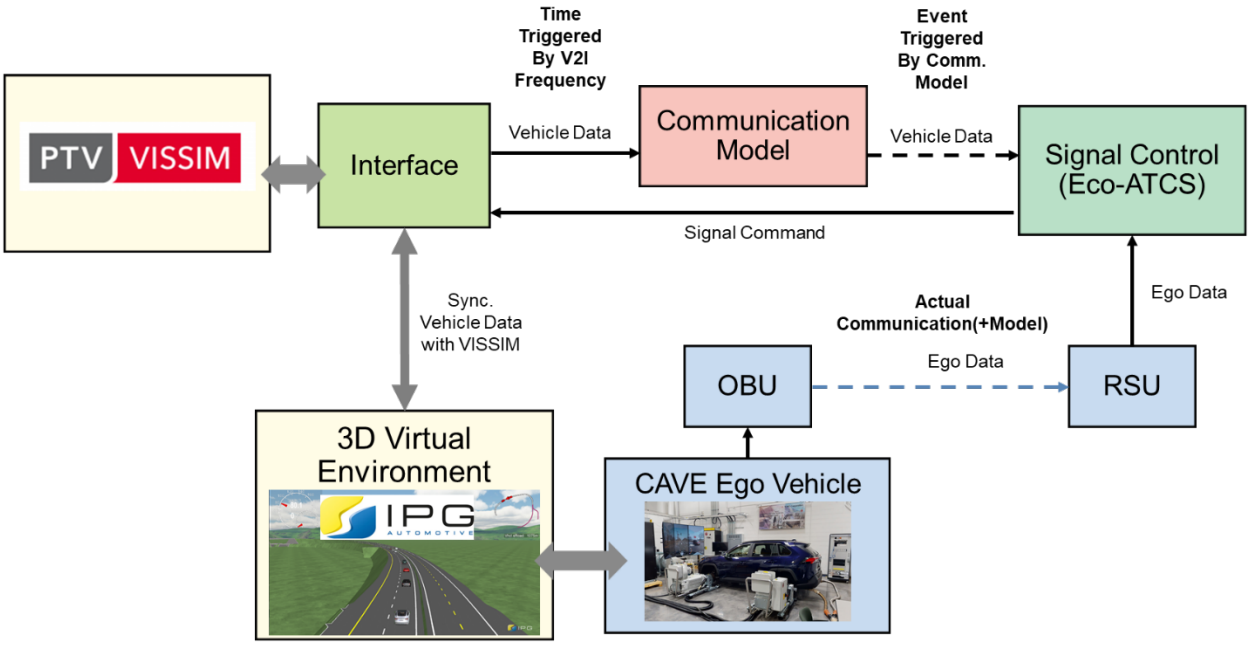

Fig. 25: CAVE lab HIL architecture including communication model

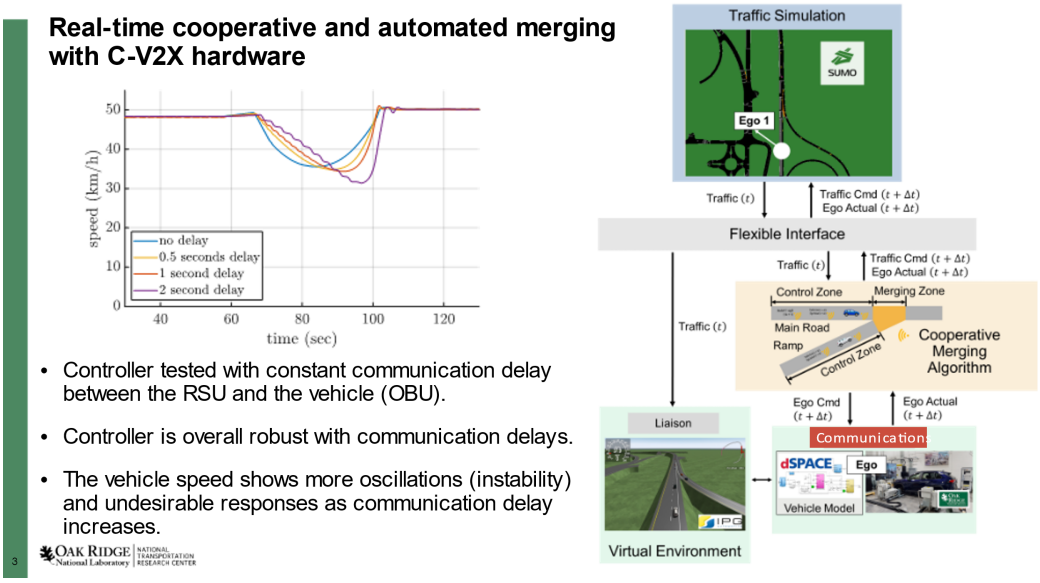

Fig. 26: Example of CAVE lab application quantifying the effect of communications on connected vehicles during traffic merging optimization

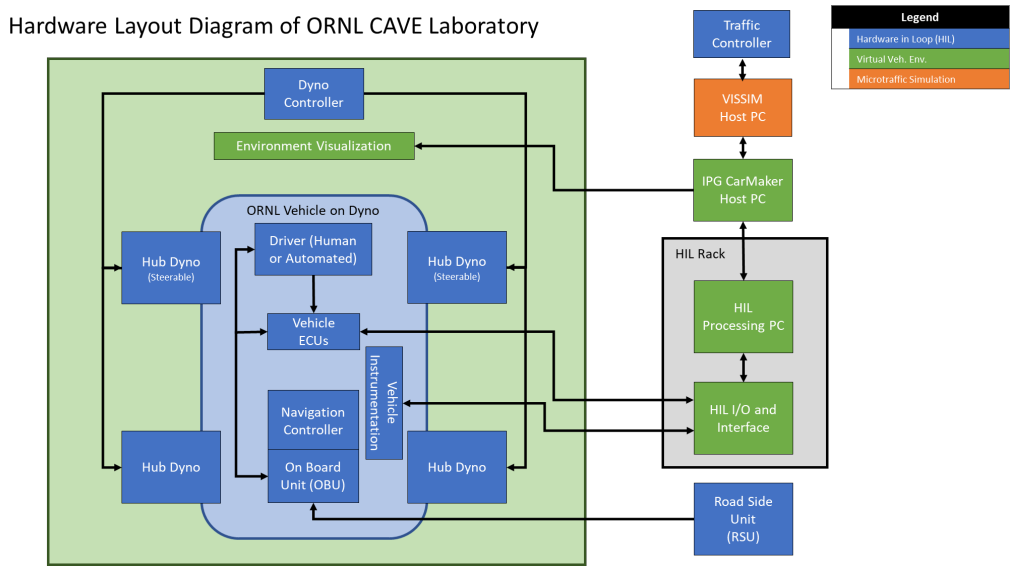

Figure 27: CAVE lab HIL architecture diagram

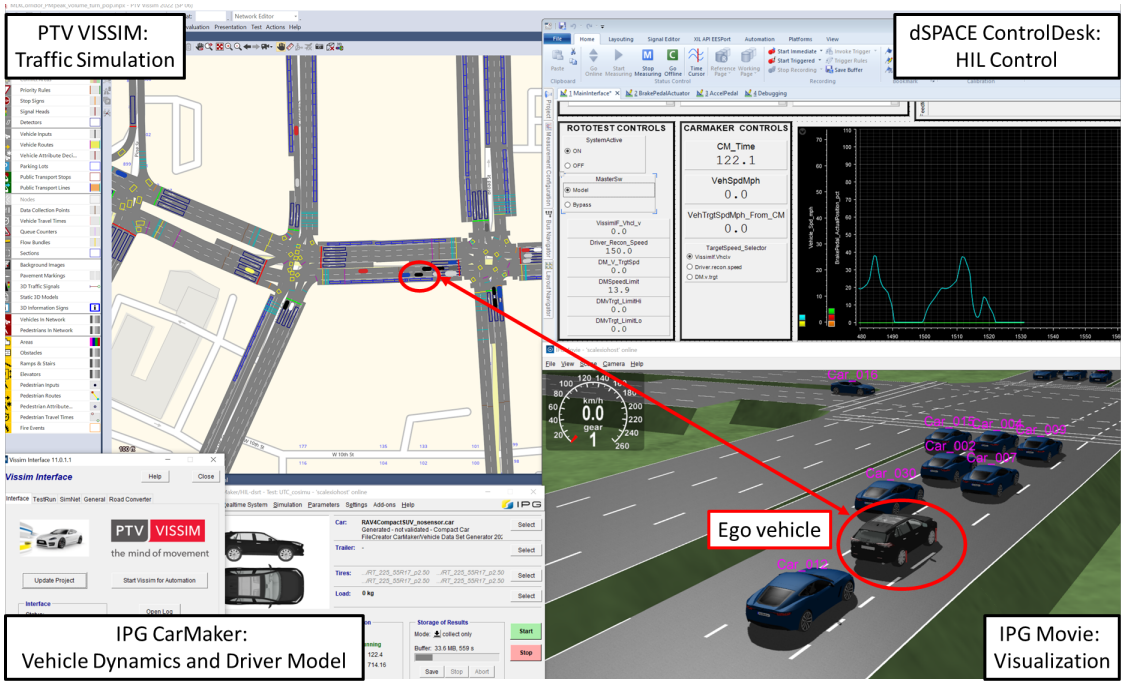

Figure 28: HIL architecture demonstration with VISSIM in the CAVE lab

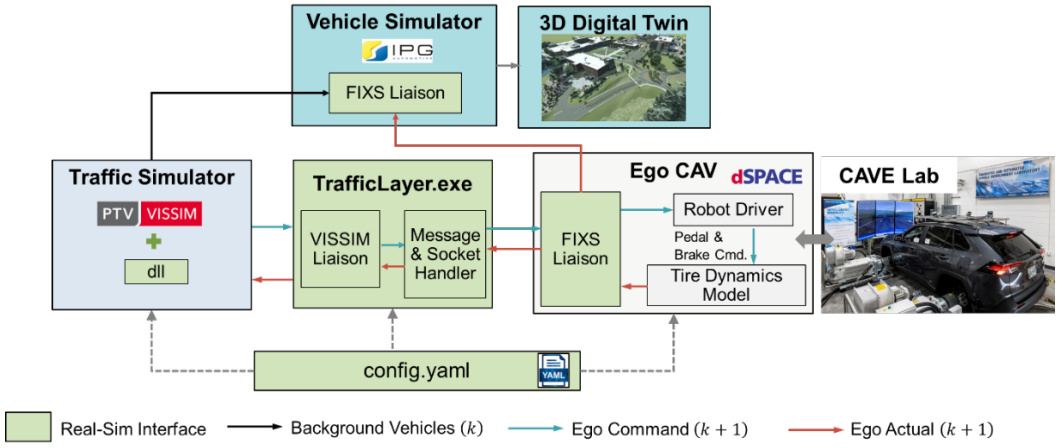

Figure 29: HIL architecture integrating Vissim MLK model with Ford Mach E

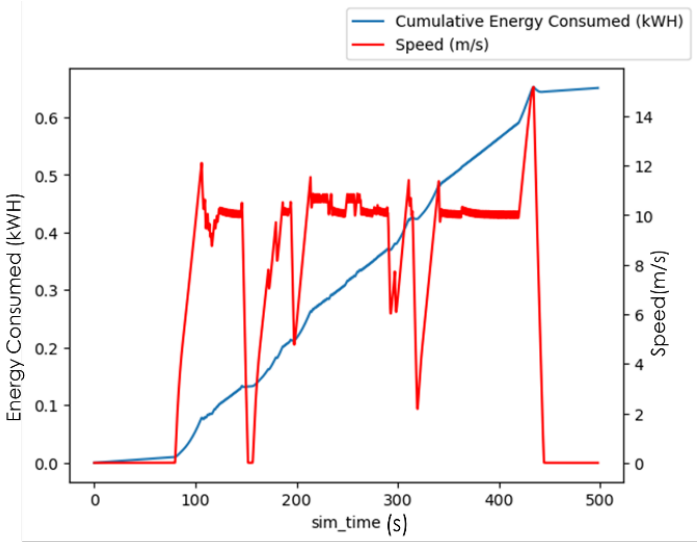

Figure 30: Power consumption and speed of ego vehicle in the MLK Vissim simulation for a single run across the corridor in Eastbound direction.

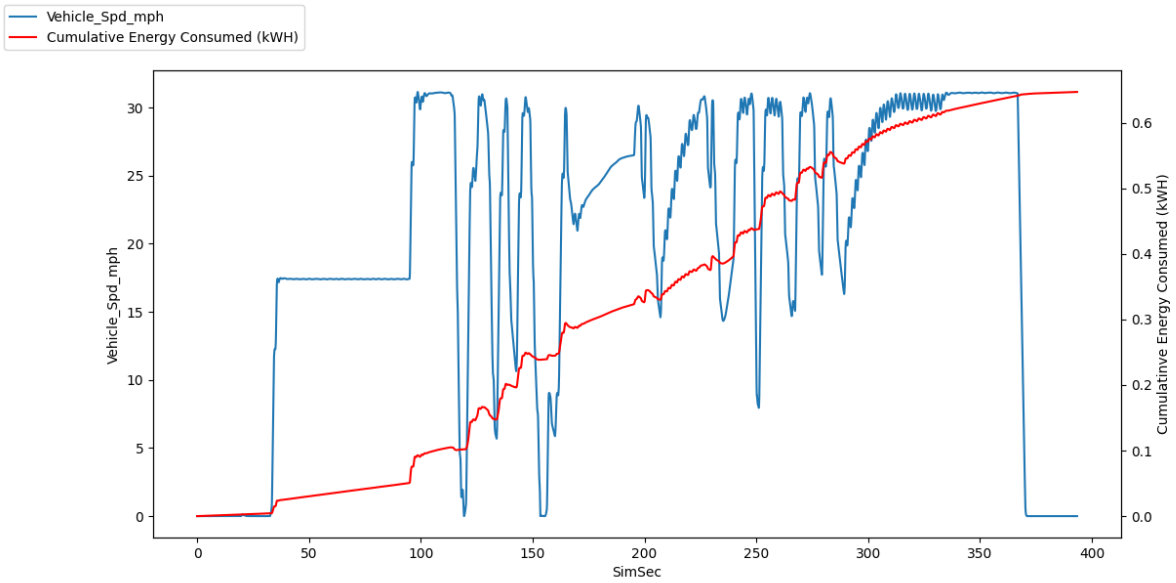

Figure 31: Actuated signal controls Ego vehicle speed and cumulative energy consumption – Mach E

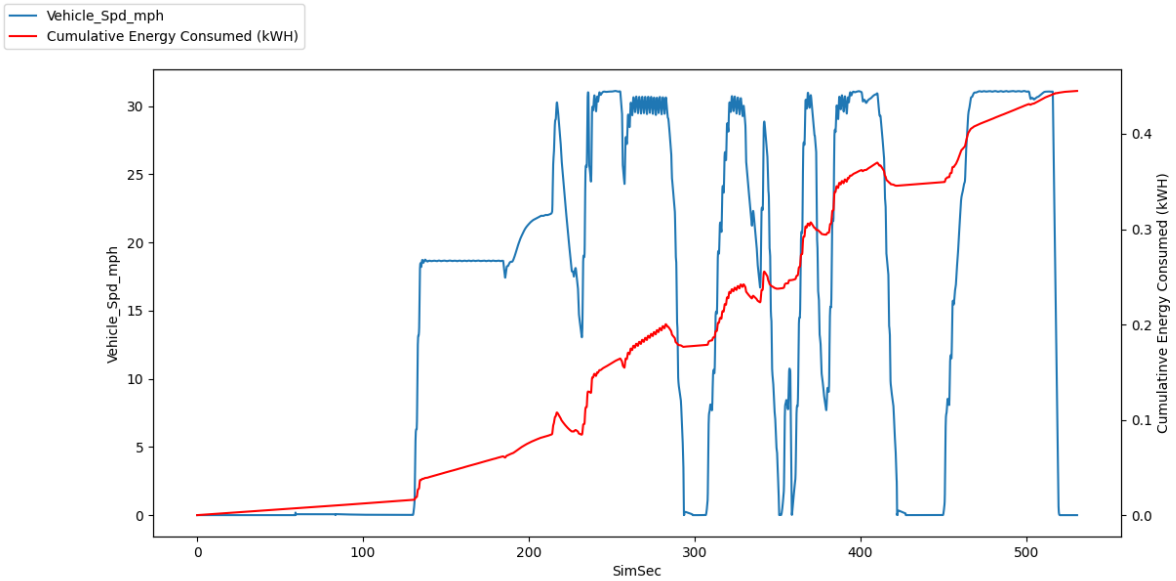

Figure 32: DGMARL signal controls Ego vehicle speed and cumulative energy consumption – Mach E

Figure 33: AVL Plutron Fuel Flow Meter installed on RAV4 in CAVE Laboratory

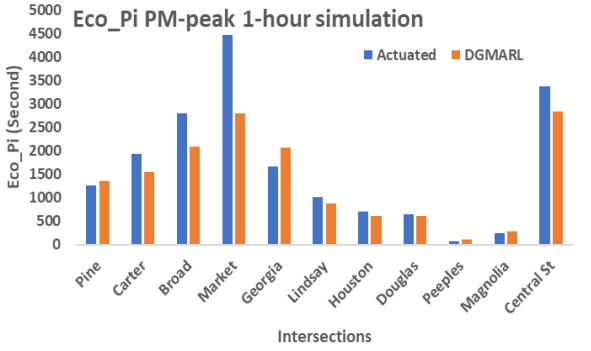

Node	Actuated	DGMARL	%
Pine	1264.765704	1360.566	-7.57%
Carter	1938.054917	1549.567	20.05%
Broad	2806.981228	2083.691	25.77%
Market	4466.239603	2809.791	37.09%
Georgia	1664.027442	2078.297	-24.90%
Lindsay	1019.277417	873.994	14.25%
Houston	704.1671827	610.716	13.27%
Douglas	652.0101882	604.659	7.26%
Peeples	77.02113721	107.426	-39.48%
Magnolia	252.5771327	285.469	-13.02%
Central St	3385.80875	2834.15	16.29%
Total	**18230.9307**	**15198.326**	**16.63%**

Fig. 34: PM-peak 1 Hour Simulation Test Results

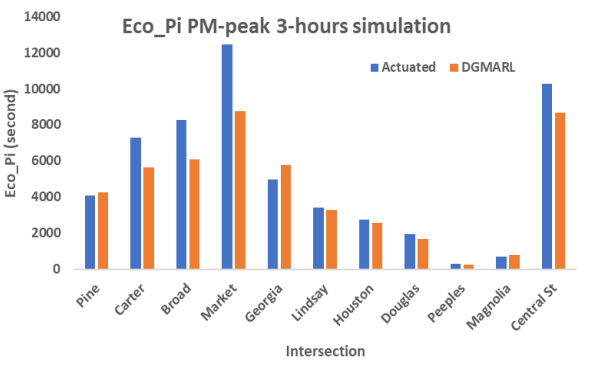

Node	Actuated	DGMARL	%
Pine	4089.825891	4240.674	-3.69%
Carter	7304.622662	5631.773	22.90%
Broad	8252.061816	6076.327	26.37%
Market	12434.08111	8737.537	29.73%
Georgia	4957.651198	5769.946	-16.38%
Lindsay	3431.395635	3284.548	4.28%
Houston	2734.583124	2591.272	5.24%
Douglas	1936.988007	1703.281	12.07%
Peeples	291.1535964	261.231	10.28%
Magnolia	693.0480542	807.524	-16.52%
Central St	10266.42646	8665.133	15.60%
Total	**56391.83755**	**47769.246**	**15.29%**

Fig. 35: PM-peak 3 Hour Simulation Test Results

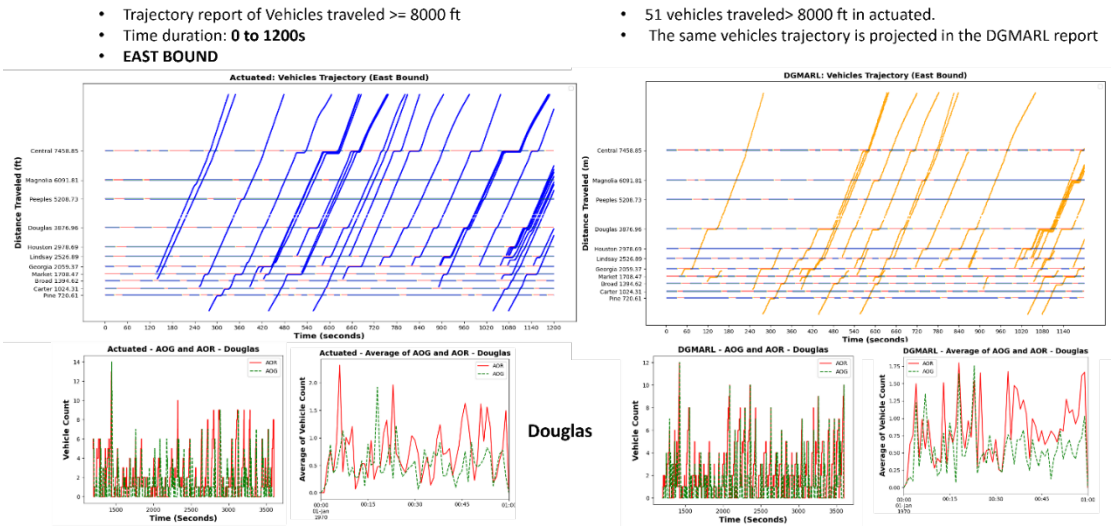

Fig 36: Eastbound: Trajectory report of vehicles traveled >= 8000ft

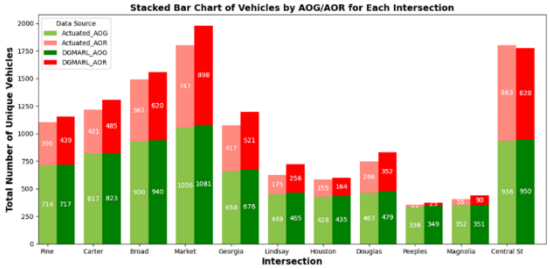

Fig.37: Arrival on green and arrival on red

Stopped vehicles speed <=3mph			
1-hr	Actuated	DGMARL	%
Pine	8206.608	8684.976	-5.83%
Carter	14024.69	9850.864	29.76%
Broad	20510.14	14065.34	31.42%
Market	25329.8	19325.07	23.71%
Georgia	12172.99	12002.76	1.40%
Lindsay	6382.125	5499.636	13.83%
Houston	5902.847	3450.75	41.54%
Douglas	8050.33	10011.97	-24.37%
Peeples	487.9753	822.1571	-68.48%
Magnolia	1607.838	2164.154	-34.60%
Central St	24768.92	14336.55	42.12%
	127444.3	**100214.2**	**21.37%**

Fig. 38: Overall Eco-PI in 1 hour simulation

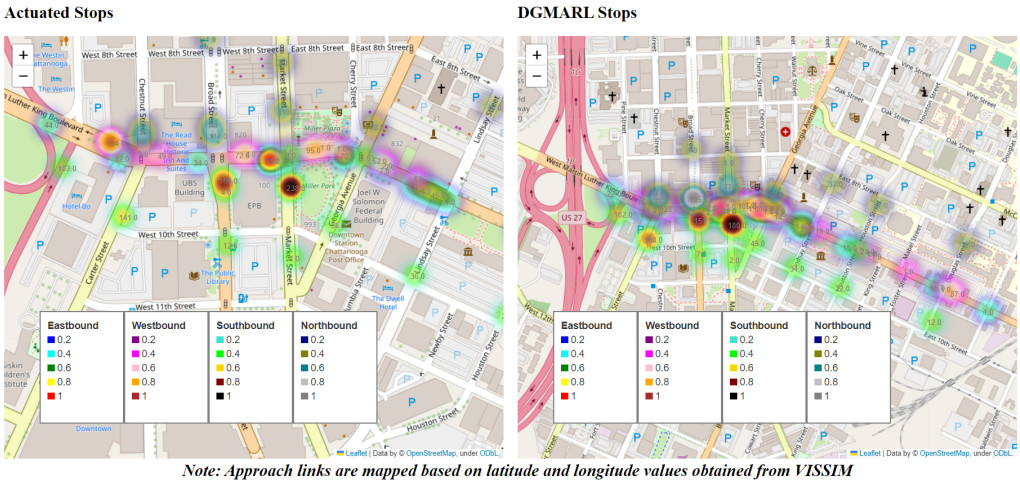

Note: Approach links are mapped based on latitude and longitude values obtained from VISSIM

Fig 39: Actuated vs DGMARL–Stops Reduced by 17.35%

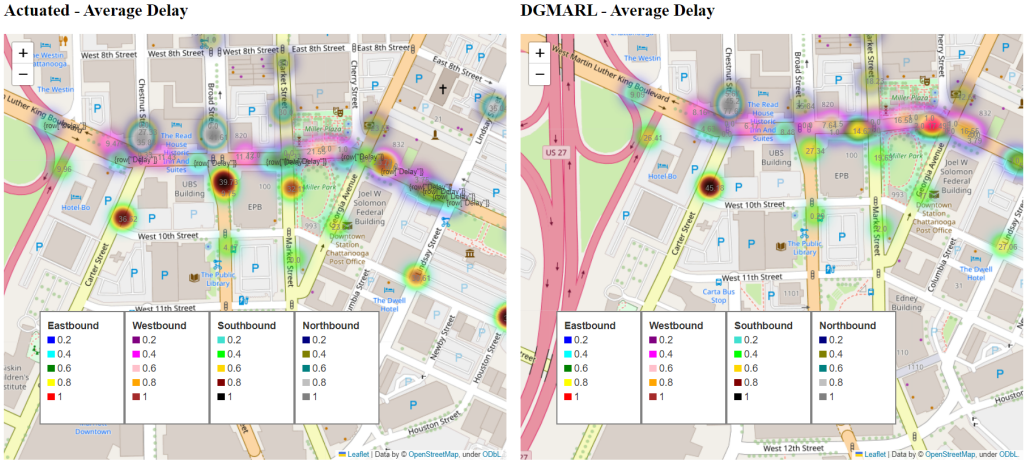

Note: Approach links are mapped based on latitude and longitude values obtained from VISSIM

Fig. 40: Actuated vs DGMARL–Delay Reduced by 32.78%

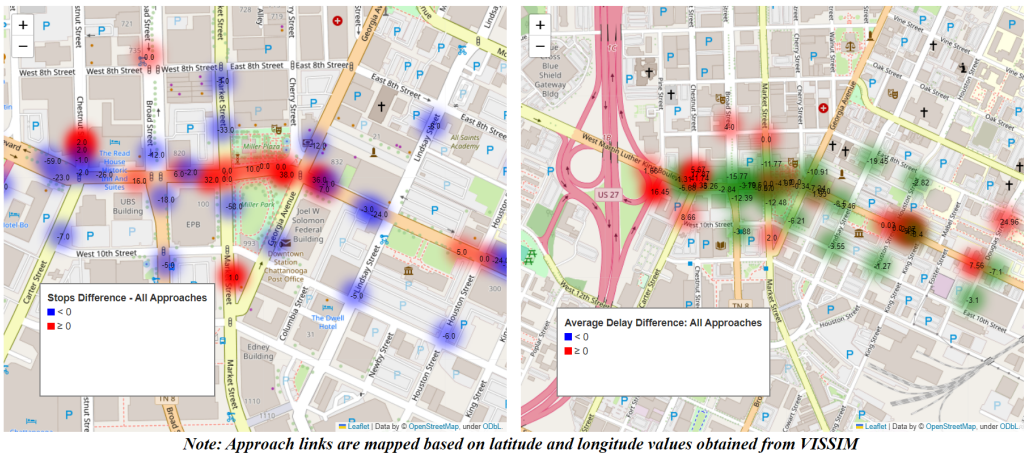

Note: Approach links are mapped based on latitude and longitude values obtained from VISSIM

Fig. 41: Difference in Stops and Delays (DGMARL minus Actuated)

Performance Measurement	Value
Total no. of pedestrians arrived	458
Total no. of vehicles traveled	2825
Actuated: Avg. of peds. serving time	22.51s
DGMARL PedRecal: Avg. of peds. serving time	22.51s
DGMARL Automated: Avg. of peds serving time	21.84s

Fig. 42: Overall Traffic and Serving State

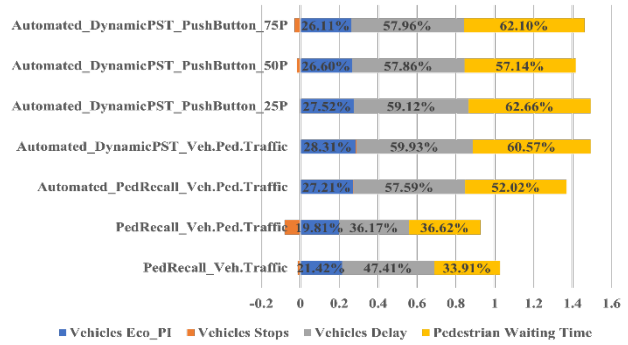

Fig. 43: Automated pedestrian traffic detection with dynamic pedestrian signal timing performance improvements compared to pedestrian recall.

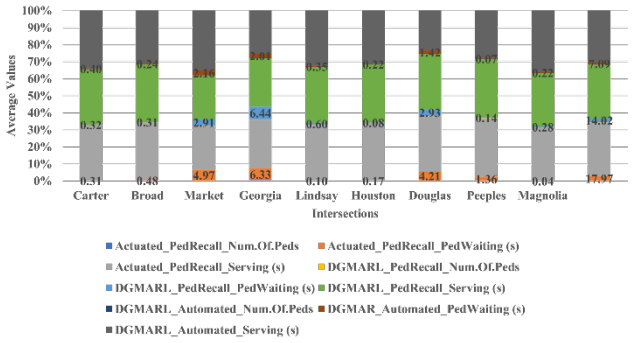

Fig. 44: Pedestrian traffic, waiting time, and serving time comparison.

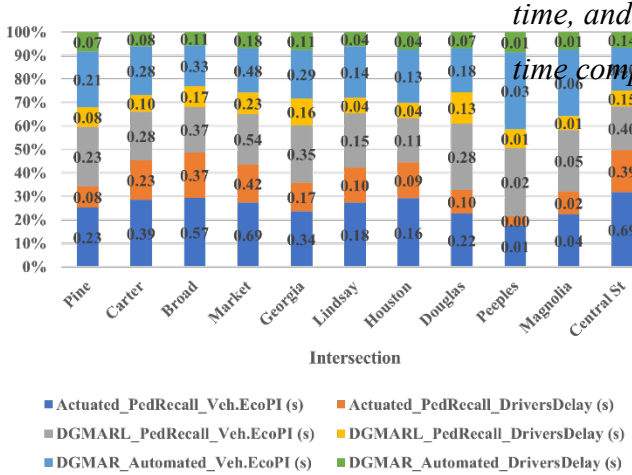

Fig. 45:(23) Vehicles Eco-PI and drivers waiting time comparison

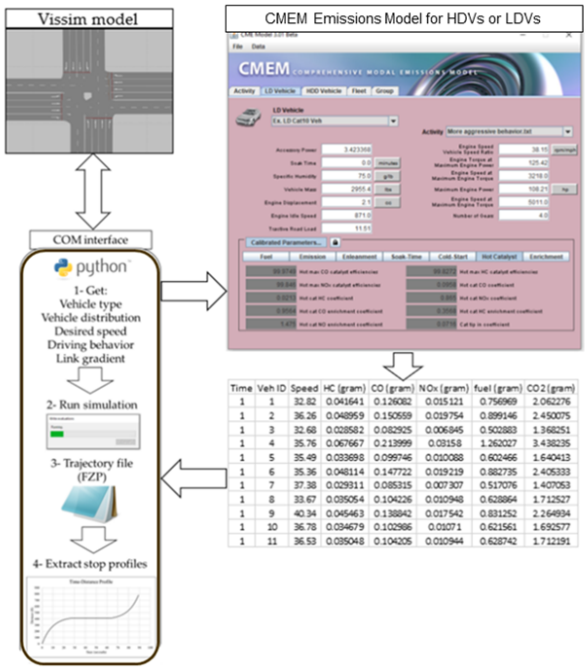

Fig. 46: Processing trajectories in CMEM emissions model

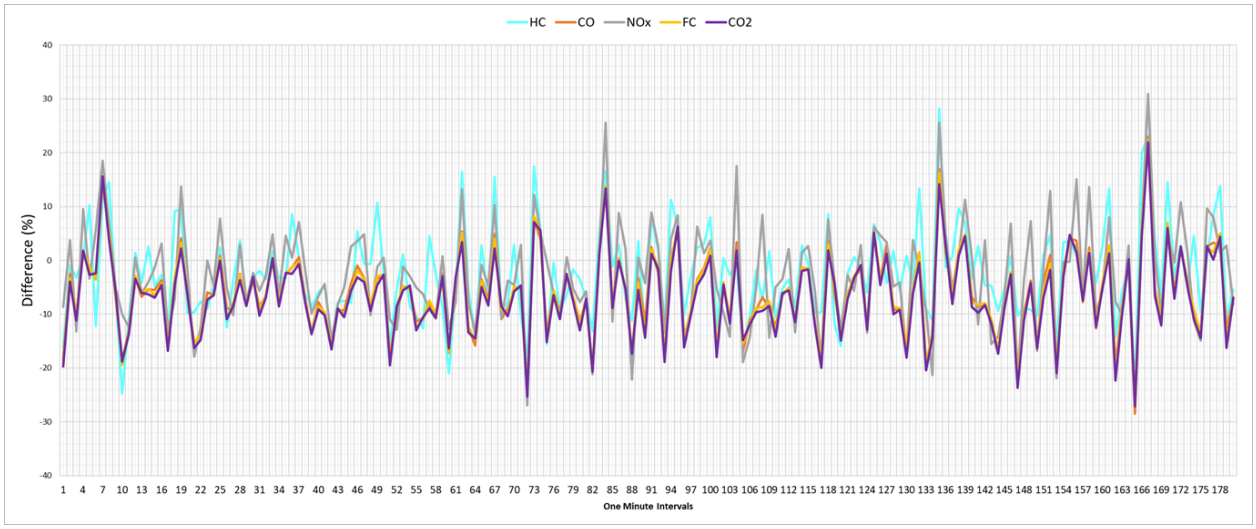

Fig. 47: CMEM results per minute – MLK corridor

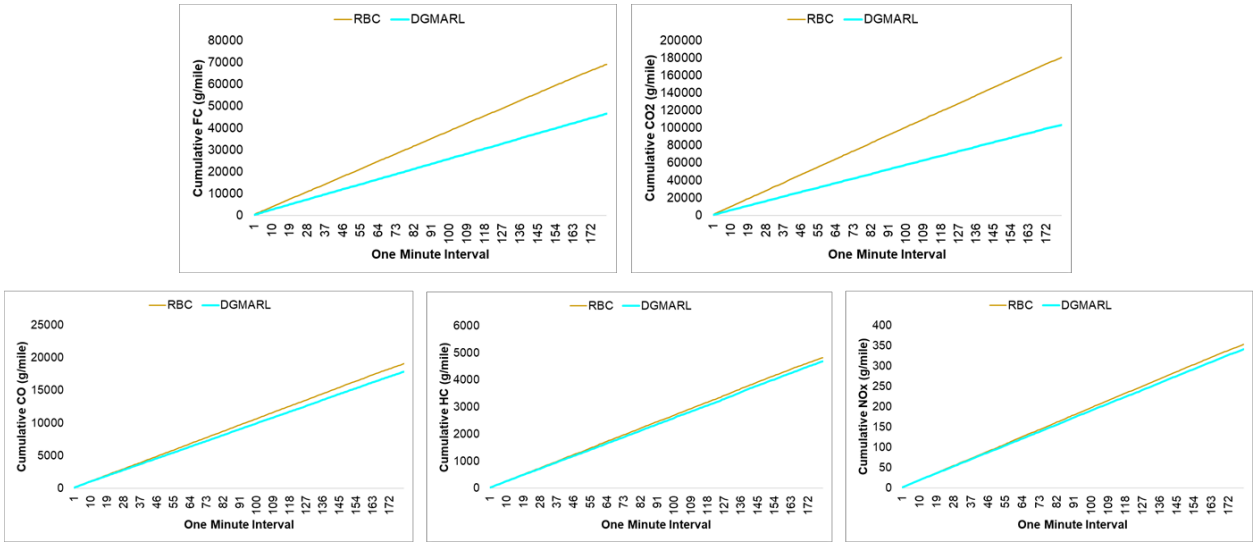

Figure 48: Cumulative emissions and FC

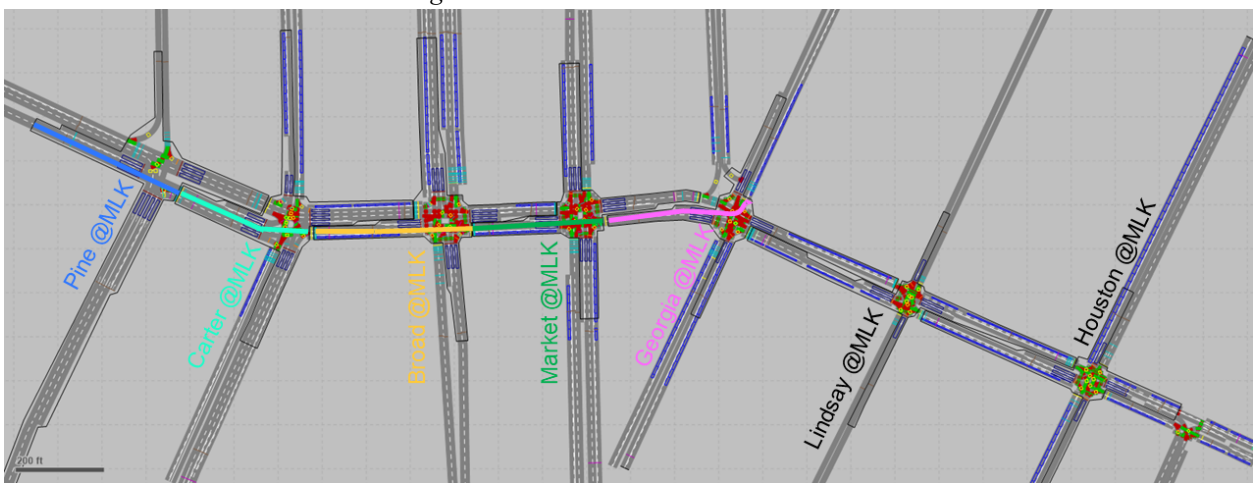

Fig. 49: FC and emissions analysis per intersection

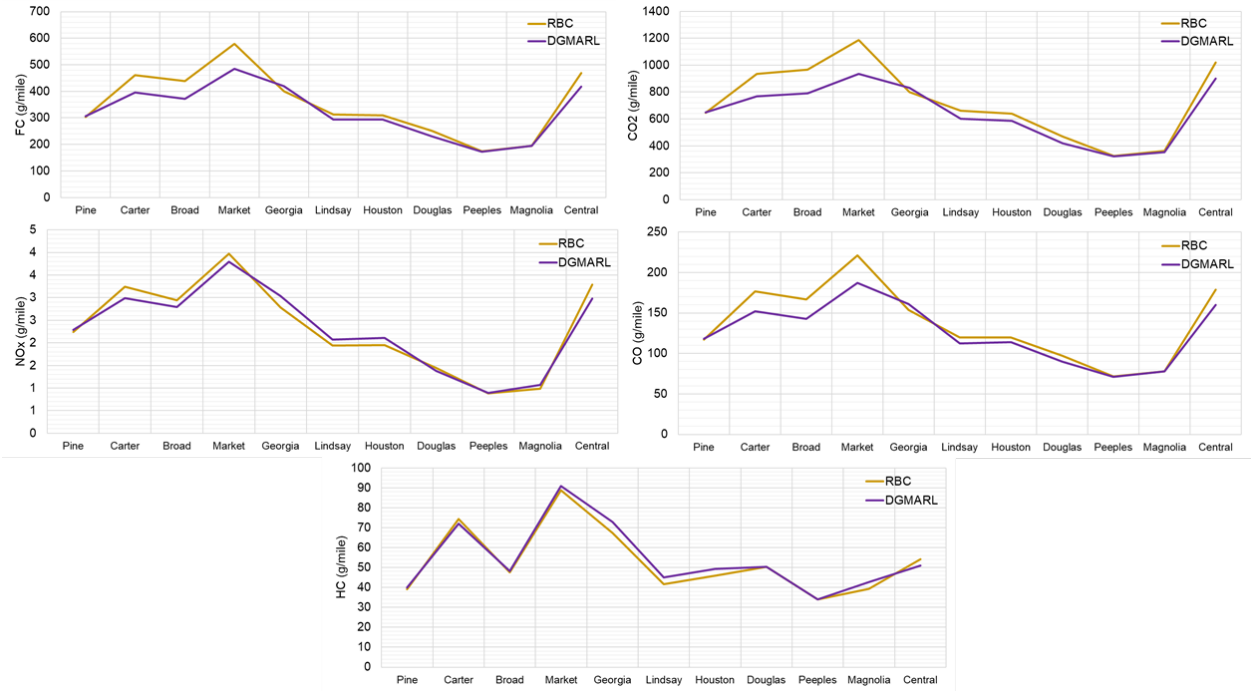

Fig. 50: CMEM results per intersection

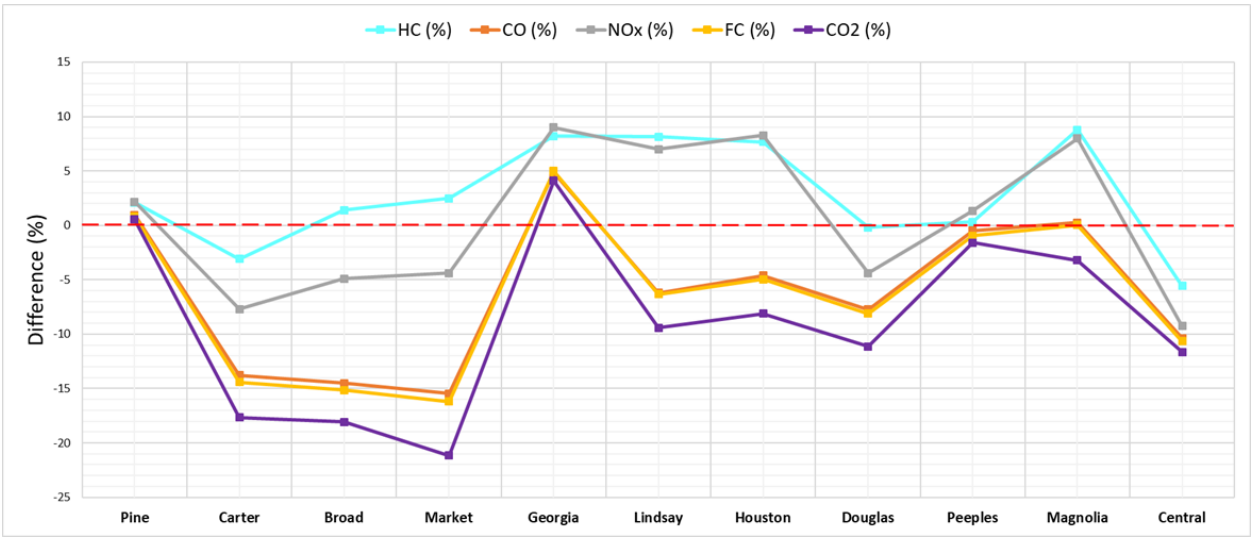

Fig. 51 Difference achieved by DGMARL per intersection

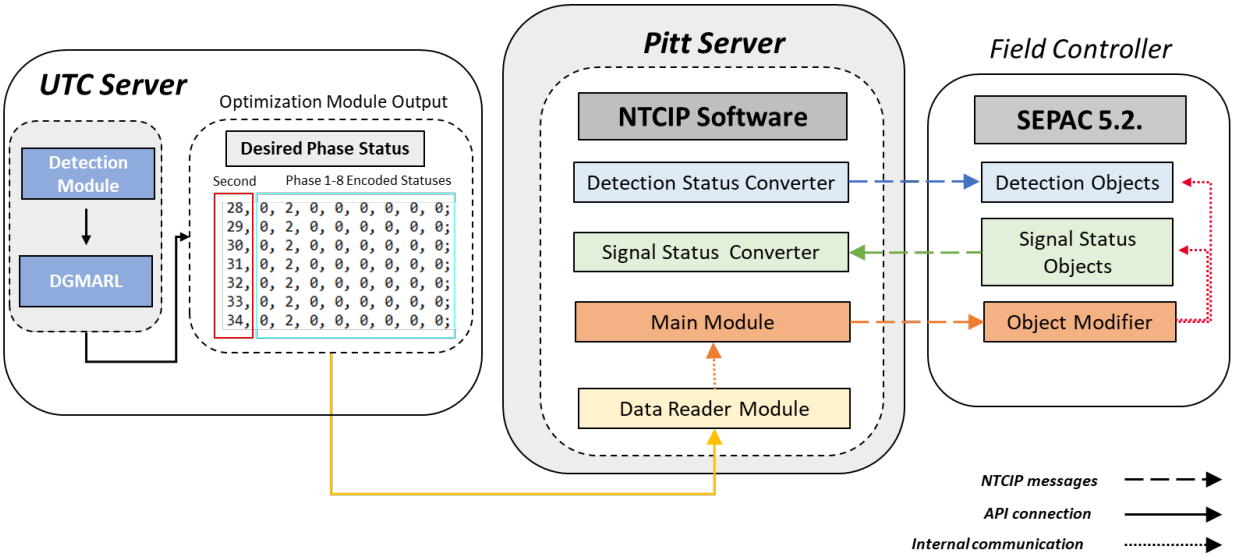

Fig. 52: Framework for Online Adaptive Logic Implementation

Appendix B: Tables

Table 1: Input and Output of DGMARL

DGMARL Input		
Runtime Properties Needed from Field	**Sub algorithm – Eco_PI Calculation**	**Static Properties or Configurations available from the field**
1. Detector's value - Traffic Occupancy 2. Each signal's current status 3. Number of vehicles in each lane - every second	Vehicle_ID, LaneID, Vehicle_speed	Intersection Id, Associated Signal Controller Id, Signal Group ids and Associated Phases, Left turn phases, Link Ids and Lanes - associated to phases, Detectors Ids associated to phases, MinGreen, RedClearanceTime, YellowTime, Ped Recall, Walk time, Flashing Don't Walk time
DGMARL Output		
Action: 0 : Stay in current phase 1 & Phase_id: Switch to the Phase_id which has highest traffic demand		

Table 2 Variables for various operational conditions impacting FC

Vehicle type		Fleet distribution		Driver behavior		Road gradient		Cruising speed		Wind effect	
Variable	FC (g)	Variable	FC (g)	Variable	FC (g)	Variable	FC (g)	Variable	FC (g)	Variable	FC (g)
LDV1	56.6	100:0	56.6	Func1	45.7	-7	34.8	20	16.1	50 tailwinds	473.8*
LDV2	57.2	99:1	62.5	Func2	47.2	-6	37.6	25	21.8	40 tailwinds	505.6
LDV3	55.5	98:2	68.7	Func3	49.5	-5	40.8	30	27.2	30 tailwinds	510.8
LDV4	52.5	97:3	74.4	Func4	51.9	-4	43.5	35	36.7	20 tailwinds	513.3
LDV5	57.8	96:4	80.1	Func5	53.2	-3	46.3	40	46.4	10 tailwinds	525.6
LDV6	54.6	95:5	86.5	Func6	55.4	-2	49.6	45	56.6	No wind	549.0
LDV7	55.5	94:6	92.3	Func7	56.3	-1	52.7	50	70.3	10 headwinds	587.2
LDV8	59	93:7	98.4	Func8	58.4	0	56.6	55	85.5	20 headwinds	628.5
LDV9	58.7	92:8	104.1	Func9	60.5	1	59.2	60	106.6	30 headwinds	690.8
LDV10	111.2	91:9	110.9	Func10	62.2	2	63.7	65	135.3	40 headwinds	835.4
LDV11	56.8	90:10	117.6	Func11	63.7	3	67.1			50 headwinds	979.5
LDV12	55.9			Func12	65.4	4	71.1				
HDDV1	816.5					5	75.0	Not applicable		*Values are for HDDVs	
HDDV2	894.4	Not applicable		Not applicable		6	80.2				
HDDV3	549.0					7	85.6				

Table 3 Regression equations to compute the stop penalty

Factor	Equation	Range	R^2
x_{pHV}: % of HDV	$K = 129.37 \cdot e^{0.0615 \cdot x_{pHV}}$	$x_{pHV} = [0, 10]$	0.6273
x_{RG}: Road gradient (%)	$K = 122.19 \cdot e^{0.0648 \cdot x_{RG}}$	$x_{RG} = [-7, 7]$	0.8335
x_{cs}: Cruising speed (mph)	$K = 14.761 \cdot e^{0.0467 \cdot x_{cs}}$	$x_{cs} = [20, 65]$	0.9645
x_{WE}: Wind effect (mph)	$K = 0.1613 \cdot {x_{WE}}^2 + 9.6642 \cdot x_{WE} + 1244.6$	$x_{WE} = [-50, 50]$	0.9389

Table 4 Required data for estimating delay and number of stops

Optimization type \ Data attribute	Type	Source	Spatial coverage	Temporal coverage	Importance
Vehicle arrivals downstream					
Offline - Pretimed	Traffic counts	GridSmart TMCs / Counts	Intersection movement	15-minutes bins / Second-by-second	High
Online - Adaptive	Traffic counts	GridSmart Counts	Intersection movement	Second-by-second	High

Online CV – Adaptive CV	Traffic counts	CV data (BSM)	Exact location of vehicle	Same as Online	Medium
Vehicle arrivals upstream					
Offline - Pretimed	Traffic counts	GridSmart Counts	After upstream intersection	Aggregated based on second-by-second data	Low
Online - Adaptive	Traffic flow rate	GridSmart Counts / Video data	After upstream intersection	Second-by-second / TBD (resolution of video analytics)	High
Online CV – Adaptive CV	Traffic flow rate	CV data (BSM)	Exact location of vehicle	Second-by-second	Medium
Signal phasing and timing data					
Offline - Pretimed	Signal timing elements	Signal timing sheets	Intersection movement	Peak period or hour	High
Online - Adaptive	Signal timing elements	GridSmart Events	Intersection movement	Second-by-second	High
Online CV – Adaptive CV	Signal timing elements	Same as Online	Same as Online	Same as Online	Medium

Table 5 Required data for each of the factors impacting the stop penalty

Optimization type \ Data attribute	Type	Source	Spatial coverage	Temporal coverage	Importance
Fleet composition and Vehicle type					
Offline - Pretimed	Vehicle shape	GridSmart Counts	Intersection movement	Second-by-second	Medium
Online - Adaptive	Vehicle shape	Video data / GridSmart Counts	Intersection movement	TBD (resolution of video analytics) / Second-by-second	High
Online CV – Adaptive CV	Exact vehicle model	CV data (Embed in BSM)	Exact location of vehicle	Second-by-second	High
Driving behavior					
Offline - Pretimed	Trajectory data	Probe GPS / Video data	Before & After StopLine/ TBD (camera view)	Second-by-second / TBD (resolution of video analytics)	High
Online - Adaptive	Trajectory data	Video data	TBD (camera view)	TBD (resolution of video analytics)	Medium
Online CV – Adaptive CV	Trajectory data	CV data (BSM), individual CV	Same as Online and for multiple intersections	Second-by-second	High
Road gradient					
Offline - Pretimed	Grade of the terrain	Maps with altitude	Intersection approach	NA	High
Online - Adaptive	Grade of the terrain	Same as Offline	Same as Offline	Same as Offline	Low
Online CV – Adaptive CV	Grade of the terrain	Same as Offline + BSM	Exact location of vehicle	Second-by-second	Medium
Cruising speed					
Offline - Pretimed	Speed limit	Google maps	Intersection approach	NA	High
Online - Adaptive	Speed distribution	Video data /GridSmart Realtime	TBD (camera view) / Intersection movement	TBD (temporal resolution of video analytics) / Second-by-second	Medium
Online CV – Adaptive CV	Speed distribution	CV data (BSM)	Exact location of vehicle	Second-by-second	Medium
Wind effect					
Offline - Pretimed	Wind speed & direction	Dark Sky	TBD	TBD	Low
Online - Adaptive	Wind speed & direction	Dark Sky (API)	TBD	TBD	Medium
Online CV – Adaptive CV	Wind speed & direction	Dark Sky (API)	Same as Online	Same as Online	Medium

Table 6 Cruising speeds and road gradients on intersections of the area of study

Intersection	Parameter/movement	EB RT	EB TH	EB LT	WB RT	WB TH	WB LT	NB RT	NB TH	NB LT	SB RT	SB TH	SB LT
Carter St	Initial speed (mph)	30	30	30	25	25	25	30	30	30	30	30	30
	Final speed(mph)	30	30	30	25	25	25	30	30	25	25	30	30
	Deceleration slope (%)	-0.8	-0.8	-0.8	-0.1	-0.1	-0.1	0.1	0.1	0.1	-0.4	-0.4	-0.4
	Acceleration slope (%)	0.2	-0.2	0.4	0.3	0.3	0.1	0.4	0.2	0.1	0.3	-0.1	0.0
Broad St	Initial speed (mph)	30	30	30	25	25	25	30	30	30	20	20	20
	Final speed(mph)	20	25	30	30	30	25	30	20	25	25	30	30
	Deceleration slope (%)	0.2	0.2	0.2	-1.6	-1.6	-1.6	-0.2	-0.2	-0.2	0.0	0.0	0.0
	Acceleration slope (%)	0.5	1.1	0.8	0.3	-0.1	0.0	0.9	0.3	0.0	-0.3	0.0	1.1
Market St	Initial speed (mph)	25	25	25	25	25	25	30	30	30	30	30	30
	Final speed(mph)	30	25	30	30	25	30	25	30	25	25	30	25
	Deceleration slope (%)	1.5	1.5	1.5	-1.9	-1.9	-1.9	-0.5	-0.5	-0.5	1.5	1.5	1.5
	Acceleration slope (%)	1.0	2.0	-1.1	-1.9	-1.7	0.3	1.9	-1.7	-1.3	-0.9	1.1	2.2
Georgia St	Initial speed (mph)	25	25	25	25	25	25	30	30	30	30	30	30
	Final speed(mph)	30	25	30	30	25	30	25	30	25	30	25	30
	Deceleration slope (%)	1.9	1.9	1.9	-1.0	-1.0	-1.0	-0.9	-0.9	-0.9	-1.1	-1.1	-1.1
	Acceleration slope (%)	0.7	1.4	1.3	0.3	-1.9	-0.1	1.3	0.6	-1.7	-2.3	0.0	0.8
Lindsay St	Initial speed (mph)	25	25	25	25	25	25	30	30	30	30	30	30
	Final speed(mph)	30	25	30	30	25	30	25	30	25	30	25	30
	Deceleration slope (%)	1.3	1.3	1.3	1.7	1.7	1.7	-1.7	-1.7	-1.7	-3.7	-3.7	-3.7
	Acceleration slope (%)	1.3	-1.1	1.9	2.2	-1.0	1.1	-1.2	1.8	-0.8	-1.3	0.7	-1.5
Houston St	Initial speed (mph)	25	25	25	25	25	25	30	30	30	30	30	30
	Final speed(mph)	30	25	30	30	25	30	25	30	25	30	25	30
	Deceleration slope (%)	-1.6	-1.6	-1.6	2.3	2.3	2.3	-1.1	-1.1	-1.1	-4.3	-4.3	-4.3
	Acceleration slope (%)	0.8	-1.5	1.7	4.4	0.9	0.3	-1.4	5.0	1.2	0.8	-0.4	-1.8
Douglas St	Initial speed (mph)	25	25	25	25	25	25	30	30	30	30	30	30
	Final speed(mph)	30	25	30	30	25	30	25	30	25	30	25	30
	Deceleration slope (%)	-0.5	-0.5	-0.5	-1.0	-1.0	-1.0	0.4	0.4	0.4	-2.3	-2.3	-2.3
	Acceleration slope (%)	-0.3	1.1	1.9	2.2	0.3	-0.5	1.1	1.8	0.7	-0.2	-0.9	0.2
Peeples St	Initial speed (mph)	25	25	-	-	25	25	30	-	30	-	-	-
	Final speed(mph)	30	25	-	-	25	30	25	-	25	-	-	-
	Deceleration slope (%)	0.3	0.3	-	-	-1.5	-1.5	3.3	-	3.3	-	-	-
	Acceleration slope (%)	-2.3	1.4	-	-	0.5	-1.9	1.3	-	0.9	-	-	-
Magnolia St	Initial speed (mph)	25	25	25	25	25	25	30	30	30	30	30	30
	Final speed(mph)	30	25	30	30	25	30	25	30	25	30	25	30
	Deceleration slope (%)	3.3	3.3	3.3	-4.3	-4.3	-4.3	3.2	3.2	3.2	-1.8	-1.8	-1.8
	Acceleration slope (%)	-1.8	3.7	2.2	1.1	-3.2	-2.6	3.6	1.4	-2.0	-3.1	-1.6	2.4
Central St	Initial speed (mph)	35	35	35	35	35	35	30	30	30	30	30	30
	Final speed(mph)	30	35	30	30	35	30	35	30	35	30	35	30
	Deceleration slope (%)	-5.4	-5.4	-5.4	5.8	5.8	5.8	-1.7	-1.7	-1.7	-0.4	-0.4	-0.4
	Acceleration slope (%)	1.2	-5.5	-1.5	1.5	5.1	5.1	-5.7	-1.4	2.6	4.4	1.1	-3.3

Tables 7-11

Total Eco_PI – 5% HDV

Test - 80007

	Actuated	DGMARL	%
Pine	26991.12	30428.89	-12.74%
Carter	57094.26	46794.52	18.04%
Broad	64535.16	51103.28	20.81%
Market	95568.8	68690.66	28.12%
Georgia	34127.16	41003.34	-20.15%
Lindsay	25395.81	22719.74	10.54%
Houston	21812.12	16759.19	23.17%
Douglas	24803.67	34139.17	-37.64%
Peeples	1957.362	2421.52	-23.71%
Magnolia	4593.444	4420.578	3.76%
Central St	78523.56	48949.88	37.66%
	435402.5	**367430.8**	**15.61%**

Total Eco_PI – 4% HDV

Test - 80008

	Actuated	DGMARL	%
Pine	24956.75	27515.2	-10.25%
Carter	55420.46	46314.24	16.43%
Broad	62387.07	51228.14	17.89%
Market	93576.75	60697.98	35.14%
Georgia	32370.87	38559.85	-19.12%
Lindsay	24614.08	20679.51	15.99%
Houston	21726.01	16187.48	25.49%
Douglas	22691.93	32832.43	-44.69%
Peeples	2156.546	1811.461	16.00%
Magnolia	4685.571	4880.236	-4.15%
Central St	73120.13	43622.82	40.34%
	417706.2	**344329.3**	**17.57%**

Total Eco_PI – 3% HDV

Test - 80009

	Actuated	DGMARL	%
Pine	26876.46	26576.07	1.12%
Carter	56642.02	45916.48	18.94%
Broad	64473.02	49426.02	23.34%
Market	82221.34	58018.87	29.44%
Georgia	35025.02	37918.21	-8.26%
Lindsay	24921.98	20094.77	19.37%
Houston	20555.69	14239.56	30.73%
Douglas	25899.19	32822.78	-26.73%
Peeples	1422.154	1830.014	-28.68%
Magnolia	4618.953	5516.213	-19.43%
Central St	72600.75	42307.93	41.73%
	415256.6	**334666.9**	**19.41%**

Total Eco_PI – 2% HDV

Test - 80010

	Actuated	DGMARL	%
Pine	24081.56	24793.27	-2.96%
Carter	50174.58	45763.32	8.79%
Broad	58851.8	46836.02	20.42%
Market	75300.72	53083.14	29.51%
Georgia	31339.99	34086.17	-8.76%
Lindsay	22369.66	18513.47	17.24%
Houston	21062.65	14610.07	30.64%
Douglas	21579.61	31090.11	-44.07%
Peeples	1672.345	1751.771	-4.75%
Magnolia	4023.593	4327.326	-7.55%
Central St	68926.94	42560.51	38.25%
	379383.5	**317415.2**	**16.33%**

Total Eco_PI – 1% HDV

Test - 80011

	Actuated	DGMARL	%
Pine	22414.17	24861.13	-10.92%
Carter	48304.07	38906.22	19.46%
Broad	56874.65	41201.3	27.56%
Market	85438.29	54420.59	36.30%
Georgia	29541.67	33941.8	-14.89%
Lindsay	21951.49	17900.08	18.46%
Houston	19898.14	14551.83	26.87%
Douglas	21451.33	31266.32	-45.75%
Peeples	1587.332	1881.436	-18.53%
Magnolia	3861.027	4327.243	-12.07%
Central St	66225.3	38970.97	41.15%
	377547.5	**302228.9**	**19.95%**

Table 12

Model	Simulation Hour(s)	Original Timing	Improved Timing	Output(s)
Actuated	**1-hour**	2 hours, 34 minutes	23 minutes, 59 seconds	Eco_PI, Vehicles in Net, Signal State
	3-hours	Around 5 hours	1 hour, 4 minutes	
DGMARL	**1-hour**	3 hours, 38 minutes	1 hour, 36 minutes	Eco_PI, Vehicles in Net, Signal State, Node State and other details
	3-hours	Around 12 hours	4 hours, 55 minutes	

Table 13

Without Message Passing

1-hr sim	Actuated	DGMARL	%
Pine	8532.522	9078.161	-6.39%
Carter	15010.87	10692.89	28.77%
Broad	22306.46	14976.2	32.86%
Market	29651.8	24204.07	18.37%
Georgia	13007.5	12652.69	2.73%
Lindsay	7422.028	7334.966	1.17%
Houston	5200.612	3425.311	34.14%
Douglas	9298.906	10600.68	-14.00%
Peeples	520.0162	926.8122	-78.23%
Magnolia	1783.23	1488.852	16.51%
Central St	25359.28	15550.25	38.68%
	138093.2	**110930.9**	**19.67%**

Previous approach – With Message Passing

1-hr sim	Actuated	DGMARL	%
Pine	8532.522	8832.619	-3.52%
Carter	15010.87	10918.25	27.26%
Broad	22306.46	15447.74	30.75%
Market	29651.8	23137.99	21.97%
Georgia	13007.5	13723.71	-5.51%
Lindsay	7422.028	6644.614	10.47%
Houston	5200.612	3930.351	24.43%
Douglas	9298.906	11076.56	-19.12%
Peeples	520.0162	850.8524	-63.62%
Magnolia	1783.23	1624.885	8.88%
Central St	25359.28	16730.18	34.03%
	138093.2	**112917.8**	**18.23%**

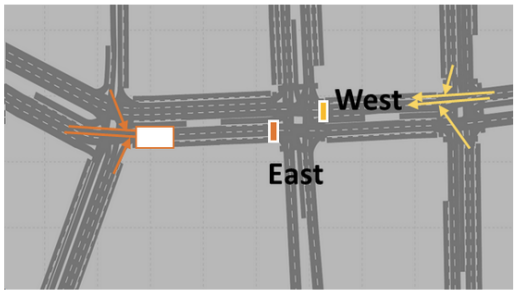

NEW - With Message Passing

1-hr	Actuated	DGMARL	%
Pine	6956.699	6963.358	-0.10%
Carter	12658.01	8579.315	32.22%
Broad	18768.45	12117.76	35.44%
Market	25233.92	17294.65	31.46%
Georgia	10705.41	10331.45	3.49%
Lindsay	5786.092	4716.866	18.48%
Houston	5362.982	3488.379	34.95%
Douglas	7093.474	9352.383	-31.84%
Peeples	356.3135	612.2733	-71.84%
Magnolia	1459.848	1867.387	-27.92%
Central St	22217.69	12457.45	43.93%
	116598.9	**87781.28**	**24.72%**

Table 14: DGMARL–Improved Intersections Coordination and Average Eco-PI: 26.52%

	Actuated	Previous Alg.		New Alg. Test 1		New Alg. Test 2		New Alg. Test 3		New Alg. Test 4		New Alg. Test 5	
Pine	8185.241	8684.976	-6.11%	7979.621	2.51%	7116.527	13.06%	6990.358	14.60%	6896.521	15.74%	7154.246	12.60%
Carter	13902.52	9850.864	29.14%	13424.57	3.44%	13761.67	1.01%	13776.82	0.90%	14400.02	-3.58%	13914.22	-0.08%
Broad	20382.28	14065.34	30.99%	13822.61	32.18%	14478.4	28.97%	14857.32	27.11%	14301.52	29.83%	13946.63	31.57%
Market	25006.75	19325.07	22.72%	18557.74	25.79%	18310.03	26.78%	17891.16	28.45%	17042.08	31.85%	17959.51	28.18%
Georgia	12131.55	12002.76	1.06%	11204.29	7.64%	12203.93	-0.60%	12497.34	-3.02%	12278.29	-1.21%	11561.31	4.70%
Lindsay	6376.639	5499.636	13.75%	4274.406	32.97%	4912.883	22.95%	4447.026	30.26%	4352.152	31.75%	4581.422	28.15%
Houston	5871.748	3450.75	41.23%	3893.175	33.70%	3520.334	40.05%	3275.001	44.22%	2794.201	52.41%	3913.558	33.35%
Douglas	8050.33	10011.97	-24.37%	5327.777	33.82%	5357.547	33.45%	5453.206	32.26%	6156.63	23.52%	5732.179	28.80%
Peeples	487.9753	822.1571	-68.48%	308.687	36.74%	305.2768	37.44%	278.1765	42.99%	330.3526	32.30%	321.9541	34.02%
Magnolia	1597.224	2164.154	-35.49%	1451.924	9.10%	1386.026	13.22%	1293.778	19.00%	1224.132	23.36%	1300.444	18.58%
Central St	24678.95	14336.55	41.91%	12856.28	47.91%	12287	50.21%	12419.58	49.68%	12208.88	50.53%	13097.94	46.93%
	126671.2	**100214.2**	**20.89%**	**93101.09**	**26.50%**	**93639.63**	**26.08%**	**93179.76**	**26.44%**	**91984.79**	**27.38%**	**93483.41**	**26.20%**

Table 15: DGMARL–Improved Intersections Coordination and Average STOPS: 17.91%

	Actuated	Previous Alg.		New Alg. Test 1		New Alg. Test 2		New Alg. Test 3		New Alg. Test 4		New Alg. Test 5	
Pine	285	313	-9.82%	194	31.93%	192	32.63%	182	36.14%	191	32.98%	181	36.49%
Carter	339	371	-9.44%	291	14.16%	289	14.75%	297	12.39%	284	16.22%	304	10.32%
Broad	455	490	-7.69%	387	14.95%	412	9.45%	403	11.43%	417	8.35%	396	12.97%
Market	598	643	-7.53%	582	2.68%	563	5.85%	557	6.86%	522	12.71%	546	8.70%
Georgia	355	404	-13.80%	373	-5.07%	394	-10.99%	395	-11.27%	397	-11.83%	380	-7.04%
Lindsay	171	214	-25.15%	130	23.98%	142	16.96%	141	17.54%	141	17.54%	143	16.37%
Houston	155	130	16.13%	110	29.03%	110	29.03%	98	36.77%	86	44.52%	113	27.10%
Douglas	232	287	-23.71%	156	32.76%	145	37.50%	146	37.07%	179	22.84%	159	31.47%
Peeples	24	33	-37.50%	16	33.33%	16	33.33%	15	37.50%	17	29.17%	16	33.33%
Magnolia	45	76	-68.89%	27	40.00%	29	35.56%	27	40.00%	29	35.56%	26	42.22%
Central St	633	542	14.38%	433	31.60%	425	32.86%	426	32.70%	425	32.86%	457	27.80%
	3292	**3503**	**-6.41%**	**2699**	**18.01%**	**2717**	**17.47%**	**2687**	**18.38%**	**2688**	**18.35%**	**2721**	**17.35%**

Table 16: DGMARL–Imrpoved Intersections Coordination and Average DELAY: 33.49%

	Actuated	Previous Alg.		New Alg. Test 1		New Alg. Test 2		New Alg. Test 3		New Alg. Test 4		New Alg. Test 5	
Pine	2954.1	2995.5	-1.40%	4601.7	-55.77%	3771.2	-27.66%	3875.8	-31.20%	3556.3	-20.39%	4025.7	-36.28%
Carter	8156.6	3308.1	59.44%	8628.8	-5.79%	8996.8	-10.30%	8847.7	-8.47%	9655.2	-18.37%	8942.4	-9.63%
Broad	13416.9	6256.6	53.37%	7598.4	43.37%	7862.9	41.40%	8310.2	38.06%	7723.3	42.44%	7746.3	42.26%
Market	15011.7	8389.2	44.12%	8537.3	43.13%	8367	44.26%	8296.3	44.73%	7956.9	47.00%	8523.2	43.22%
Georgia	6234.1	5310.7	14.81%	5133	17.66%	5630	9.69%	5706	8.47%	5394.2	13.47%	5300.3	14.98%
Lindsay	3451.8	1668.8	51.65%	2059.9	40.32%	2415.8	30.01%	2077.5	39.81%	1952.9	43.42%	2126.2	38.40%
Houston	3096.8	1101.9	64.42%	1889.1	39.00%	1595.3	48.49%	1554.7	49.80%	1303.5	57.91%	1894.7	38.82%
Douglas	3542.7	4593	-29.65%	2425.3	31.54%	2705.2	23.64%	2726.2	23.05%	2845.9	19.67%	2800.5	20.95%
Peeples	113.1	217.3	-92.13%	46.9	58.53%	45.1	60.12%	41.4	63.40%	57.5	49.16%	51.5	54.47%
Magnolia	689.1	494.9	28.18%	897.9	-30.30%	816.9	-18.55%	779.8	-13.16%	659.4	4.31%	802.5	-16.46%
Central St	14033.1	5226.2	62.76%	5274.2	62.42%	4957.3	64.67%	5122.8	63.49%	4880.9	65.22%	5311.2	62.15%
	70700	**39562.2**	**44.04%**	**47092.5**	**33.39%**	**47163.5**	**33.29%**	**47338.4**	**33.04%**	**45986**	**34.96%**	**47524.5**	**32.78%**

Table 17: CMEM results – MLK corridor

	RBC	DGMARL	Difference (%)
Hydrocarbons (g/mile)	11.81	11.21	-5.04%
Carbon Monoxide (g/mile)	94.57	90.33	-4.48%
Nitrogen Oxides (g/mile)	1.51	1.55	2.93%
Carbon Dioxide (g/mile)	249.59	237.41	-4.88%
Fuel Consumption (g/mile)	603.20	573.25	-4.97%

Table 18: Average difference achieved across all intersections

Average Difference (%)				
HC	CO	NO_x	FC	CO_2
2.4%	-7.6%	-1.0%	-8.0%	-10.7%

Appendix C: Equations

$$FC_{CSSP} = FC_D + FC_I + FC_A \quad (1)$$

$$FC_{DA} = K_e \cdot FC_I \quad (2)$$

$$K_e = \frac{FC_D + FC_A}{FC_I} \quad (3)$$

$$K = \frac{(FC_D + FC_A) \cdot T_I}{FC_I} \quad (4)$$

$$K_i = \frac{(FC_D + FC_A)_i \cdot T_{I_i}}{FC_{I_i}} \quad (5)$$

$$FC - PI = \sum_{i=1}^{n} D_i + \frac{(FC_D + FC_A)_i \cdot T_{I_i}}{FC_{I_i}} \cdot S_i \quad (6)$$

$$EcoPI_{total}^{i} = \sum_{m=1}^{8} d_{m_i} + K_{m_i} * N_{m_i} \quad (7)$$

$$d_{m_i} = \frac{0.38 * CL^i\left(1 - g_{m_i}/CL^i\right)^2}{1 - y_{m_i}} * PF_{m_i} \quad (8)$$

$$PF_{m_i} = \frac{1 - POG_{m_i}}{1 - g_{m_i}/CL^i} * \frac{1 - y_{m_i}}{1 - y_{m_i} * \left(\frac{CL^i}{g_{m_i}}\right) * POG_{m_i}}$$

$$* \left[1 + y_{m_i} * \frac{1 - POG_{m_i} * CL^i/g_{m_i}}{1 - g_{m_i}/CL^i}\right] \quad (9)$$

$$N_{m_i} = 0.9 \times \frac{1 - g_{m_i}/CL^i}{1 - y_{m_i}} \qquad (10)$$

$$CL^i_{min} = \frac{L}{1 \; - \; \frac{\sum AoR_{m_{i_{critical}}}}{0.5 \times CL^i_{previous}}} \qquad (11)$$

$$CL^i_{min} = L_i + \left(AoR_{\phi 1} + AoR_{\phi 2} + AoR_{\phi 3} + AoR_{\phi 4}\right) * h_{sat} \qquad (12)$$

$$L_i = \sum_{m'} \quad L_{\phi_{m'}} \qquad (13)$$

$$L_{\phi_{m'}} = \left(l_{1_{m'}} + y_{m'} + ar_{m'} - e_{m'}\right) \qquad (14)$$

$$AoR_{\phi_{m'}} = \left\{AoR_{\phi 1_{m'}}, \ldots, AoR_{\phi 4_{m'}}\right\} \qquad (15)$$

$$g_{min_{\phi_{m'}}} = L_{\phi_{m'}} + \; AoR_{\phi_{m'}} * h_{sat} \qquad (16)$$

$$CL^{group}_{min} = \left(CL^i_{min}\right) \qquad (17)$$

$$g_{extension1-4} = \left((CL^{group}_{min_{EcoPI}} + \Delta) - CL^{group}_{min_{EcoPI}}\right) \times \frac{AoR_{m_i} * K_{m_i} * q_{m_i} \; for \; \phi_{1-4}}{\sum AoR_{m_i} * K_{m_i} * q_{m_i}} \qquad (18)$$

$$EcoPI^i_{total} = \sum_{m\,=\,1}^{8} \quad d_{m_i} + K_{m_i} * N_{m_i} \qquad (19)$$

$$d_{m_i} = \frac{0.38 * CL^i\left(1 - g_{m_i}/CL^i\right)^2}{1 - y_{m_i}} * PF_{m_i} \qquad (20)$$

$$PF_{m_i} = \frac{1 - POG_{m_i}}{1 - g_{m_i}/CL^i} * \frac{1 - y_{m_i}}{1 - y_{m_i} * \left(\frac{CL^i}{g_{m_i}}\right) * POG_{m_i}}$$

$$* \left[1 + y_{m_i} * \frac{1 - POG_{m_i} * CL^i/g_{m_i}}{1 - g_{m_i}/CL^i}\right] \quad (21)$$

$$N_{m_i} = 0.9 \times \frac{1 - g_{m_i}/CL^i}{1 - y_{m_i}} \quad (22)$$

$$CL_{EcoPI}^{group} = \left(CL_{EcoPI}^{i}\right) \quad (23)$$

$$CL_{min_q}^{i} = \frac{Total\ Lost\ Time}{1 - \frac{\sum AOR_{m_{i_{critical}}}}{0.5 \times CL^i}} \quad (24)$$

$$g_{min_{q1}} = CL_{min_q}^{i} \times \frac{\left(AOR_{1,5}\right)}{\sum AOR_{m_{i_{critical}}}} \quad (25)$$

$$g_{min_{q2}} = CL_{min_q}^{i} \times \frac{\left(AOR_{2,6}\right)}{\sum AOR_{m_{i_{critical}}}} \quad (26)$$

$$g_{min_{q3}} = CL_{min_q}^{i} \times \frac{\left(AOR_{3,7}\right)}{\sum AOR_{m_{i_{critical}}}} \quad (27)$$

$$g_{min_{q4}} = CL_{min_q}^{i} \times \frac{\left(AOR_{4,8}\right)}{\sum AOR_{m_{i_{critical}}}} \quad (28)$$

$$g_{extension1-4} = \left(CL_{EcoPI}^{group} - CL_{min_q}^{i}\right) \times \frac{critical\ movement\ based\ on\ AoG_{m_i} * K_{m_i}\ for\ phase\ 1-4}{\sum critical\ movement\ based\ on\ K(AoG)} \quad (29)$$

$$g_{total_{1-4}} = g_{min_{q1-4}} + g_{extension1-4} \quad (30)$$